

Towards Mechanical Reinforcement in Polymer Layered Silicates Nanocomposites of the Second Generation

Dissertation

zur Erlangung des akademischen Grades

Doktor der Naturwissenschaften (Dr. rer. nat.)

im Promotionsprogramm Materialchemie und Katalyse

an der Bayreuther Graduiertenschule

für Mathematik und Naturwissenschaften (BayNAT)

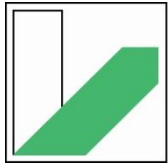
der Universität Bayreuth

vorgelegt von

Mazen Ziadeh

Geboren in Aleppo (Syrien)

Bayreuth – 2014



**UNIVERSITÄT
BAYREUTH**

Die vorliegende Arbeit wurde in der Zeit von Juni 2010 bis Dezember 2013 am Lehrstuhl für Anorganische Chemie I (ACI) an der Universität Bayreuth unter der Betreuung von Herrn Professor Dr. Josef Breu angefertigt.

Vollständiger Abdruck der von der Bayreuther Graduiertenschule für Mathematik und Naturwissenschaften (BayNAT) der Universität Bayreuth genehmigten Dissertation zur Erlangung des akademischen Grades eines Doktors der Naturwissenschaften (Dr. Rer. Nat.).

Dissertation eingereicht am: 07.02.2014

Zulassung durch die Prüfungskommission: 24.02.2014

Wissenschaftliches Kolloquium: 02.06.2014

Amtierender Direktor: Prof. Dr. Franz Xaver Schmid

Prüfungsausschuss:

Prof. Dr. Josef Breu (Erstgutachter)

Prof. Dr.-Ing. Volker Altstädt (Zweitgutachter)

Prof. Dr. Georg Papastavrou (Vorsitzender)

Prof. Dr. Peter Strohriegl

To my Parents Elias and Mary

إلى والدي و والدي الأعماء

“Only those who will risk going too far
can possibly find out how far one can go.”

T. S. Eliot

Table of Contents

List of abbreviations	vi
Summary.....	1
Zusammenfassung	3
1. Introduction	6
1.1. Structure of layered silicates.....	9
1.2. Classification of layered silicates	10
1.3. The 2:1 silicate layer–smectite	11
1.4. Modification of layered silicates.....	12
1.5. Polymer layered silicates nanocomposites	13
1.5.1. Mechanical properties.....	14
1.5.2. Reinforcement in nanocomposites.....	15
1.5.3. Dispersing methods and efficiency	17
1.6. Aims and addressed problems	19
2. Synopsis	20
2.1. Maximizing the aspect ratio.....	22
2.2. Optimizing the specific interface.....	25
2.3. Reinforcement and fracture toughness	28
2.4. Dispersion quality and the specific interface	31
3. References.....	33
4. Publications.....	36
4.1. A simple approach for producing high aspect ratio fluorohectorite nano-platelets by utilizing a stirred media mill (ball mill).....	37
4.2. Towards completely miscible PMMA nanocomposites reinforced by shear-stiff, nano-mica.....	59
4.3. Impact of large aspect ratio, shear-stiff, mica-like clay on mechanical behaviour of PMMA/clay nanocomposites	88
4.4. On the importance of specific interface area in clay nanocomposites of PMMA filled with synthetic nano-mica.....	112
List of publications and conferences.....	146
Acknowledgment.....	148
Erklärung des Verfassers.....	150

List of abbreviations

ATRP	atom transfer radical polymerization
BET	Brunauer-Emmett-Teller equation
CEC	cation exchange capacity
<i>d</i>	density of layered silicates (g cm ⁻³)
<i>d</i> _{GM}	diameter of grinding media (mm)
DMAc	dimethylacetamide
DMAEMA	2-dimethylaminoethyl methacrylate
DMSO	dimethylsulfoxid
DP	degree of polymerization
E	Young's modulus
<i>E</i> _{hyd}	enthalpy of hydration (KJ mol ⁻¹)
<i>E</i> _s	specific energy (KJ Kg ⁻¹)
Ebib	ethyl 2-bromoisobutyrate
FT-IR	Fourier transform infrared analysis
FWHM	full width at half maximum
GM	grinding media
HEMA	2-hydroxyethyl methacrylate
HDPE	high density polyethylene
<i>K</i> _{IC}	critical intensity factor (MPa m ^{1/2})
<i>h</i>	thickness of a tactoid
Hect	fluorohectorite
L	lateral extension (μm)
MI ⁿ⁺	polycationic macro-initiator
MMA	methyl methacrylate
MMT	montmorillonite
<i>M</i> _n	number average molecular weight (g mol ⁻¹)
<i>M</i> _w	weight average molecular weight (g mol ⁻¹)
<i>m</i> _p	solid content (wt.%)
<i>N</i> _A	Avogadro constant
(Na, Mg, K)-hect	fluorohectorite with corresponding interlayer cation

O-lect	organo-fluorohectorite
PLSN	polymer layered-silicate nanocomposites
PSD	particle size distribution
PTFE	polytetrafluoroethylene
PXRD	powder X-ray diffraction
OTR	oxygen transmission rate ($\text{cm}^3 \text{m}^{-2} \text{day}^{-1} \text{bar}^{-1}$)
SEC	size exclusion chromatography
SEM	scanning electron microscopy
SI-ATRP	surface initiated polymerization
SLS	static light scattering
TEM	transition electron microscopy
THF	tetrahydrofuran
T_g	glass transition temperature ($^{\circ}\text{C}$)
TGA	thermogravimetric analysis
TPU	thermoplastic polyurethane
trien	triethylenetetramine
V_t^2	velocity of the agitator (m s^{-1})
α	aspect ratio
Φ / vol.	volume fraction (%)
wt.-	weight percent (%)
ρ_{GM}	density of grinding media (kg l^{-1})
λ	wave length (\AA)
φ	filling volume (%)
ΔE	energy input (KW h)
μ -CT	micro-computer tomography
σ	grafting density (chain per nm^2)

Summary

This dissertation focuses on the optimization of nanofillers based on synthetic layered silicates for preparation of nanocomposites with improved mechanical reinforcement. The mechanical characterization was done in collaboration with the Polymer Engineering Department at Bayreuth University in the frame work of SFB 840 (Project B3).

The synthetic Na-fluorohectorite clay applied in this thesis differs from conventionally used natural montmorillonites (MMT) in respect to three main features: the charge density of the clay and thus the interface chemistry is much more homogeneous and may be adjusted to any desired value. The nanoplatelet diameter is more than an order of magnitude larger, and it is of high phase purity with limited, if any accessory minerals present. In respect to reinforcement, these features allow to eliminate internal shear planes to realize stiffer platelets with higher surface area. Moreover, the larger diameter of the nanoplatelets is beyond the size of typical microcracks and the number of platelets acting as stress concentrators is two orders of magnitude lower at any given filler content.

The synthetic Na-fluorohectorite was prepared by melt synthesis in a well optimized process at the Department of Inorganic Chemistry I. This material has huge lateral extension ($\geq 20 \mu\text{m}$) and superb layer charge homogeneity.

In order to maximize the aspect ratio (α) the nanoplatelets were exfoliated into thinner tactoids by mechanical shearing. A cation exchange of the interlayer Na^+ cations with Mg^{2+} allowed a higher hydration state and produced a 'shear-labile' material with reduced Coulomb forces between the layers. Applying shear forces generated in a stirred media mill led to exfoliation of the tactoids with minimal breakage and consequently larger aspect ratio. This process was optimized by investigating the main parameters controlling the exfoliation efficiency such as: solid content, grinding media size, and number of passages in the milling chamber. A subsequent cation exchange with K^+ cations yielded collapsed and shear-stiff, mica-like nanofiller with no interlamellar reactivity.

The collapsed state, moreover, allowed a selective organophilization of external basal surfaces of the tactoids using a polycationic macro-initiator (MI^{n+}) with no

signs of intercalation. The multiple electrostatic anchoring groups not only provided reliable adhesion but at the same time allowed adjusting the degree of protonation to match the surface charge. Dispersing the large aspect ratio MI^{n+} /nano-mica by melt compounding in poly(methyl methacrylate) (PMMA) showed significantly enhanced mechanical properties. These nanoplatelets promoted additional energy dissipating mechanisms in the nanocomposites such as crack deflection, crack pinning as well as debonding effects leading to improved fracture toughness, such improvements have never been reported for MMT-nanocomposites.

Optimization of the interfacial interaction towards complete miscibility with the PMMA-matrix was attempted by attaching a PMMA brushes on the external basal surfaces. This was done in a grafting-from process *via* surface initiated atom transfer radical polymerization (SI-ATRP). Highly stable suspensions of the coated nanofiller in organic solvent showing birefringence of a nematic phase were observed. Although a significantly improved stiffness as compared to MI^{n+} /nano-mica-filled composites was achieved, still the full potential, as predicted by Halpin-Tsai equations, could not be utilized. This was attributed to a non-wetting character of the densely packed PMMA on the surface preventing chain interdigitation needed for good wetting.

Finally, two compounding techniques were compared to probe the influence of the dispersion quality. PMMA-nanocomposites filled with MMT and MI^{n+} /nano-mica were made by melt compounding and solution blending, respectively. Gas barrier measurements proved to be an additional independent and very sensitive probe for the dispersion quality. The solution blended samples and melt compounded samples showed permeation reductions by 60% and 30%, respectively. Maximizing the interface area by optimum dispersion not only reduced the oxygen permeation but also improved the reinforcement and fracture toughness especially at low clay content. These results highlighted the prime importance of the dispersion quality to exploit the full potential of nanofillers. Mediocre compounding may easily counterpoise advantages of superior fillers.

Zusammenfassung

Diese Arbeit konzentriert sich auf die Optimierung von Nanofüllstoffen auf Basis synthetischer Schichtsilikate zur Herstellung von Nanokompositen mit mechanischer Verstärkung. Die mechanische Charakterisierung der Nanokomposite wurde in Zusammenarbeit mit dem Lehrstuhl Polymere Werkstoffe der Universität Bayreuth im Rahmen des SFB 840 (Teilprojekt B3) durchgeführt.

Die synthetischen Schichtsilikate (Na-Fluorohectorit) in dieser Arbeit unterscheiden sich von konventionell verwendetem, natürlichem Montmorillonit (MMT) in Bezug auf die drei wichtigsten Eigenschaften: Die Ladungsdichte der synthetischen Schichtsilikate und damit die Grenzflächenchemie ist viel homogener und kann auf jeden gewünschten Wert eingestellt werden. Ihr Plättchendurchmesser ist mehr als eine Größenordnung höher und sie besitzen eine hohe Phasenreinheit mit wenig oder kaum Nebenphase. In Bezug auf die Verstärkung ermöglichen diese Eigenschaften interne Scherflächen zu beseitigen und steifere Plättchen mit höherer Oberfläche zu realisieren. Darüber hinaus liegt der vergrößerte Durchmesser der Plättchen über der Größe von typischen Mikrorissen und die Anzahl der Plättchen, die als Spannungskonzentratoren wirken, ist bei jedem gegebenen Füllstoffgehalt um zwei Größenordnungen niedriger.

Der synthetische Na-Fluorohectorit wurde durch Schmelzsynthese in einem optimierten Prozess am Lehrstuhl Anorganische Chemie I hergestellt. Dieses Material hat eine sehr große laterale Ausdehnung ($\geq 20 \mu\text{m}$) und eine hervorragende Homogenität der Schichtladung.

Um das Aspektverhältnis (α) zu maximieren, wurden die Plättchen durch mechanisches Scheren in dünnere Taktoide exfoliert. Ein Kationenaustausch der Zwischenschicht Na^+ -Kationen durch Mg^{2+} ermöglichte einen höheren Hydratationszustand und erzeugte ein „scherlabiles“ Material mit verringerten Coulomb-Kräften zwischen den Schichten. Das Einbringen von Scherkräften in einer Rührwerkskugelmühle führte zu einer Exfolierung der Taktoide mit minimalem Bruch und infolgedessen hohem Aspektverhältnis. Die Exfolierungseffizienz dieses Prozess wurde durch die Untersuchung der

wichtigsten Parameter optimiert: Feststoffgehalt, Kugelmediengröße und Anzahl der Zyklen. Ein nachfolgender Kationenaustausch mit K^+ -Kationen resultierte in kollabierten, „schersteifen“ Glimmer-ähnlichen Nanofüllstoffen.

Der kollabierte Zustand ermöglichte eine selektive Organophilierung der externen Basaloberflächen der Taktoide mit einem polykationischen Makroinitiator (MI^{n+}) ohne Anzeichen einer Interkalation. Die multiplen elektrostatischen Ankergruppen bieten nicht nur eine zuverlässige Anbindung, sondern erlauben gleichzeitig die Einstellung des Protonierungsgrades auf die entsprechende Oberflächenladung. Die Dispergierung des MI^{n+} /nano-Glimmers mit großem Aspektverhältnis durch Schmelz-compoundierung in Polymethylmethacrylat (PMMA) zeigte deutlich verbesserte mechanische Eigenschaften. Diese Nanoplättchen förderten zusätzliche Energiedissipationsmechanismen wie Rissablenkung, Risspinning, sowie Ablösungseffekte in den Nanokompositen, die zu einer verbesserten Bruchzähigkeit führten, wie sie nie zuvor für MMT-Nanokomposite berichtet wurde.

Die Optimierung der Grenzflächen-Wechselwirkungen hin zu einer vollständigen Mischbarkeit mit der PMMA-Matrix wurde durch Anbringen von PMMA-Bürsten auf die externen Basalflächen erreicht. Dies wurde durch einen ‚grafting-from‘ Prozess via oberflächeninitiiertes Atom Transfer Radikal Polymerisation (ATRP) erreicht. Es wurden sehr stabile Suspensionen des beschichteten Nanofüllstoffes in einem organischen Lösungsmittel beobachtet, die Doppelbrechung einer nematischen Phase zeigten. Obwohl eine deutlich verbesserte Steifigkeit im Vergleich zu MI^{n+} /nano-Glimmer gefüllten Verbundwerkstoffen erzielt wurde, konnte das volle Potenzial, das von den Halpin-Tsai Gleichungen prognostiziert wird, nicht erreicht werden. Dies wird dem nicht-benetzbarkeit Charakter des dicht gepackten PMMA auf der Oberfläche zugeschrieben, das eine für eine gute Benetzung notwendige Kettenverzahnung verhindert.

Schließlich wurden zwei Mischtechniken verglichen, um den Einfluß der Dispersionsqualität zu untersuchen. PMMA/Nanokomposite, die mit MMT und MI^{n+} /nano-Glimmer gefüllt wurden, wurden durch Schmelz-compoundierung und solution blending hergestellt. Gasbarrieremessungen erwiesen sich als zusätzliche, unabhängige und sehr empfindliche Methode zur Überprüfung der

Dispersionsqualität. Die in Lösung vermischten und schmelz-compoundierten Proben zeigten eine Senkung der Permeation von 60% und 30%. Die Maximierung der Grenzfläche durch optimale Dispergierung verringerte nicht nur die Sauerstoffdurchlässigkeit, sondern verbesserte auch die Verstärkung und Bruchzähigkeit bei niedrigem Füllstoffgehalt. Diese Ergebnisse heben die vorrangige Bedeutung der Dispersionsqualität hervor, die notwendig ist um das volle Potenzial der Nanofüllstoffe nutzen zu können. Eine mittelmäßige Compoundierung kann den Vorteilen überlegener Füllstoffe leicht entgegenwirken.

1

1. Introduction

Man has combined two or more materials with different physical and/or chemical properties to make composite with desired properties for several thousand years. From early bricks made of straw and mud to modern days nanocomposites, these composite materials have become essential products for modern daily life [1]. In the last two decades a huge demand on high performance materials started to rise in various industrial fields. Such materials even paved the way for new technological applications. In particular, advanced polymeric materials emerge as an appealing candidate to replace expensive and rather heavy metals and ceramics for more sustainable and affordable products, especially in automotive and aviation industry where weight is a major factor [2,3].

More recently the field gained significant momentum by introducing robust nanoscale fillers with high modulus to enhance the performance of composites. Nanofillers are a class of materials having at least one dimension in the nanometre scale. Switching from the micrometer to nanometre scale fillers increases the surface area/volume ratio by three orders of magnitude [4]. Appropriate compounding transforms the surface into specific interface areas that extend their influence into the bulk of the matrix generating a large interphase volume with modified properties. Even for moderate filler contents, this interphase volume might actually comprise the complete nanocomposite volume.

Significant progress not only led to the developing of new type of fillers but also in controlling the structure and the dimension of fillers on the nanometre scale. The incorporation of various nanoparticles ranging from isotropic to highly anisometric shapes has been already reported intensively in literature [5,6]. It is noteworthy to mention that, although many nanoparticles have been investigated

to produce polymer nanocomposites, unfortunately most are relatively difficult to produce or handle and thus nanocomposites might become quite expensive compared to conventional composites. The industrial costs might in fact be one of the main reasons limiting a real large scale application of polymer nanocomposites. For a breakthrough, cheap and abundant nanofillers are needed.

The morphological characteristic of the filler is of a fundamental importance for the structure-property relationship of composites. An essential aspect is the surface area/volume ratio of the nanofiller. The small scale of the nanofillers leads to an exceptionally large interfacial area in the composites. The interface controls the degree of interaction between the filler and the polymeric matrix which in relation controls the final properties of the composite [7].

The specific interface area is, however, not only determined by the size but is also significantly influenced by the shape of the filler particles. Common nanofiller geometries and their respective surface area/volume ratios are shown in **Figure 1**.

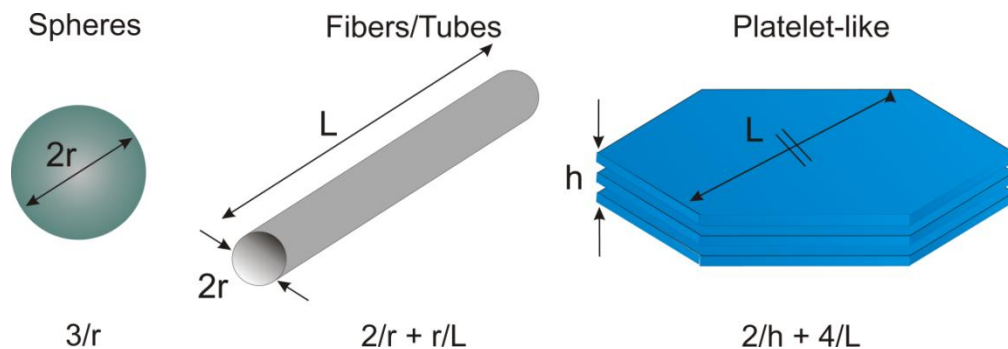


Figure 1. Surface area/volume relations of various nanofillers geometries.

In the case of spherical nanoparticles the surface area per unit volume depends on the radius (r) of the sphere, whereas in layered materials and fibres, the surface area per unit volume is inversely proportional to the material's lateral extension (L). Low dimensional morphologies with high aspect ratio like platelets are therefore advantageous over spherical nanoparticles due to their higher specific interface area. For that reason, layered materials have emerged as the most promising candidates for the preparation of polymeric based nanocomposites.

Among the plethora of anisotropic layered materials known such as layered double hydroxides (LDH) [8,9], graphene-based materials [10,11], and layered silicates [12], swelling 2:1 layered silicates (LS) stand out due to their rich interlamellar

reactivity. This characteristic, allows for facile tuning of the strength of the interactions between layers in the tactoid. Consequently, the mechanical properties of LS can be varied depending on the nature of the interlayer cation [13]. The combination the unique physical and chemical properties (i.e. thermal stability, mechanical strength and high aspect ratio) of these LS with neat polymers created a special class of high performance polymer layered silicate nanocomposites (PLSN). The incorporation of nanoscale LS have recently been used in various new fields of nanotechnology; for instance, for superb diffusion barriers [14,15], flame retardancy [16,17], and for mechanical reinforcement [12,18]. In particular the latter application is the main focus of this research.

The fabrication of PLSN affords four major consecutive steps (**Figure 2**): i. The synthesis or in the case of natural sources, the purification of the clay. ii. The tailoring of the morphology and mechanical properties, if possible. iii. Modification of the external basal planes to adjust the surface tensions of filler and matrix (organophilization). Ideally the modification should also optimize the interaction with the matrix to allow for an efficient stress transfer. iv. Homogenous dispersion of the filler in to the matrix. Ideally the complete surface area provided by the nanofiller should be converted into interface area.

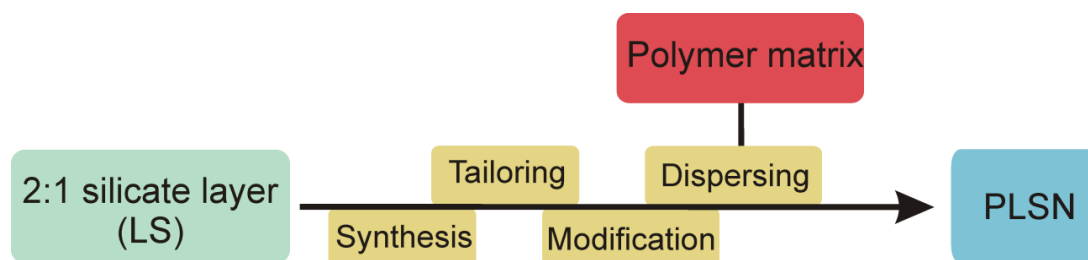


Figure 2. A schematic representation towards a successful combination of the 2:1 silicate layer into the polymer matrix for the preparation of nanocomposites.

1.1. Structure of layered silicates

As the name layered silicates (LS) suggests, it is made up by two-dimensional sheets. These sheets create a layer (*lamella*) and the parallel arrangements of a number of layers create a tactoid (*lamellae*) with a certain distance depending on the nature of the interlayer ions. The interlayer ions play an important role through determining the interlamellar interaction and cohesion, and thus the macroscopic properties [19]. There are two types of sheets, a tetrahedral sheet (T) and an octahedral sheet (O) which are connected by a common anion plane. The periodic stacking of the layers forms a one-dimensional lattice, with layers of approximately 0.96 nm thickness [24].

1.1.1. Tetrahedral sheet

The tetrahedral sheet of layer silicates are composed of SiO_4^{4-} or AlO_4^{5-} , which are linked together by sharing three corners of the basal oxygen atoms O_b , the fourth being the apical oxygen atom O_a . Each of the basal O^{2-} connects two tetrahedral. The basal oxygen atoms form a two-dimensional lattice exhibiting hexagonal cavities as shown in (Figure 3).

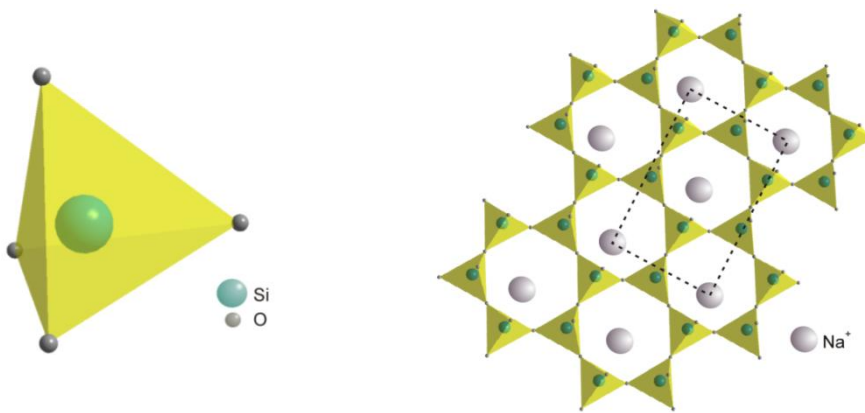


Figure 3. Tetrahedron and a tetrahedral sheet (T) arrangement showing the interlayer cations in the cavities.

1.1.2. Octahedral sheet

The octahedral sheet holds various cations such as: Al^{3+} , Fe^{3+} , Mg^{2+} , Fe^{2+} , Li^+ , Mn^{2+} , Co^{2+} , Ni^{2+} , Cu^{2+} , Zn^{2+} , V^{3+} , and Ti^{4+} . Where these cations are coordinated by four oxygen atoms shared with the tetrahedral sheet and two additional hydroxyl or fluoride groups (Figure 4) [21].

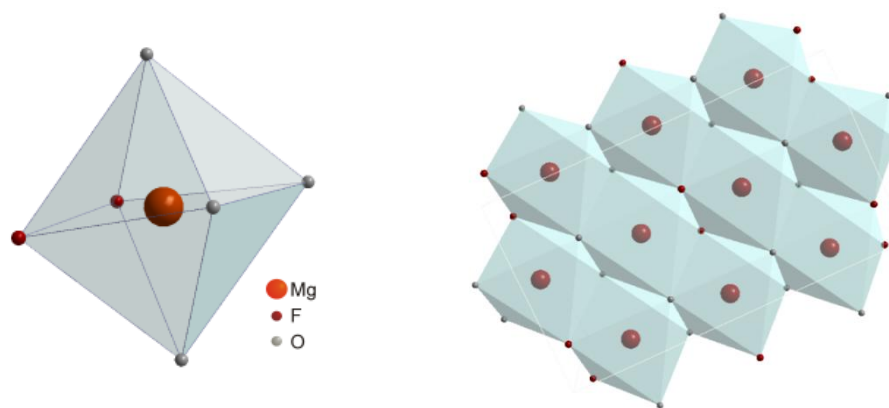


Figure 4. Octahedron and an octahedral sheet (O) arrangement.

1.2. Classification of layered silicates

Layered silicates can be categorized depending on the packing arrangement of the tetrahedral and octahedral sheets. The first type is the 1:1 layer structure which is formed by one T sheet and one O sheet (T-O). The alternative one is the 2:1 layer structure, in which there are two T sheets having the O sheet sandwiched between (T-O-T) [21,22]. Each layer is separated from its neighbours by a gap called *interlayer* or *gallery*, so that these layers organize themselves to form tactoids hold together by relatively weak forces. Isomorphic substitution within the layers (for example, Al^{3+} replaced by Mg^{2+} or by Fe^{2+}) generates negative charges that are counterbalanced by alkali or alkaline earth cations placed in the galleries. Structures where all of the six octahedral sites are occupied are referred to as trioctahedral and where only four of the six sites are occupied then they are known as dioctahedral.

A simple approach to classify the various types of layered silicate is depending on the structure and composition of the octahedral sheet (OS) and the layer charge (X). The layer charge in the 1:1 layer structure is close to zero and varies in the 2:1 layer structure from 0.2 (smectites) to 2.0 in brittle mica. The layer charge is calculated on the basis of layered silicates structural formulae (half unit-cell content) (**Table 1**) [23].

Table 1. Classification of layered silicates and their corresponding layer charge

Group	Layer charge (X per Si ₄ O ₁₀)	Octahedral character*	Name
<i>1:1 layer structure</i>			
Serpentine- Kaolinite	X~0	Di Tri	Kaolinite Serpentine
<i>2:1 layer structure</i>			
Talc-pyrophyllite	X~0	Di Tri	Pyrophyllite Talc
Smectite ^a	X~0.2-0.6	Tri Di	Hectorite, Saponite Montmorillonite,
Vermiculite ^b	X~0.6-0.9	Tri Di	Trioct. Vermiculite Dioct. Vermiculite
True mica ^b	X~0.6-1.0	Tri Di	Muskovite, Illite Phlogopite
Brittle mica ^c	X~1.8-2.0	Tri Di	Margarite Bityite, Anandite

^ahydrated and exchangeable cation, ^bnon-hydrated monovalent cations

^cnon-hydrated divalent cations

*Di = dioctahedral and Tri= trioctahedral

1.3. The 2:1 silicate layer–smectite

One of the most important groups of the 2:1 family is smectite family, which due to its intermediate X has rich intercrystalline reactivity (**Figure 5**). This pronounced interlamellar reactivity results from hydration and exchange of the interlayer cations. Moreover, hydration of interlayer cations or cation exchange concomitantly increases the basal spacing and thus reduces the cohesion between layers [22]. The degree of swelling of 2:1 LS is determined by the nature of the interlayer cations through their hydration of enthalpy (H_{Hydra} . KJ mol⁻¹). This is associated with the Coulomb attraction between silicate lamellae and interlayers and scales with the charge density.

Larger basal spacing inversely reduce the attractive Coulomb forces between the positively charged interlamellar space and the negatively charged silicate lamellae proportionally to the square of the distance between the charges ($F \sim 1/d^2$).

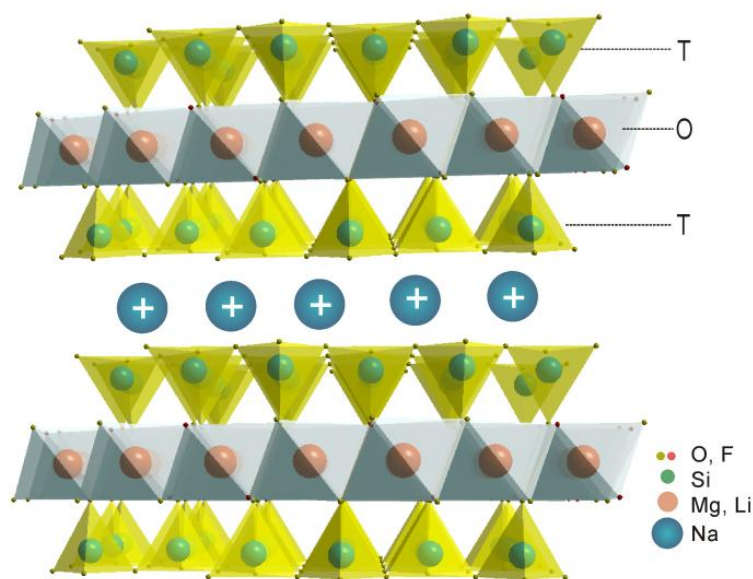


Figure 5. Structure of the 2:1 silicate layer type of Na-fluorohectorite of the smectite family. The Octahedral sheet (O) is sandwiched between two tetrahedral sheets (T) and the negative charge from the isomorphous substitution in the octahedral sheet (Mg^{2+} with Li^+) is compensated with the exchangeable interlayer cations (Na^+).

1.4. Modification of layered silicates

The reactivity of layered silicates can be related with the capacity of the interlayer cations to be replaced with other cations by exchange reaction at both external and internal surfaces. This is referred to as the CEC (Cation Exchange Capacity) and has the unit of meq./ 100 gr. With increasing diameter, the contribution of the edge surface to the total surface quickly becomes irrelevant for the surface properties of the clay. Surface chemistry of synthetic Na-fluorohectorite to a very good approximation is solely determined by external basal surfaces.

Due to inorganic cations at the external surfaces, LS are highly hydrophilic. Therefore, incorporation into hydrophobic organic polymers requires adjustment of surface tension which can be achieved by a highly favourable cation exchange with organic cations. Most commonly, alkyl-ammonium cations are used [24,25]. For natural MMT this exchange cannot be restricted to external surfaces but also cations in the interlayer are replaced. These completely organophilized layered silicates are referred to as 'Organoclay' (**Figure 6**).

More elaborate organic modifiers may, however, contain a variety of functional groups, which improve the interaction with the polymer matrix needed for effective stress transfer into the filler. Such functionalities can include polymerizable groups (e.g., vinyl) or initiating groups which can initiate a subsequent polymerization of various monomers.



Figure 6. Organophilization of layered silicates by complete exchange of the interlayer cations with organic molecules.

Moreover, the complete intercalation usually weakens the cohesion between the lamellae by increasing the interlayer spacing $d(001)$. Although in many papers it is claimed that the weakening is sufficient to trigger delamination during the subsequent melt compounding into polymeric matrices. In our own experience the shearing is at best sufficient to disaggregate the clays but not even exfoliation can be achieved. Consequently, the high organic volume in the interlayers will act like a lubricant which will be detrimental on the shearing stiffness of the filler and hence the mechanical properties of the nanocomposite. These interlayer spaces will act as inner shear planes inducing failure when introducing shear stress or load [26].

1.5. Polymer layered silicates nanocomposites

Despite the fact that PLSN had been studied for several decades, the genesis of the modern PLSNs can be traced to the seminal work done at Toyota Central Research and Development Laboratories (CRDL) in the late 1980s [27,28]. In these studies, organoclays have been employed to reinforce Nylon 6. The preparation of the Nylon 6–MMT nanocomposite was done by *in-situ* polymerizing of intercalated ϵ -caprolactam in MMT which had been ion exchanged with 12-aminolauric acid serving as catalyst for the ring opening polymerization [27]. The appropriate combination resulted in LS being fully delaminated and uniformly dispersed in the matrix. The nanocomposites showed enhanced mechanical properties compared to neat polymer stretching from higher tensile strength and moduli, decreased thermal expansion coefficient, and enhanced electrical conductivity.

1.5.1. Mechanical properties

The enhancement in mechanical properties is a significant driving force behind the development of PLSNs. The impact of LS on the reinforcement of PLSN has been evaluated by measurement of various mechanical properties of the produced nanocomposites. The fundamental mechanical properties of plastics include four aspects [29]:

- I. *Stiffness*: the extent of a material which it resists deformation in response to an applied force
- II. *Strength*: ability of a material to withstand an applied stress without failure
- III. *Formability*: the capacity of a material to become deformed under external stress
- IV. *Toughness*: ability of a material to absorb energy and plastically deform without fracturing

The first three aspects can be measured from a typical tensile test from the relationship between the stress applied on a sample being pulled apart and the strain (stretching). The modulus of elasticity (stiffness) or Young's modulus (**E**) is defined by the ratio of tensile stress over tensile strain (**Figure 7**) in the lower range of the stress-strain diagram using the following equation:

$$E = \frac{\sigma}{\varepsilon} = \frac{F/A}{\Delta L/L} \quad (1)$$

Where F is the force exerted on sample under tension, A is the cross-sectional area; ΔL is the change in length of the sample and L is the original length.

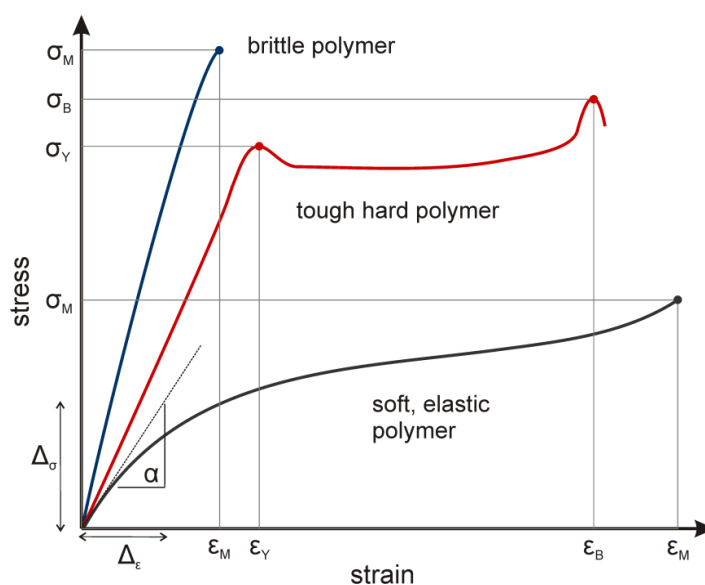


Figure 7. Full engineering stress-strain curves; these curves are typical of brittle, tough, and soft elastic polymers, respectively [29].

Beside Young's modulus, stress-strain curves give information on strength and deformation of the material (**Figure 7**):

- Tensile strength (σ_M) is the tensile stress at maximum force
- Tensile stress at break (σ_B) is the tensile stress at the moment of break
- Tensile strength at yield (σ_Y) is the tensile stress at which the slope of the change of force versus length curve equals zero for the first time
- The elongation at maximum force is described as (ϵ_M), elongation at break as (ϵ_B), and tensile strength at yield as (ϵ_Y)

1.5.2. Reinforcement in nanocomposites

By the term, reinforcement relates to the improvement of stiffness and strength in a composite material. Accumulating and understanding the relation between the type of dispersed nanofiller and the reinforcement observed in the nanocomposites requires the systematic investigation of several factors. These include the shape and dimension (i.e. aspect ratio) [12], mechanical properties of the filler [15], the interaction between nanofiller and polymer at the interface, and the dispersion quality [30].

All theoretical models predicting the increase in Young's modulus assume a complete stress transfer. For spherical filler, Fornes and Paul [31] proposed the following equation:

$$E_c = E_m \Phi_m + E_f \Phi_{mf} \quad (2)$$

where E_c , E_m and E_f are the Young's modulus of the nanocomposites, polymer matrix and nanofiller, respectively. Φ_m and Φ_f are the volume fraction of the polymer matrix and nanofiller in the nanocomposite. The aspect ratio is taken into account by the Halpin-Tsai equation [32] by the inclusion of a shape factor (Eq. 3).

$$\frac{E_c}{E_m} = \frac{1 + \xi \eta \Phi}{1 - \eta \Phi} \quad (3)$$

$$\text{where: } \xi = 2 * 0.66 * \left(\frac{L}{h}\right); \eta = \frac{\frac{E_f}{E_m} - 1}{\frac{E_f}{E_m} + \xi}$$

In this case, ξ is the shape factor depending on the filler orientation and loading direction. The value 0.66 is introduced as a modulus reduction factor taking into

account the lower contribution of platelet-like nanofiller to Young's Modulus in comparison to fibre-like fillers [33].

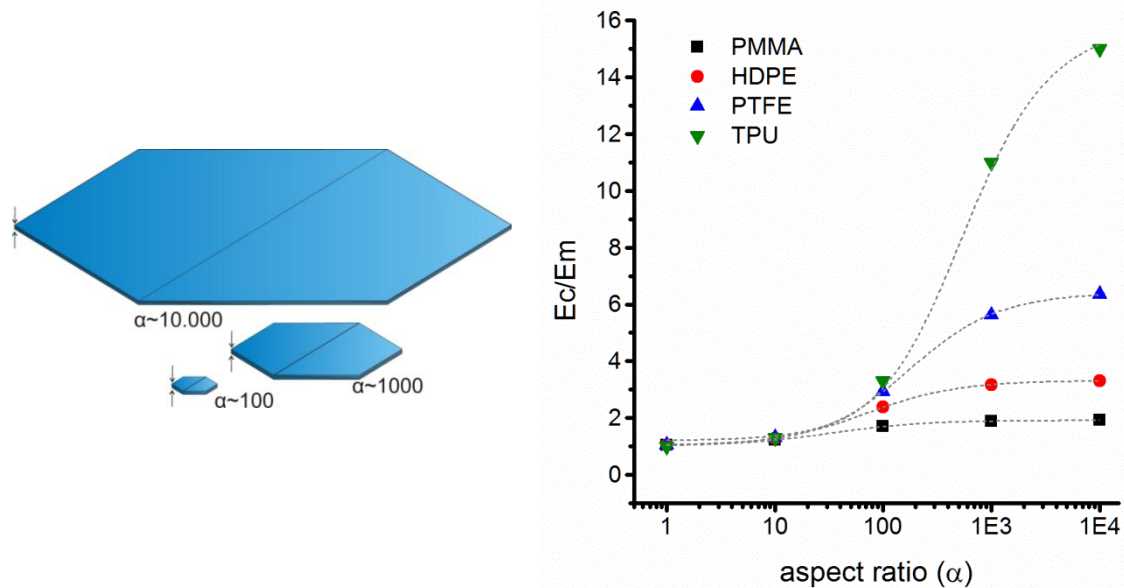


Figure 8. Left). Representation of various aspect ratio nanoplatelets having lateral extension in micrometer and thickness in the nanometre scale, Right). Reinforcement effect calculated using Halpin-Tsai equation in nanocomposites using nanofillers with different aspect ratios in various polymeric matrices; (■) PMMA $E_{m1} = 3.5$ GPa, (●) HDPE $E_{m2} = 1.7$ GPa, (▲) PTFE $E_{m3} = 0.6$ GPa and (▼) TPU $E_{m4} = 0.2$ GPa. The calculation is based on $E_f = 150$ GPa at a volume fraction of $\Phi = 0.2\%$.

The improvement of Young's modulus that may be achieved at a certain filler content and aspect ratio strongly depends on the modulus of the matrix (**Figure 8**). As a function of aspect ratio, the relative improvement of the young's modulus for all matrices approaches a plateau. The softer the matrix, however, the larger the aspect ratio must be to achieve the maximum stiffness and vice versa. For instance, for a stiff PMMA matrix incorporation of filler with aspect ratios of 300 is fully sufficient to achieve maximum reinforcement.

In reality, complete stress transfer may not be achieved due to suboptimal interfacial adhesion between the dispersed phase and the polymer matrix [34,35]. As the interfacial region increases in nanocomposites, this issue might become crucial factor for the material properties (see **Chapter 2.2**).

1.5.3. Dispersing methods and efficiency

The uniform dispersion of nanofillers in the polymer matrices is a general prerequisite for achieving desired mechanical and physical characteristics [30]. Dispersing of fillers within the polymeric matrices has been attempted using different techniques. In the following a short description of the three main methods is given for preparation of PLSNs material:

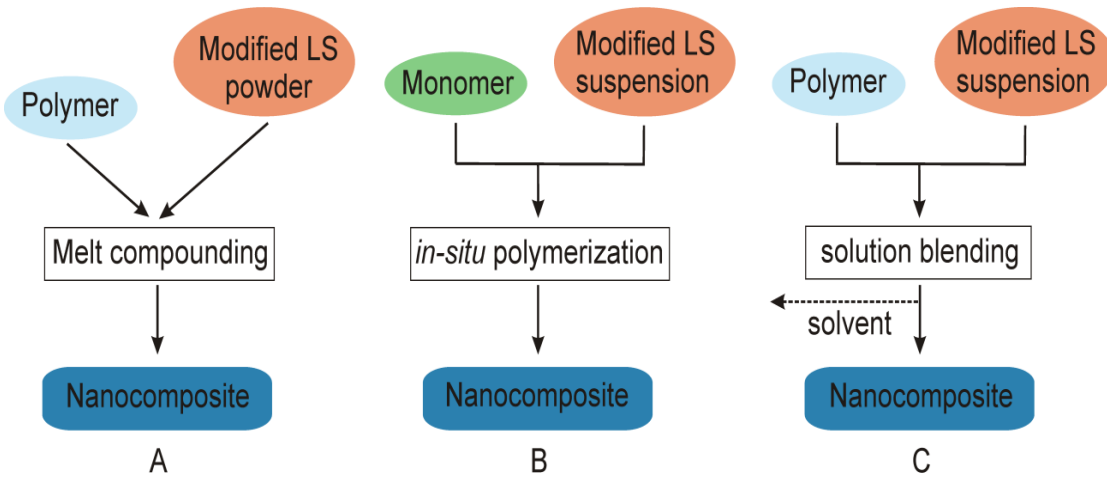


Figure 9. A schematic representation of dispersing methods for preparation of polymer layered silicates nanocomposites by a) melt compounding, b) *in-situ* polymerization, and c) solution blending.

1. Melt compounding

Melt processing is, as the name suggests, simply based on the thorough mechanical mixing of LS with the molten state of the polymer matrix in either static or flow conditions and subsequent cooling (**Figure 9a**). Melt compounding is the most convenient, economical and therefore appealing technique for industry. The dispersibility of LS in the matrix is dependent on certain factors including the polymer type, filler characteristics and the processing parameters. However, processing of commercial organoclay via melt compounding fails to delaminate tactoids, which reduces the maximal possible aspect ratio and therefore the desired final properties of PLSN [36] (**Chapter 2.3**).

II. In situ polymerization

The *in-situ* polymerization approach was first developed by Toyota's CRDL for preparation of Nylon 6–MMT nanocomposites from ϵ -Caprolactam monomer. This technique was found to be effective to disperse LS on a nanometer level in the matrix (**Figure 9b**). Polymerization of a monomer occurs in the swollen interlayer space of LS within the liquid monomer resulting in an expanded interlayer distance which additionally lead to complete delamination [37,38].

III. Solution blending

This approach is similar to the *in-situ* polymerization method except that the role of the monomer solution is replaced by polar solvent. The modified clay and the polymer are both suspended in a common solvent which allows efficient mixing (**Figure 9c**). Upon evaporation well dispersed nanocomposites are obtained (**Chapter 2.4**). Although, this strategy can provide an excellent dispersion of LS in the matrix, the large amount of solvent required is a major disadvantage from environmental and economical aspects.

Closely related to solution blending are cases where organoclays are dispersed in liquid, low viscous pre-polymers. For instance, epoxy resin clay nanocomposites may be obtained by mixing the filler into epoxy resin which is then cured by amine-catalyzed cross-linking [39].

1.6. Aims and addressed problems

Cutting-edge PLSN will only be available if various remaining fundamental challenges can be met. To start with, nanofiller of natural origin i.e. MMT, suffer from major drawbacks and limitations. These include small particle sizes inherent to the genesis of these materials which limit their aspect ratios ≤ 300 even after complete delamination. Genesis, moreover, takes place at low temperatures and consequently isomorphous substitution occurs in segregated patterns. Consequently, the charge density is heterogeneous which in turn leads to nonuniform interlamellar reactivity and surface chemistry.

Synthetic LS, such as synthetic Na-fluorohectorite prepared via a melt synthesis by a melt synthesis at temperatures >1000 °C overcome these limitations and open new opportunities for PLSN of a new generation. These material have extraordinary lateral extension (≥ 20 μm , **Figure 10**) and can be produced in a 1 Kg scale [21,40]. Furthermore, it is characterized by a uniform interlamellar reactivity and superb charge homogeneity.

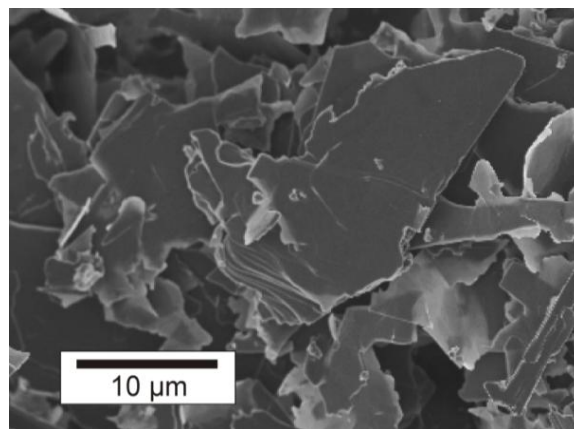


Figure 10. Scanning electron micrograph of a pristine synthetic Na-fluorohectorite showing huge lateral extension ($L \geq 20$ μm).

As already pointed out, with fixed filler content, the performance of nanocomposites may be optimized by tuning four crucial factors regarding the clay nanofiller: maximized aspect ratio (α), excellent mechanical properties (i.e., stiffness state), smart interface management, and finally an optimum dispersion in the matrix. In the course of this study, optimization of the aforementioned four critical factors of the nanofiller was carried out and the impact on the mechanical properties of the prepared PMMA/clay nanocomposites was investigated.

2

2. Synopsis

The presented dissertation consists of four publications that put the main focus on the different aspects that influence the mechanical properties of nanocomposites as discussed in the aims and addressed problems.

A graphical abstract of the workflow and the particular focus of the papers including main investigations and aspects are given in **Figure 11**:

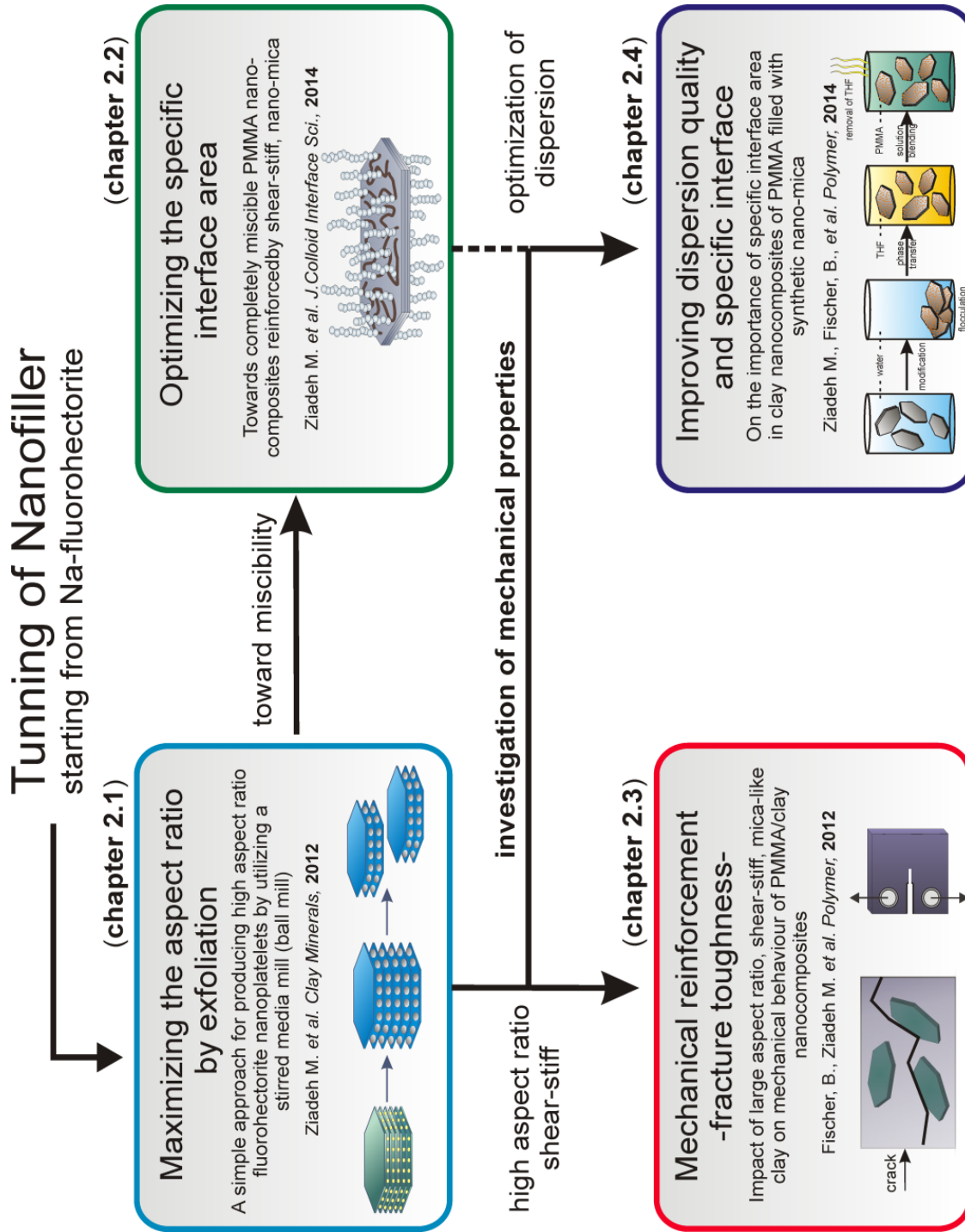


Figure 11. A schematic overview of the workflow and the particular focus of the publications.

2.1. Maximizing the aspect ratio

As previously pointed out, the synthetic Na-fluorohectorite was prepared via melt synthesis in an open system and has the following chemical formula: $\text{Na}_{0.5}[\text{Mg}_{2.5}\text{Li}_{0.5}]\text{Si}_4\text{O}_{10}\text{F}_2$ (layer charge 0.5) This synthetic LS is characterized by huge lateral extension (L) ($\geq 20 \mu\text{m}$) and a superb homogenous layer charge density and thus a uniform interlamellar reactivity. However, due to the nature of the crystal growth, the large thickness of the tactoids, the aspect ratio ($\alpha=L/h$) of the pristine material is limited to < 100 . For this reason a suitable and facile method able of shearing these tactoids and thus reducing their thickness without any significant breakage is of a great importance.

As already shown by Möller, M., et al. the interlamellar reactivity can be mainly attributed to the reactivity of the interlayer cations [13]. Therefore, by hydration of the interlayer cation (swelling), the basal spacing can be increased and concomitantly the cohesion between the lamella in the tactoids is decreased (Coulomb forces $F \sim 1/d^2$). In order to obtain a highly hydrated state, the interlayer Na^+ cations were exchanged with Mg^{2+} cations which have a higher enthalpy of hydration. This exchange increased the interlayer distance $d(001)$ from ~ 15 to $\sim 18 \text{ \AA}$, respectively yielding a highly 'shear-labile' material.

Exfoliation was done in this state using a wet milling technique in a stirred media mill *LabStar LS1* from Netzsch GmbH (Germany). The exfoliation process was achieved through the induced shear forces generated inside the milling chamber. The tactoids were subjected to the shear forces between the grinding media and/or between the slurry and the inner walls of the chamber. The specific energy was mainly affected by the solid content of the aqueous suspensions and was correlated with the degree of exfoliation. Furthermore, the stress energy generated by the grinding media was an important factor influencing the exfoliation process. Therefore, two different grinding media were employed to generate low and high stress energies.

Subsequent to the exfoliation in the stirred media mill the Mg^{2+} interlayer cations were exchanged with K^+ cations yielding a collapsed material with $d(001) = 9.9 \text{ \AA}$ (**Figure 12**). This material represents shear-stiff, mica-like nanofiller with no interlayer reactivity.

In this case the specific surface area (SSA) and the cation exchange capacity (CEC) were only attributed to the external basal surfaces.

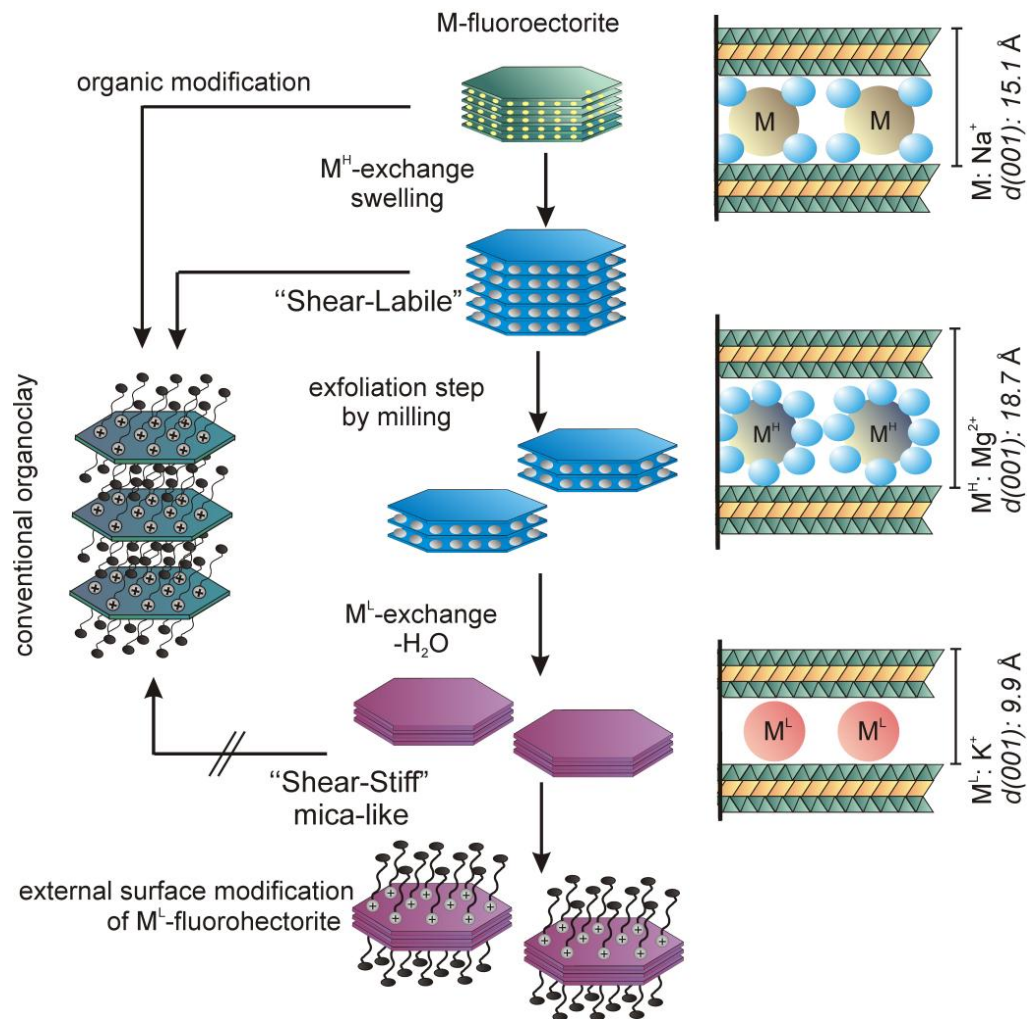


Figure 12. Tailoring of the hydration state in fluorohectorite where M , M^H , and M^L indicate interlayer cations with $|E_{\text{hyd}}|: M^L < M < M^H$.

The exfoliation efficiency was evaluated using various measurements including light scattering for of particle size distribution, specific surface area by the adsorption/desorption isotherms of N_2 , and powder X-ray diffraction. The aspect ratio was roughly estimated using a calculation model which correlates the tactoid thickness as determined by the Scherrer equation with the value of the total specific surface area. The milling parameters were systematically varied depending on the solid content of the suspension, grinding media diameter and time of milling (number of passages in the milling chamber).

Summary

- a) Highly hydrated shear-labile, Mg-fluorohectorite was obtained by exchanging the Na⁺ in the interlayer by Mg²⁺ cations.
- b) The shear-labile tactoids were exfoliated by shear forces generated in the milling chamber of a stirred media mill.
- c) Evaluation of the exfoliation efficiency was done by various means such as PXRD, BET, SLS and SEM micrographs.
- d) The wet milling approach was able to tune the average thickness of the tactoids by controlling the milling parameters.
- e) The reduction of the tactoid thickness by exfoliation produced nanoplatelets with a significantly high aspect ratio ($\alpha \sim 600$).
- f) Shear-stiff, mica-like nanoplatelets were obtained by exchanging the interlayer cations with K⁺ cations.

2.2. Optimizing the specific interface

Improving the adhesion between the nanofiller and the polymeric matrix is a key factor to achieve an effective stress transfer. In the course of the study a coating of the external basal surfaces of tailored high aspect ratio nano-mica (**Chapter 2.1**) with polymer brushes by a 'grating-from' technique was done. A polycationic macro-initiator (MI^{n+}) was designed and employed for modification of the nano-mica (**Figure 13**).

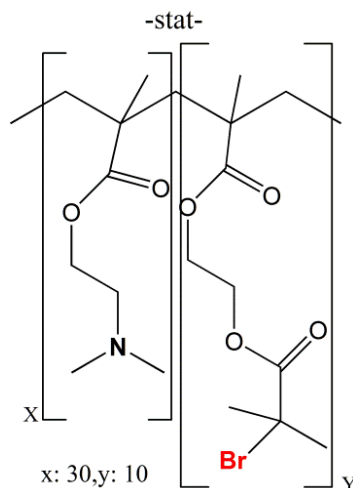


Figure 13. A statistical polycationic macro-initiator (MI^{n+}) used for modification of LS after protonation of the dimethylamine group in DMAEMA.

MI^{n+} consists of a statistical copolymer of DMAEMA and BIEM in a 3:1 ratio with an average degree of polymerization (DP) of 40 units. This polymeric modifier is unable to intercalate between the silicate layers and the cation exchange is restricted to outer basal surfaces. Moreover, the multiple electrostatic anchoring by ammonium groups incorporated in the backbone of MI^{n+} allow for a more reliable adhesion as compared to isolated mono-cations and at the same time the degree of protonation can be varied (charge density of MI^{n+}) to match the charge density of the clay surface. Furthermore, each MI^{n+} chain bears an average of ten potential initiator groups for a surface-initiated (SI)-ATRP, subsequently enabling a controlled grafting of polymeric brushes of poly(methyl methacrylate) (PMMA) from the surface of the modified nano-mica. (**Figure 14**).

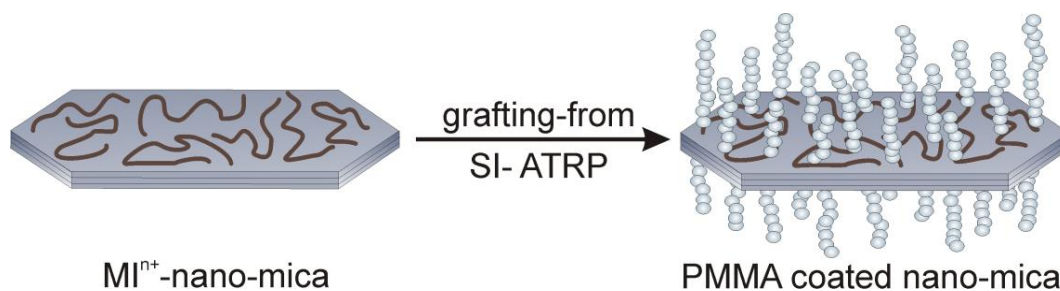


Figure 14. Selective surface modification of nano-mica by the MI^{n+} followed by a subsequent SI-ATRP to produce planar PMMA brushes.

Monitoring of the polymerization kinetics of PMMA was facilitated by analysis of free chains formed in solution using a sacrificial-initiator which has structural similarity to the incorporated BIEM in the MI^{n+} . This technique allowed the preparation of PMMA coated nano-mica with different chain lengths and narrow PDI. The obtained coated nanoplatelets were suspended in organic solvents and a vivid birefringence of a nematic phase was observed with the naked eye alongside a remarkable stability. This phenomenon cannot be observed for organoclays simply modified using only the macro-initiator.

Finally, PMMA nanocomposites with 5 wt% clay content were made by solution blending of two different nano-micas modified by MI^{n+} and PMMA brushes of length below and above the critical entanglement length of PMMA, respectively. Dispersion quality in the translucent nanocomposites was determined by transmission electron microscopy (TEM). The reinforcement effect on the produced PLSN was evaluated using stress-strain curves to obtain the tensile strength and Young's modulus. Although significantly improved mechanical properties could be achieved as compared to nanocomposites made with conventional clay fillers, the full potential, as expressed by Halpin-Tsai equations, of the PMMA coated nano-mica still cannot be realized. This is attributed to the non-wetting character of the densely packed PMMA brushes attached to planar nanoplatelets. In this line, no significant differences could be observed in respect to the length of the PMMA brush because the grafting density was too high to allow for entanglement and therefore no efficient stress transfer into the matrix.

Summary

- a) Altering the interlamellar reactivity enables tailoring of shear-stiff, nano-mica.
- b) Selective modification of the external basal surfaces of nano-mica was done using a polycationic macro-initiator (MI^{n+}).
- c) The protonation degree of MI^{n+} was tuned to match the charge densities of the LS surface.
- d) SI-ATRP of MMA from the modified surfaces produced chains with a narrow PDI and controlled molecular weight.
- e) The PMMA coated nano-micas yielded long-term stable suspensions in THF that showed a vivid birefringence of a nematic phase.
- f) Significantly improved mechanical properties could be achieved as compared to PLSN made with conventional clay fillers.
- g) The non-wetting character of the densely packed PMMA brushes to planar surfaces restricted the stress transfer into the matrix.

2.3. Reinforcement and fracture toughness

The performance of high aspect ratio shear-stiff, mica-like nanoplatelets and conventional nanofiller in respect to mechanical reinforcement of PLSN was compared. The controlled exfoliation process of thick tactoids by the wet milling allowed tuning of high aspect ratio nanoplatelets with an estimated $\alpha \sim 600$ (**Chapter 2.1**). Moreover, altering the interlamellar reactivity led to a unique shear-stiff, mica-like material. To emphasize on the importance of the aspect ratio, a pristine material with low aspect ratio ($\alpha \sim 50$) was used for comparison. A surface modification of the hydrophilic nanoplatelets with a polycationic macro-initiator renders it hydrophobic to improve compatibility with the PMMA matrix. As previously discussed in **Chapter 2.2**, the employed micro-initiator allows for a selective surface modification of external basal surfaces of the mica-like material without any intercalation.

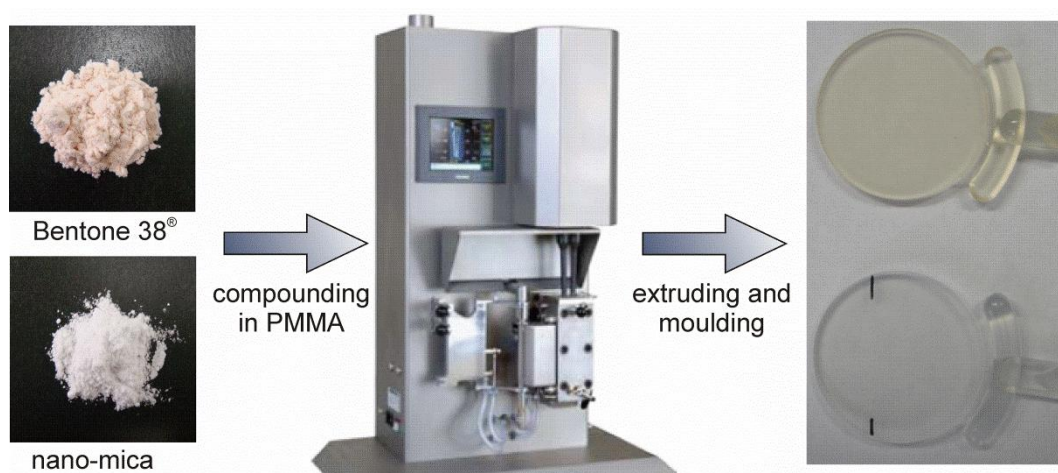


Figure 15. Preparation of PMMA/clay nanocomposites, the different nanofillers (freeze-dried) were dispersed in a PMMA matrix by a melt compounding technique using a twin-screw microcompounder and mould injected into required testing specimen.

The modified nanoplatelets were freeze-dried and dispersed into a PMMA matrix with conventional melt compounding technique using a twin-screw microcompounder (**Figure 15**). A series of PMMA/clay nanocomposites (1,2 and 4 wt.-%) were prepared and mechanically characterized by tensile testing and fracture toughness (K_{Ic}). The results were compared to conventional nanocomposites

prepared using commercial organoclay (Bentone 38®) with low aspect ratio ($\alpha \sim 50$)¹.

Using high aspect ratio mica-like material, most notable the fracture toughness could be increased by 66% at 4 wt.-% loading. For the first time for a nanocomposite such an improvement of fracture toughness could be achieved without sacrificing tensile strength (**Figure 16**). The filler promoted a number of toughening mechanism in the nanocomposite as probed by scanning electron microscopy (SEM) of the corresponding fracture surfaces.

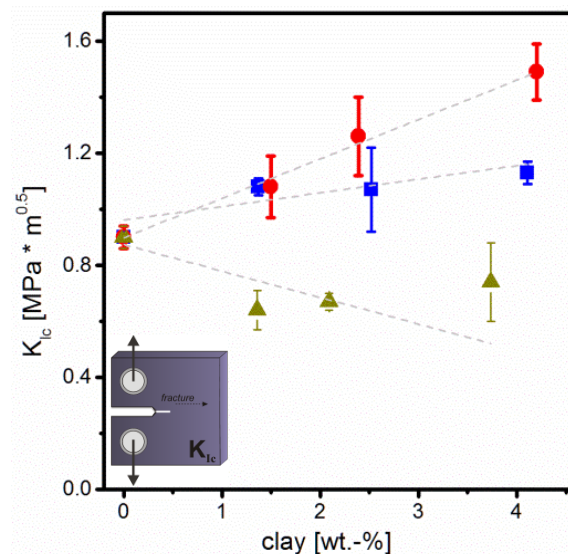


Figure 16. Effect of clay amount on fracture toughness (K_{Ic}) of PMMA/clay nanocomposites (\blacktriangle) Bentone ($\alpha \sim 50$), (\blacksquare) O-hect ($\alpha \sim 50$) and (\bullet) O-hect ($\alpha \sim 600$).

The large nanoplatelets varied the local stress state in the matrix and promoted additional energy dissipating mechanisms such as crack deflection, crack pinning and debonding effects with platelets pull-out.

It is noteworthy to mention, that the conventional MMT led to an increase in modulus on the expenses of reduced strength and fracture toughness as expected.

1. Bentone 38® is a trade mark for a commercial organic derivate of hectorite clay supplied by Elementis Specialties. The cation exchange is complete of the external and internal surface with various alkyl-ammonium chains (C14-C18). The organic content was determined by TGA to be ~ 38 wt.-%

Summary

- a) High aspect ratio nanofiller ($\alpha \sim 600$) was prepared by exfoliation of thick tactoids ($\alpha \sim 50$) in a stirred media mill (Chapter 2.1).
- b) Shear-stiff, mica-like nanoplatelets with no interlayer reactivity allowed a selective modification restricted to the external basal surfaces.
- c) The influence of different clay content (1–4 wt.-%) on mechanical properties of PMMA/clay nanocomposites was studied for two aspect ratios ($\alpha \sim 50$ and $\alpha \sim 600$) and was compared to natural MMT (Bentone 38).
- d) The high aspect ratio mica-like-filled nanocomposites offered improved toughness and stiffness without promoting any embrittlement.
- e) The first report showing different occurring toughening mechanisms in nanocomposites leading to an increase in fracture toughness by 66% at 4wt.-%.

2.4. Dispersion quality and the specific interface

An appropriate dispersion of the nanofiller in the polymeric matrix is a key factor for maximizing the specific interface area. While melt compounding was found to provide a decent dispersion on a macroscopic level (**Chapter 2.3**), on a microscopic level some smaller aggregates were detected. This suggested that the specific interface area could not be maximized. Achieving a perfect dispersion for such huge nanoplatelets by conventional melt compounding proved to be impossible.

Selective modification of shear-stiff, mica-like material with a macro initiator altered their inherited hydrophilic nature to hydrophobic allowing a good dispersion in organic solvents (**Chapter 2.2**). Upon complete removal of solvent, the high aspect ratio nanoplatelets are arranged in band-like structured aggregates. Therefore, solution blending was chosen as a processing method which strictly avoids powdered samples in order to fully exploit the potentials of such high aspect ratio nanofiller (**Figure 17**).

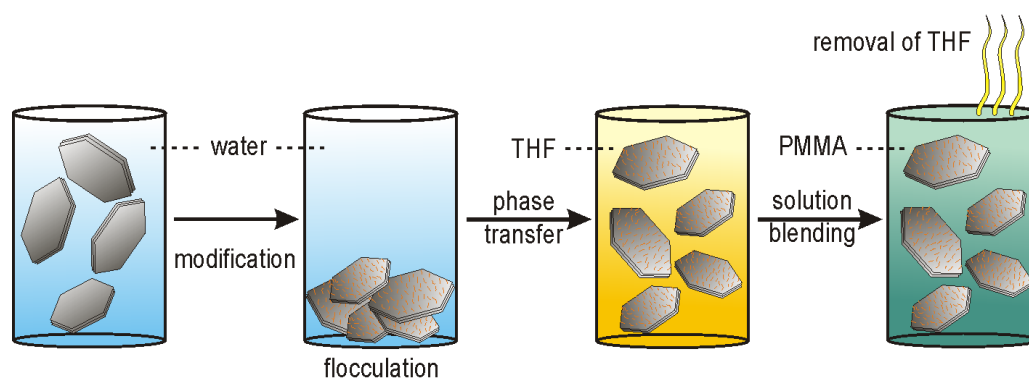


Figure 17. A schematic representation towards preparation of PMMA/clay nanocomposites ‘masterbatch’ via solution blending technique.

A much improved dispersion quality was achieved with almost perfectly dispersed clay tactoids as indicated by both computer micro-tomography (μ -CT) and transmission electron microscopy (TEM). Moreover, gas barrier measurements served as an additional independent indication to probe the dispersion quality. Improved dispersion in nanocomposites reduced the oxygen permeation as much as 60% compared to only 30% for nanocomposites having a mediocre dispersion as achieved by melt compounding.

Furthermore, mechanical properties were characterized by tensile testing and fracture toughness (K_{Ic}) measurements and were correlated with the improved morphology to establish structure-property relationships.

Significantly higher stiffness was obtained without any embrittlement of the nanocomposites for the nano-mica-filled composites. A maximum increase in fracture toughness of 63% was achieved at only 0.8 vol.-% while achieving a similar value with inferior melt compounding needed 1.85 vol.-%. No further increase in fracture toughness with increasing clay content was observed due to an increased restriction in plastic deformation as indicated by a reduced elongation at break. The property improvements observed with solution blending highlight the importance of the dispersion quality. To exploit the full potential of superior nanofillers, dispersion must be optimized since improvements in filler properties can easily be counterpoised by a mediocre dispersion quality.

Summary

- a) Solution blending was carried out in order to overcome the limitations of melt compounding to disperse large nanoplatelets.
- b) Optimally dispersed clay tactoids in the PMMA matrix was achieved as indicated by μ -CT and TEM micrographs.
- c) Gas barrier measurements served as indirect sensitive probe the dispersion quality. A much improved dispersion reduced the oxygen permeation by 60% at 1.6 vol.-% content.
- d) Fracture toughness was increased by 63% at only 0.8 vol.-% content.
- e) The results underline the importance of dispersion quality to exploit the full potential of the nanofiller.

3

3. References

1. Annabi-Bergaya, F. Layered clay minerals. Basic research and innovative composite applications. *Microporous and Mesoporous Mater.* **2008**, *107*, 141-148.
2. Schadler, L. S. Polymer-Based and Polymer-Filled Nanocomposites. *Nanocomposite Science and Technology*; Wiley-VCH Verlag GmbH & Co. KGaA: **2003**; pp 77-153.
3. Thostenson, E. T.; Li, C.; Chou, T. W. Nanocomposites in context. *Compos. Sci. Technol.* **2005**, *65*, 491-516.
4. Paul, D. R.; Robeson, L. M. Polymer nanotechnology: Nanocomposites. *Polymer.* **2008**, *49*, 3187-3204.
5. Coleman, J. N.; Khan, U.; Blau, W. J.; Gun'ko, Y. K. Small but strong: A review of the mechanical properties of carbon nanotube-polymer composites. *Carbon.* **2006**, *44*, 1624-1652.
6. Shipp, D. A. Polymer-layered silicate nanocomposites. *Comprehensive Nanoscience and Technology*; Editors-in-Chief:-David, L. A.; Gregory, D. S.; Gary, P. W., Eds.; Academic Press: Amsterdam, **2011**; pp 265-276.
7. Fu, S. Y.; Feng, X. Q.; Lauke, B.; Mai, Y. W. Effects of particle size, particle/matrix interface adhesion and particle loading on mechanical properties of particulate-polymer composites. *Composites Part B.* **2008**, *39*, 933-961.
8. Schütz, M. R.; Schedl, A. E.; Wagner, F. E.; Breu, J. Complexing agent assisted synthesis of high aspect ratio Fe³⁺/Mg²⁺ layered double hydroxides. *Appl. Clay Sci.* **2011**, *54*, 281-286.
9. Troutier-Thuilliez, A. L.; Hintze-Bruening, H.; Taviot-Gueho, C.; Verney, V.; Leroux, F. Exfoliation and liquid crystal phase formation of layered double hydroxide into waterborne polyurethane coatings. *Soft Matter.* **2011**, *7*, 4242-4251.
10. Yoonessi, M.; Scheiman, D. A.; Dittler, M.; Peck, J. A.; Ilavsky, J.; Gaier, J. R.; Meador, M. A. High-temperature multifunctional magnetoactive nickel graphene polyimide nanocomposites. *Polymer.* **2013**, *54*, 2776-2784.
11. Zhang, X.; Fan, X.; Li, H.; Yan, C. Facile preparation route for graphene oxide reinforced polyamide 6 composites via in situ anionic ring-opening polymerization. *J. Mater. Chem.* **2012**, *22*, 24081-24091.

12. Fischer, B.; Ziadeh, M.; Pfaff, A.; Breu, J.; Altstädt, V. Impact of large aspect ratio, shear-stiff, mica-like clay on mechanical behaviour of PMMA/clay nanocomposites. *Polymer*. **2012**, *53*, 3230-3237.
13. Möller, M. W.; Handge, U. A.; Kunz, D. A.; Lunkenbein, T.; Altstädt, V.; Breu, J. Tailoring Shear-Stiff, Mica-like Nanoplatelets. *ACS Nano*. **2010**, *4*, 717-724.
14. Kunz, D. A.; Schmid, J.; Feicht, P.; Erath, J.; Fery, A.; Breu, J. Clay-Based Nanocomposite Coating for Flexible Optoelectronics Applying Commercial Polymers. *ACS Nano*. **2013**, *7*, 4275-4280.
15. Möller, M. W.; Kunz, D. A.; Lunkenbein, T.; Sommer, S.; Nennemann, A.; Breu, J. UV-Cured, Flexible, and Transparent Nanocomposite Coating with Remarkable Oxygen Barrier. *Adv. Mater.* **2012**, *24*, 2142-2147.
16. Schütz, M. R.; Kalo, H.; Lunkenbein, T.; Breu, J.; Wilkie, C. A. Intumescent-like behavior of polystyrene synthetic clay nanocomposites. *Polymer*. **2011**, *52*, 3288-3294.
17. Schütz, M. R.; Kalo, H.; Lunkenbein, T.; Groschel, A. H.; Müller, A. H. E.; Wilkie, C. A.; Breu, J. Shear stiff, surface modified, mica-like nanoplatelets: a novel filler for polymer nanocomposites. *J. Mater. Chem.* **2011**, *21*, 12110-12116.
18. Götter, L. A.; Lee, K. Y.; Thakkar, H. Layered silicate reinforced polymer nanocomposites: Development and applications. *Polymer Rev.* **2007**, *47*, 291-317.
19. Laird, D. A. Influence of layer charge on swelling of smectites. *Appl. Clay Sci.* **2006**, *34*, 74-87.
20. Kalo, H.; Milius, W.; Breu, J. Single crystal structure refinement of one- and two-layer hydrates of sodium fluorohectorite. *RSC Adv.* **2012**, *2*, 8452-8459.
21. Breu, J.; Seidl, W.; Senker, J. Synthesis of threedimensionally ordered intercalation compounds of hectorite. *Z. Anorg. Allg. Chem.* **2004**, *630*, 80-90.
22. Brigatti, M. F.; Galán, E.; Theng, B. K. G. Chapter 2 - Structure and Mineralogy of Clay Minerals. *Handbook of Clay Science Fundamentals*; Bergaya, F.; Lagaly, G., Eds.; Elsevier: **2013**; pp 21-81.
23. Bergaya, F.; Lagaly, G. Chapter 1 - General Introduction: Clays, Clay Minerals, and Clay Science. *Handbook of Clay Science Fundamentals*; Bergaya, F.; Lagaly, G., Eds.; Elsevier: **2013**; pp 1-19.
24. Prado, L. A. S.; Karthikeyan, C. S.; Schulte, K.; Nunes, S. P.; de Torriani, I. L. Organic modification of layered silicates: structural and thermal characterizations. *J. Non-Cryst. Solids.* **2005**, *351*, 970-975.
25. Ke, Y. C.; Stroeve, P. Chapter 2 - Modification and Dispersion of Silicate and Silica. *Polymer-Layered Silicate and Silica Nanocomposites*; Elsevier Science: Amsterdam, **2005**; pp 69-118.
26. Brune, D. A.; Bicerano, J. Micromechanics of nanocomposites: comparison of tensile and compressive elastic moduli, and prediction of effects of

- incomplete exfoliation and imperfect alignment on modulus. *Polymer*. **2002**, *43*, 369-387.
27. Kojima, Y.; Usuki, A.; Kawasumi, M.; Okada, A.; Kurauchi, T.; Kamigaito, O. Synthesis of nylon 6-clay hybrid by montmorillonite intercalated with ε-caprolactam. *J. Polym. Sci. A Polym. Chem.* **1993**, *31*, 983-986.
 28. Usuki, A.; Kojima, Y.; Kawasumi, M.; Okada, A.; Fukushima, Y.; Kurauchi, T.; Kamigaito, O. Synthesis of Nylon 6-Clay Hybrid. *J. Mater. Res.* **1993**, *8*, 1179-1184.
 29. Van Krevelen, D. W.; Te Nijenhuis, K. Chapter 13 - Mechanical Properties of Solid Polymers. *Properties of Polymers (Fourth Edition)*; Elsevier: Amsterdam, **2009**; pp 383-503.
 30. Vaia, R. A.; Wagner, H. D. Framework for nanocomposites. *Mater. Today*. **2004**, *7*, 32-37.
 31. Fornes, T. D.; Paul, D. R. Modeling properties of nylon 6/clay nanocomposites using composite theories. *Polymer*. **2003**, *44*, 4993-5013.
 32. Halpin, J. C.; Kardos, J. L. Halpin-Tsai Equations - Review. *Polym. Eng. Sci.* **1976**, *16*, 344-352.
 33. Wu, Y. P.; Jia, Q. X.; Yu, D. S.; Zhang, L. Q. Modeling Young's modulus of rubber-clay nanocomposites using composite theories. *Polymer Testing*. **2004**, *23*, 903-909.
 34. Gay, C. Wetting of a polymer brush by a chemically identical polymer melt. *Macromolecules*. **1997**, *30*, 5939-5943.
 35. Zheng, X.; Sauer, B. B.; Van Alsten, J. G.; Schwarz, S. A.; Rafailovich, M. H.; Sokolov, J.; Rubinstein, M. Reptation Dynamics of a Polymer Melt near an Attractive Solid Interface. *Phys. Rev. Lett.* **1995**, *74*, 407-410.
 36. Sheng, N.; Boyce, M. C.; Parks, D. M.; Rutledge, G. C.; Abes, J. I.; Cohen, R. E. Multiscale micromechanical modeling of polymer/clay nanocomposites and the effective clay particle. *Polymer*. **2004**, *45*, 487-506.
 37. Zhao, H.; Argoti, S. D.; Farrell, B. P.; Shipp, D. A. Polymer-silicate nanocomposites produced by in situ atom transfer radical polymerization. *J. Polym. Sci. A Polym. Chem.* **2004**, *42*, 916-924.
 38. Yan, D.; Xie, T.; Yang, G. In situ synthesis of polyamide 6/MWNTs nanocomposites by anionic ring opening polymerization. *J. Appl. Polym. Sci.* **2009**, *111*, 1278-1285.
 39. Triantafyllidis, K. S.; LeBaron, P. C.; Park, I.; Pinnavaia, T. J. Epoxy-Clay Fabric Film Composites with Unprecedented Oxygen-Barrier Properties. *Chem. Mater.* **2006**, *18*, 4393-4398.
 40. Kalo, H.; Möller, M. W.; Ziadeh, M.; Dolejs, D.; Brey, J. Large scale melt synthesis in an open crucible of Na-fluorohectorite with superb charge homogeneity and particle size. *Appl. Clay Sci.* **2010**, *48*, 39-45.

4

4. Publications

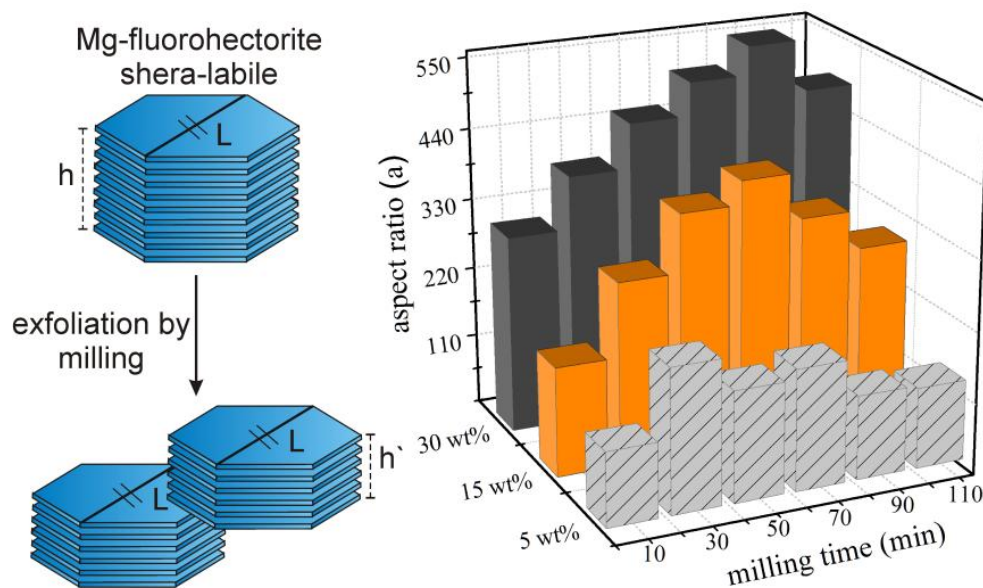
This chapter contains the four publications as follow:

- 4.1. A simple approach for producing high aspect ratio fluorohectorite nanoplatelets by utilizing a stirred media mill (ball mill).
- 4.2. Towards completely miscible PMMA nanocomposites reinforced by shear-stiff, nano-mica.
- 4.3. Impact of large aspect ratio, shear-stiff, mica-like clay on mechanical behaviour of PMMA/clay nanocomposites.
- 4.4. On the importance of specific interface area in clay nanocomposites of PMMA filled with synthetic nano-mica.

4.1. A simple approach for producing high aspect ratio fluorohectorite nanoplatelets by utilizing a stirred media mill (ball mill)

Mazen Ziadeh^a, Bettina Chwalka^a, Hussein. Kalo^a, Michael R. Schütz^a, Josef Breu^{a}*

Published in: Clay Minerals (2012), 47 (3), 341-353



^aLehrstuhl für Anorganische Chemie I, Universität Bayreuth,
Universitätstr. 30,95447 Bayreuth

*Corresponding Author: josef.breu@uni-bayreuth.de (J. Breu)

Author's individual contributions:

My contribution to this publication was the investigation of a facile approach for exfoliation of thick layered silicates tactoids. Exfoliation was achieved by wet milling using aqueous Mg-fluorohectorite suspensions in a stirred media mill. I have done all the milling trails including the operation of the mill and variation of the milling parameters. This included the preparation of a series of solid content: 5, 15 and 30 wt.-% and employing two different grinding media to tune the stress intensity.

Evaluation of the degree of exfoliation was done using a number of characterization methods. I have done all the characterization techniques such as: PXRD, SLS and BET.

The synthetic Na-fluorohectorite for the experiments was prepared by *Hussien Kalo*. Both *Bettina Chwalka* and *Michael Schütz* contributed to the discussion of the results.

The academic writing was done mainly by me with the help of Prof. Dr. *Josef Breu* and the manuscript was published in a special issue of **Clay minerals** dedicated to EUROCLAY 2011 conference.

My contribution to this publication is 80%.

A Simple Approach for Producing High Aspect Ratio Fluorohectorite Nanoplatelets by Utilizing a Stirred Media Mill (Ball Mill)

Mazen Ziadeh, Bettina Chwalka, Hussien Kalo, Micheal. R. Schütz, Josef Breu*

Lehrstuhl für Anorganische Chemie I, Universität Bayreuth, 95440 Bayreuth, Germany

* E-mail: josef.breu@uni-bayreuth.de

(Received 31 December 2011; revised 29 March 2012; Editor: Enver Murad)

ABSTRACT

The potential of platy nanofillers like clays in polymer nanocomposites is mostly determined by their aspect ratio. The degree of improvements that may be achieved in respect to reinforcement, gas-barrier, and flame retardancy critically depends on aspect ratio. Thus, increasing the aspect ratio is highly desirable in order to explore the full potential of the clay filler. Mechanical shear stress as generated in the grinding chamber of a stirred media mill (ball mill) proved to induce an efficient exfoliation of highly hydrated and therefore 'shear-labile' synthetic Mg-fluorohectorite in aqueous dispersion. The attainable degree of exfoliation can be tuned and controlled through the shear forces applied by changing process parameters such as solid content and grinding media diameter.

Characterization and evaluation of the exfoliation efficiency during milling was achieved by combining and cross-validating data obtained by powder X-ray diffraction (PXRD), static light scattering (SLS), specific surface measurements applying the Brunauer-Emmett-Teller (BET) equation, and scanning electron microscopy (SEM) images. This led to the identification of optimal processing parameters allowing for controlling the degree of exfoliation and consequently the aspect ratio of the nanoplatelets. Not surprisingly, besides exfoliation, increasing the magnitude of the shear stress also resulted in some reduction in platelet size.

The clay platelets obtained showed a high average aspect ratio (>600) being several times greater than that of pristine synthetic fluorohectorite. The increase of aspect ratio was reflected in a significant enhancement of both, specific surface area and cation exchange capacity (CEC) of the external basal surfaces. This

method has substantial advantages as compared to microfluidizer processing in respect to feasibility, batch size, and particle diameter size preservation. The exfoliated nanoplatelets obtained by milling have great potential to improve mechanical properties of polymer layered silicate nanocomposites (PLSN).

Keywords: stirred media mill, aspect ratio, fluorohectorite, exfoliation.

1. INTRODUCTION

In comparison with neat polymer matrices, polymer layered silicate nanocomposites (PLSN's) exhibit and provide significant improvements at much lower filler volume fraction as compared to microfillers [Kumar et al., 2009; Schmidt et al., 2002]. These enhanced properties include thermal stability, flame retardancy, advanced mechanical response and reduced gas diffusion rates [Chevigny et al., 2011; Mittal, 2008; Möller et al., 2010b, Schütz et al., 2011; Zanetti et al., 2001]. The rapid development of these composite materials requires and demands a constant progress and enhancement of the properties of the employed layer silicates as nanofiller [Zartman et al., 2010]. The key factor to achieve significant improvement of the properties is the aspect ratio α of the filler material [Möller et al., 2010a; Tamura et al., 2008]. For nanocomposite materials, this ratio α is often expressed as the ratio of lateral extension L divided by height h :

$$\alpha = L/h \quad (1)$$

Decreasing the height of the tactoid while at the same time preserving the lateral platelet size (exfoliation as defined by Lagaly et al. [Gardolinski & Lagaly, 2005]) will increase the aspect ratio. The maximum aspect ratio will be achieved when the material is delaminated (as defined by Lagaly et al. [Gardolinski & Lagaly, 2005]) into singular 2:1 lamellae. We have previously reported [Kalo et al., 2010] a large-scale melt synthesis of swelling 2:1 synthetic Na-fluorohectorite clay with superb charge homogeneity and large lateral extension (median 20 μm).

Moreover, control of charge density interplaying with the charge homogeneity allowed for fine-tuning the intracrystalline reactivity of the synthetic fluorohectorite in a way that permitted switching between a highly swollen and 'shear-labile' state and a collapsed 'shear-stiff' state. Cations with high enthalpy of hydration such as Mg^{2+} (-1922 kJ mol⁻¹) give a highly hydrated state, while upon

exchanging the interlayer cations with K^+ (-322 kJ mol^{-1}) collapse into a non-swollen 'shear-stiff', mica-like material was induced with no intracrystalline reactivity. Please note that the intracrystalline reactivity differs significantly from natural K-clays because of both homogeneity of layer charge and a comparatively higher charge density. The PXRD patterns in Fig. 1 illustrate three different stages of hydration for the same clay depending on the interlayer cation (Na, Mg, and K, respectively). The highly hydrated state led to an increase in the basal spacing thus reducing the Coulomb forces between the positively charged interlamellar space and the negatively charged silicate lamellae. We have previously shown that 'shear-labile' state is favoured to achieve efficient exfoliation of the clay tactoids using a microfluidizer [Möller et al., 2010a].

However, the microfluidizer method has some drawbacks affecting the final product quality including; (i) the lateral extension of the processed clay nanoplatelets is limited by the diameter of the interaction channels, (ii) the maximum solid content of the dispersion that can be handled is low (1.5 wt%), which severely hampers up-scaling of the process and finally (iii) process parameters (e.g. pressure, diameter of interaction channel) are invariable and do not allow much of optimization. Ball milling (stirred media milling) has been recognized as an alternative method to produce very high shear stress and efficient particle size reduction is feasible [Kwade, 2003; Vodovic et al., 2010]. In the following, we investigate the efficiency of stirred media milling for improving the aspect ratio of synthetic fluorohectorites.

2. MATERIALS AND METHODS

2.1. Materials and chemicals

Na-fluorohectorite $Na_{0.5}[Mg_{2.5}Li_{0.5}]Si_4O_{10}F_2$ was prepared via melt synthesis as reported previously [Kalo et al., 2010]. The synthetic Na-fluorohectorite had a CEC of 110 meq./100g, as determined by the copper complex ($[Cu(\text{trien})]^{2+}$) method. The inorganic salts ($MgCl_2$, KCl) used for cation exchange were purchased from *Grüssing GmbH Analytika*, Germany.

Cation exchange was achieved by repeatedly treating the pristine Na-fluorohectorite with the corresponding salt followed by washing several times with deionized water until it was free from chloride ions and the $AgNO_3$ -test for Cl^-

was negative. Three different Mg-fluorohectorite dispersions with solid contents of 5, 15, and 30 wt% were prepared for the milling experiments. Following the exfoliation process in the stirred media mill, the Mg^{2+} ions were exchanged with K^+ ions which yielded a collapsed and non-swollen 'shear-stiff' mica-like material.

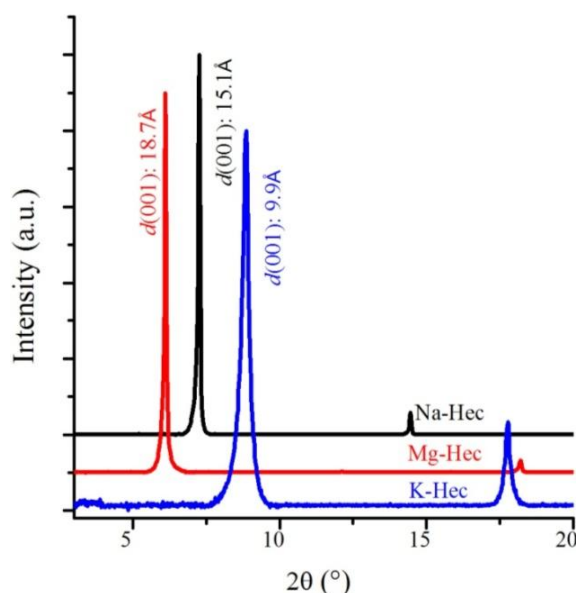


Fig 1. PXRD patterns of different stages of hydration of synthetic fluorohectorite (moist samples).

2.2. Grinding media

A high wear resistant commercial grinding media (GM) ZY premium type of yttrium stabilized Zirconia (ZrO_2), (SiLi beads, Germany) with two different diameters [$d_{GM1} = 0.6\text{-}0.8$ mm, and $d_{GM2} = 1.4\text{-}1.6$ mm] were used in the milling experiments. The grinding media had different bulk densities due to the production method [$\rho_{GM1} = 3.65$ kg/l, and $\rho_{GM2} = 3.77$ kg/l]. The exact roundness as well as the smooth and polished surface of beads contributed to the low wear rate, which meant nearly no contamination of the grinding product and therefore, the highest product qualities could be obtained. The filling ratio in the grinding chamber with grinding beads was fixed $\varphi_{GM} = 80\%$.

2.3. Milling set-up

A laboratory stirred media mill LabStar LS 1 (Netzsch, Germany) equipped with a geometric grinding system ZETA was used for the study. All milling experiments in aqueous dispersions were carried out in a three disc stirred media mill. The agitator with the perforated discs was installed on a horizontal driven shaft. The

grinding chamber was lined for wear protection reasons with silicon carbide/polyurethane. The grinding chamber was equipped with a double wall water jacket which is connected to an internal water cooling system to allow proper cooling during the milling. The dispersion was pumped using a hose pump from the stirring vessel into the grinding chamber, after passing through the chamber the dispersion was discharged through a sieve with a screen size of 0.2 mm which prevented grinding media from leaving the chamber. The dispersion then flowed back to the stirring vessel where samples were collected. The experimental set-up provided a circuit milling mode of the dispersion, a schematic diagram of the experimental set-up of the stirring media mill and the stirred vessel is shown in Fig. 2.

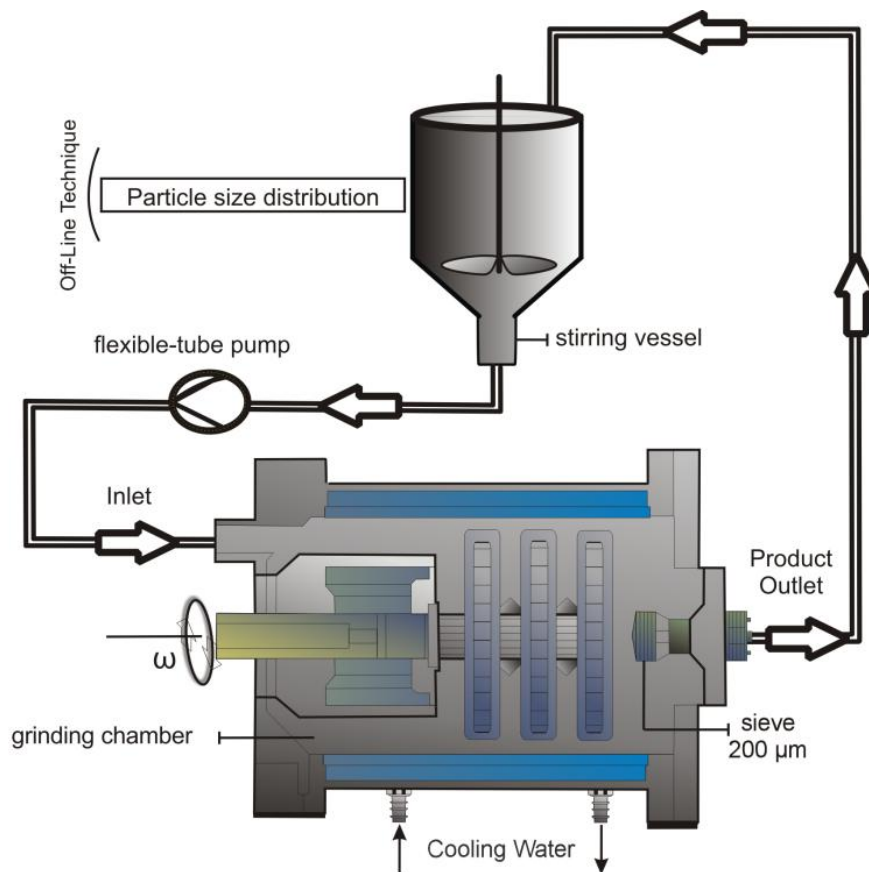


Fig 2. Schematic diagram of the stirred media mill LabStar LS1 connected with a stirring vessel for circuit milling operation.

The energy input was recorded during milling using an energy meter and the experimental grinding conditions and set-up are given in Table 1.

TABLE 1. Set of fixed and variable operating parameters in the stirred media mill

Diameter of grinding media	d_{GM1} : 1.4-1.6 mm / d_{GM2} : 0.6-0.8 mm
Density of grinding media	ρ_{GM1} : 3.773 kg/l. / ρ_{GM2} : 3.652 kg/l
Filling ratio of media in chamber	$\varphi=80$ %
Volume of grinding chamber	approx. 0.12 l
Volume of dispersion	approx. 0.3 l
Solid content of dispersions	5, 15 and 30 wt%
Flow rate of dispersion	12.4 cm ³ /s
Agitator velocity	2050 rpm ~ 6.43 m/s
Separating sieve screen size	200 μ m
Temperature	20 °C

2.4. Methods and instruments

The degree of exfoliation of Mg-fluorohectorite during the milling process was determined by PXRD. The PXRD patterns were obtained in reflection mode using nickel filtered Cu-K α radiation $\lambda = 1.54187$ Å on a Bragg-Brentano-geometry diffractometer (PANalytical Xpert-Pro) equipped with an X'Celerator Scientific RTMS detector. A divergence slit of 1/4 ° as well as a detector slit of 1/8 ° were used. Oriented samples were prepared by evaporation of aqueous suspensions of clay on flat glass slides (Menzel Gläser).

The specific surface areas of freeze-dried K-fluorohectorite samples were calculated using the BET equation from the adsorption/desorption isotherms. Measurements were carried out on a Quantachrome Nova 2000e analyzer. The specific surface area was determined using 5-points within the range of $0.09 < p/p_0 < 0.3$ using N₂ as adsorption gas. All samples were carefully degassed overnight at 150 °C under ultra high vacuum to remove adsorbed water prior to measurements.

CECs were determined by means of a photometric method applying a Varian Cary 3 UV-Vis spectrometer and [Cu(trien)]²⁺ as a dye. CuSO₄ (99.99+%) and triethylene tetramine (>97%, trien) were purchased from Sigma Aldrich. The preparation of the complex and the CEC measurements were performed according to procedures described in details in the literature [Ammann et al., 2005; Meier & Kahr, 1999].

For the determination of CEC values of the external surfaces, 200 mg of shear-stiff K-fluorohectorite (freeze dried) was weighed into 20 ml centrifuge tubes. In the copper complex method, 8 ml of the 0.01 M complex solution were added and the

sample was shaken for 10 min. The exchange occurs very quickly for the external basal planes. The samples were centrifuged and 3 ml of the supernatant were transferred into plastic cuvettes. The adsorption was measured using monochromatic light at 577 nm.

Particle size distribution measurement was implemented to investigate the changes in the platelets morphologies during the milling process. The particle size distributions curves were recorded from aqueous dispersions (~1% solid content) of the treated Mg-fluorohectorite on a Retsch Horiba LA-950 static light scattering (SLS) instrument. The calculation of the particle size distribution was performed according to the Mie scattering theory using the following refraction index (RI_{sample} : 1.590, RI_{water} : 1.333).

SEM images were obtained using a LEO 1530 FESEM (Carl Zeiss GmbH) with an acceleration voltage of 5 kV with EDX-detector from Thermo Electron. The fluorohectorite samples were freeze-dried before spreading them on the conductive sample holder and were sputtered with carbon. The prepared sample was dried for half an hour under dust free conditions prior to measurement.

3. RESULTS AND DISCUSSION

For ball milling the most 'shear-labile' Mg-fluorohectorite was used. Exchanging the interlayer Na^+ cations with Mg^{2+} which possess higher enthalpy of hydration resulted in an increase in the interlayer distance (d -spacing) from 15.1 Å to 18.7 Å (Fig. 3a). In the grinding chamber, the slurry composed of the aqueous dispersion of the clay and the grinding media, is subjected to shear forces generated due to the rotation of the agitator. The maximum shearing stress is produced when the fluid is squeezed out just before two balls or a ball and the chamber wall collide. Additional shear stress results from the rotation of the balls as shown in Fig. 3b. Alongside with exfoliation of the clay tactoids some breakage of the platelets will occur.

In order to be able to distinguish between internal (interlamellar) and external CEC, subsequent to milling, all samples were transformed to a mica-like material by exchanging with K^+ cations. The exchange led to a collapsed state with interlayer distance of 9.9 Å. Consequently, only the K^+ cations bound to the

external surfaces were available for further ion exchange [Möller et al., 2010a]. This helped us to selectively monitor the increase of just external basal surface in respect to different milling parameters. The milling parameters which mostly affect the shear stress ((i) clay content of dispersions and (ii) diameter of grinding media) were systematically varied and the degree of exfoliation which corresponds to the thickness of the nanoplatelets was investigated.

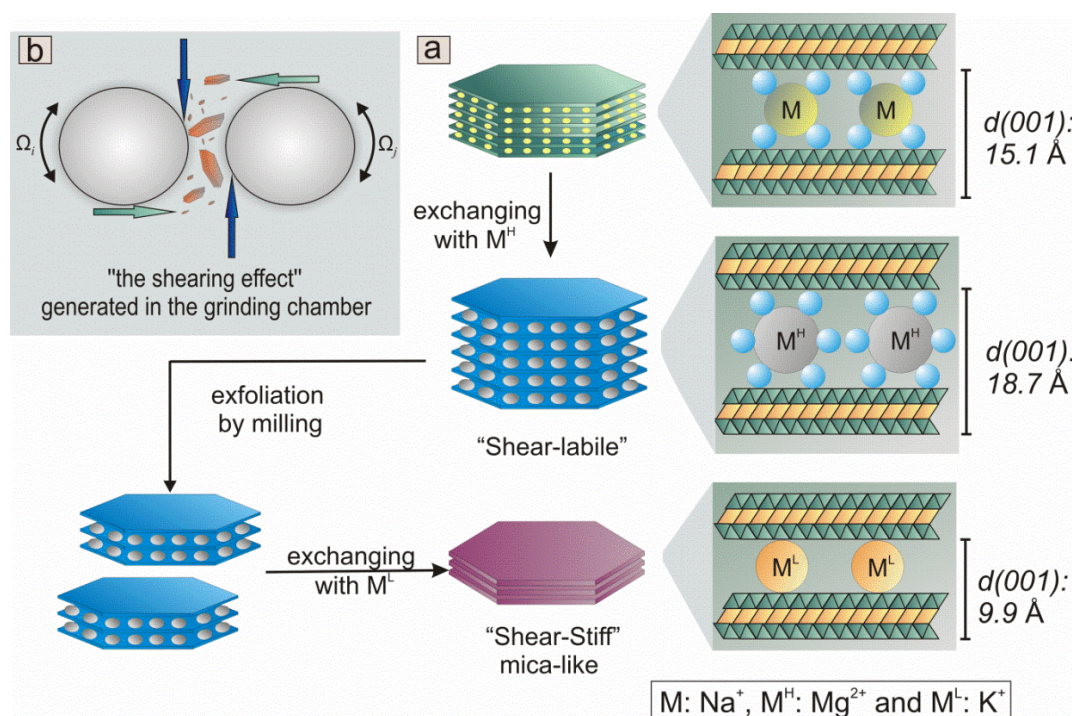


Fig 3. (a) Tuning of the hydration state in fluorohectorite where M, M^H, and M^L indicate interlayer cations with $|E_{\text{hyd}}|: M^L < M < M^H$. (b) Illustration of the shearing effect on the fluorohectorite platelets in the milling chamber.

X-ray diffraction was used as the primary tool to monitor exfoliation. The full width at half maximum (FWHM) of (001) reflections may be related to the average stack height of tactoids by applying the Scherrer equation [Burton et al., 2009; Scherrer, 1918]. We are aware that interstratification can also have a significant effect on the FWHM [Dennis et al., 2001]. However, we never saw any signs of interstratifications in our samples as would be indicated by irrationality of the basal reflection series. Therefore, we feel that the Scherrer equation is valid and allows for a, at least, semi-quantitative determination of the thickness of tactoids. Nevertheless, we prefer to compare experimentally observed FWHMs instead of derived absolute stack heights.

3.1. Effect of clay content on the exfoliation

Based on Kwade's stress model which describes the physical process in stirred media mills, there is a direct relation between the solid content of a dispersion and the specific energy [Kwade, 2003; Kwade & Schwedes, 20007]. Since the energy input ΔE is maintained constant during the milling process, the specific energy (E_s) depends directly on the solid content (m_p):

$$E_s = \frac{\Delta E}{m_p} \quad (2)$$

It becomes clear from equation (2) that lower solid content will produce higher specific energy during milling and therefore will affect the final product. In Fig. 4 we compare exfoliation efficiency through the evolution of the FWHM values of the (001) reflections for three different sets of Mg-fluorohectorite dispersions (5, 15 and 30 wt%) as a function of milling time.

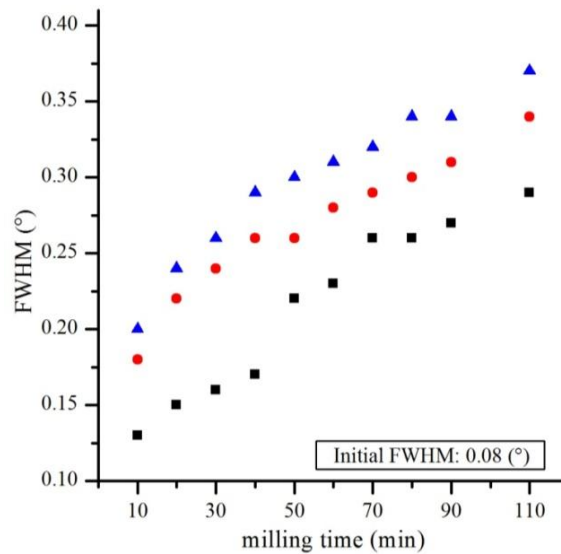


Fig 4. Influence of the solid content of three different Mg-fluorohectorite dispersions [(■) 5, (●) 15, (▲) 30 wt%] on the FWHM values under the same milling conditions.

For all three clay contents, the FWHM increase significantly with respect to milling time indicating efficient exfoliation. Higher clay contents resulted in significantly higher FWHM values as compared with lower clay content. In addition, the viscosity of the dispersions after treatment increased noticeably indicating that the number of independent (thinner) tactoids had increased during milling. It became evident that a higher degree of exfoliation can be achieved with higher clay content

of the dispersions. The changes in the particle sizes during the milling were monitored by SLS measurements. To a first approximation, the hydrodynamic radii determined from SLS can be well correlated and assigned to the lateral extension (L) [Bowen, 2002]. The results of median particle size (X_{50} and X_{90}) of dispersions of the three contents obtained at different milling times are presented in Fig. 5.

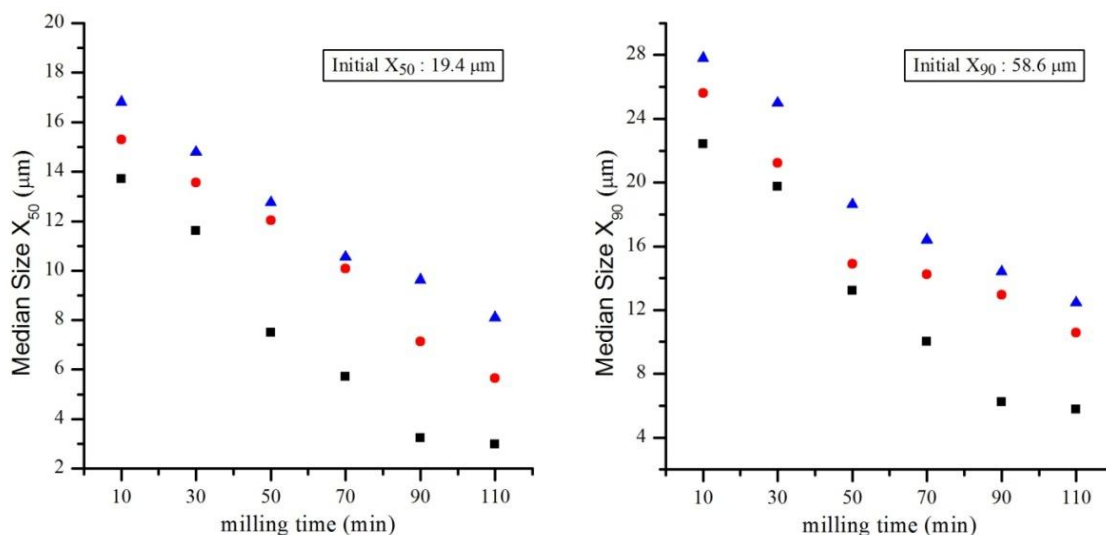


Fig 5. Median size (X_{50} and X_{90}) values obtained from SLS for three different Mg-fluorohectorite dispersions [(■) 5, (●) 15, (▲) 30 wt%] under the same milling conditions.

As synthesized, the Mg-fluorohectorite showed a broad particle size distribution after the synthesis ranging from 5 μm to 60 μm , and the initial X_{50} and X_{90} for the pristine Mg-fluorohectorite were 19.4 and 58.6 μm respectively. The size reduction upon milling starts levelling off after approximately 90 minutes and for the lowest solid content it even approaches a plateau. In the early process of milling, disaggregation is quickly achieved and consequently a rapid decrease in X_{90} was detected. Furthermore, comparing the three sets of different clay content revealed that more diluted dispersions led to smaller median size indicating that dilution favours breakage of tactoids which reduces the lateral extension as was previously also noted by [Inam et al. 2001].

Exfoliation by milling had transformed some interlamellar spaces into outer surfaces of increasingly thinner nanoplatelets. The total CEC of the synthetic Na-fluorohectorite was determined to be 110 meq. /100g. The total CEC is of course not affected by exfoliation. However, in the non-swollen K-fluorohectorite the

interlamellar space no longer contributes to the CEC. K-fluorohectorite therefore exhibits a lower CEC which was merely attributed to external basal planes of the tactoids which were still accessible. Increasing exfoliation will, however, produce more external surface and hence the CEC of external surfaces of K-fluorohectorite is expected to increase with the degree of exfoliation. Fig. 6. shows the CEC and the specific surface area values of freeze dried samples of exfoliated fluorohectorite platelets.

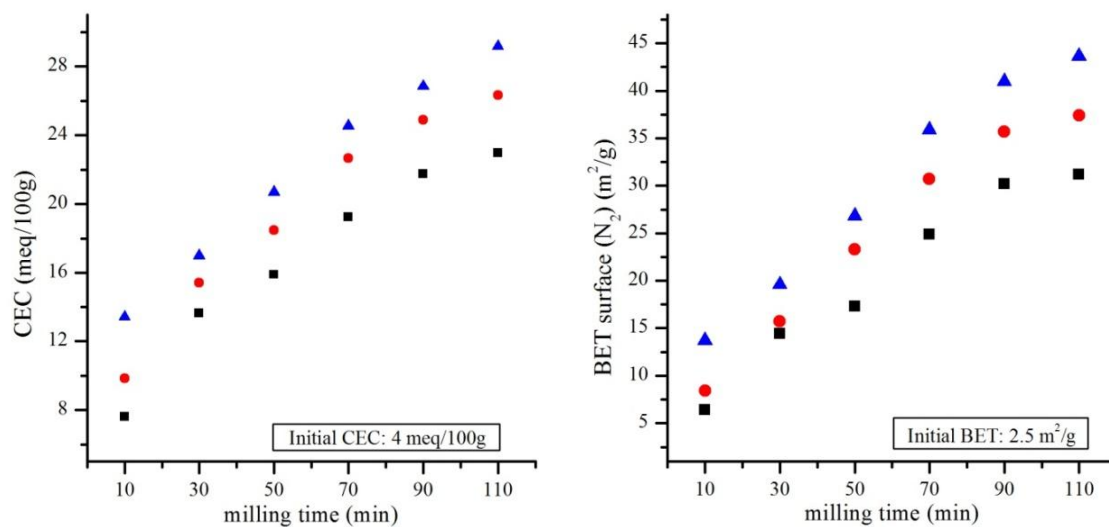


Fig 6. CEC values (left) of external surfaces and the corresponding BET values (right) for three sets of K-fluorohectorite with different solid content [(■), 5 (●), 15 (▲) 30 wt%].

A rather good correlation between CEC of external surfaces and specific surface area became obvious. This was somewhat surprising since on one hand breakage of platelets will produce additional edge surface which will contribute to the external surface area and on the other hand freeze drying might create band structures where some of the external surface is no longer available for N₂ adsorption. The observed good correlation of CEC of external surfaces would suggest that these two effects may be neglected. After 110 min. of milling the CEC of the external surfaces approached approximately a quarter of the total CEC suggesting that the average tactoid then consisted of 4 lamellae, for details of the derivation see (Möller et al., 2010a). Please note that due to the huge aspect ratio observed for the synthetic hectorites, the contribution of the edges to the CEC could be safely ignored although the relative contribution to the total surface area

increased during milling due to some breakage of platelets. High magnification SEM images provide a direct observation of individual exfoliated fluorohectorite tactoids. Fig. 7 shows the changes in the morphology of fluorohectorite platelets marked by a significant decrease in the tactoids thickness and a reduction of the platelet diameter in respect to the milling time.

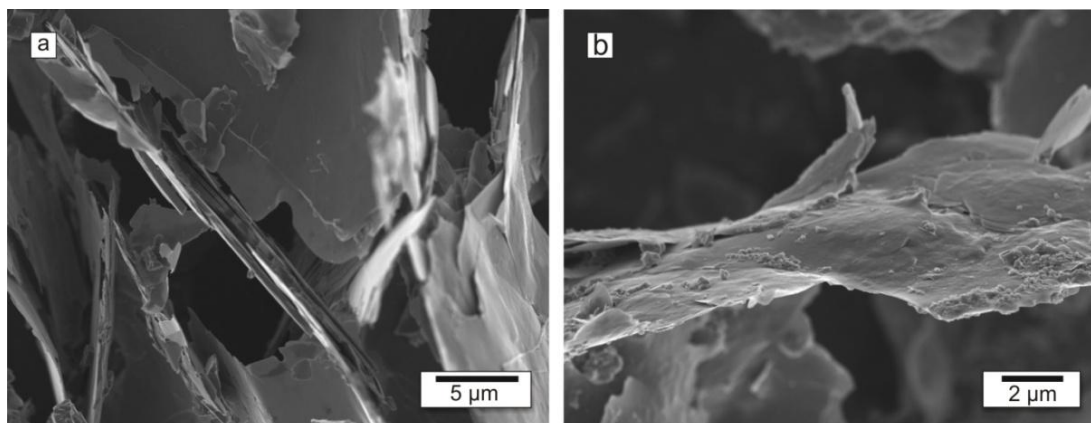


Fig 7. Representative SEM images of K-fluorohectorite before and after milling for 90 min (30 wt%).

In summary all experimental data consistently showed that exfoliation efficiency increases with the clay content of the dispersion. At the same time breakage of tactoids was least with the maximum clay content. The specific energy produced with higher concentration is far less than the energy produced with more diluted dispersions. In the grinding chamber the stress events subjected to one particle decreases with increasing the solid content. However, the probability that one particle or more are stressed between two grinding media is higher by increasing the solid content. Thus, the low specific energy apparently favoured desired exfoliation of the tactoids while detrimental breakage was minimized.

3.2. Estimation of average aspect ratios (α)

Determination of average aspect ratios would indeed require the concomitant measurement of both thickness and lateral extension of a statistical significant number of individual clay platelets. While AFM delivers height and extension of platelets concomitantly, measurement of large numbers is very time-consuming and thus impractical. Therefore, we have previously introduced a simple method that allows a rough estimate of average aspect ratios [Möller et al., 2010a]. The

method correlates the tactoid thickness as determined by the Scherrer equation with the value of the total specific surface area:

$$S_m = n_p \cdot O_p = \frac{2L \cdot \sqrt{3} + 8h}{\rho \cdot h \cdot L \cdot \sqrt{3}} \quad (3)$$

Where: S_m is the total specific surface area [m^2/g], n_p is the number of particles per gram, O_p denotes the surface area of a single hexagonal particle, L , h represent the diameter and height of tactoid in [nm] and finally ρ is the particle density and it was assumed to be 2.7 [g/cm^3]. The contribution of the edges to S_m is accounted for by assuming a uniform and ideal hexagonal morphology of the platelets. The median particle size diameter (X_{50}) is used as the lateral extension of this uniform hexagonal platelet. For details see the supporting information of Möller et al.. The specific surface area as determined by BET SSA includes contributions of quasi crystalline overlap regions [Rutherford et al., 1997]. The contributions most likely are small for the coarse grained starting material but might increase upon milling. These contributions were ignored in the derivation of the aspect ratios.

In Fig. 8. aspect ratios as estimated by applying equation (3) are compared. Again, the crucial influence of the clay content on the resulting aspect ratio becomes obvious. Moreover, while both exfoliation as indicated for instance by FWHM (Fig. 4) and breakage as indicated by particle size distribution (Fig. 5) showed no extrema, for the estimated aspect ratios maxima were observed as a function of milling time. The maximum is shifted to longer milling times with increasing clay contents of the dispersions. Interestingly, the largest aspect ratios that may be obtained increase with clay content too. Consequently, the maximum aspect ratio of all samples was observed for the highest clay content (30 wt%) after 90 min. of milling. An aspect ratio ten times higher than the pristine Na-fluorohectorite was achieved. Although SEM images might not be representative for the bulk sample, Fig. 7b where a platelet with an aspect ratio >1000 can be seen, would suggest that the real aspect ratios are even underestimated by equation (3). This might be explained by the fact that the averaged FWHM observed will overemphasize well ordered thicker platelets.

Unfortunately, the clay content cannot be increased beyond 30 wt% because the maximum value of pressure is already reached with this concentration.

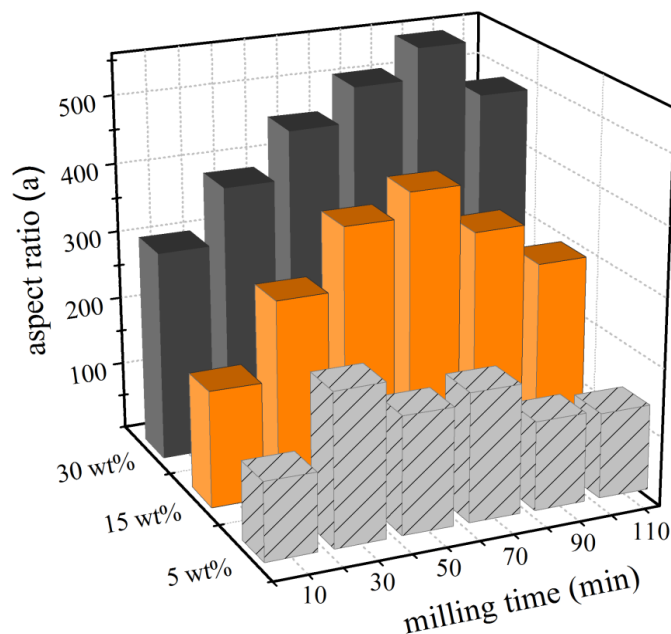


Fig 8. Evolution of estimated aspect ratios (α) values with milling time for dispersions of different clay contents (for pristine Na-fluorohectorite: $\alpha \sim 50$).

3.3. Effect of grinding media diameter on exfoliation

In addition to the influence of clay content of dispersions on the exfoliation efficiency, the effect of grinding media diameter on the final product was investigated. The optimum concentration, as identified in the previous section, of Mg-fluorohectorite dispersion (30 wt%) was used for the evaluation of two different grinding media diameters (1.4-1.6 and 0.6-0.8 mm) in respect to the degree of exfoliation. The stress energy generated by the grinding media is an important factor and is defined by the following equation:

$$Se = m_{GM} \cdot V_t^2 = d_{GM}^3 \cdot \rho_{GM} \cdot V_t^2 \quad (4)$$

Where; d_{GM} represent the diameter of the beads in [mm], ρ_{GM} represents the density of beads in [kg/m^3] and V_t is the velocity of the agitator given in [m/s].

The calculation of the stress energy for the two grinding media chosen shows, that the large grinding media GM_1 generate 10 times higher energy than the smaller GM_2 (0.527 and 0.051 Nm respectively) at a fixed agitator speed of 6.43 m s^{-1} or 2050 rpm. GM_1 has been used for all results presented in the first part where the effect of the solid content was studied. Fig. 9 shows the influence of two different grinding media diameter (GM_1 and GM_2) on the evolution of FWHM values with time.

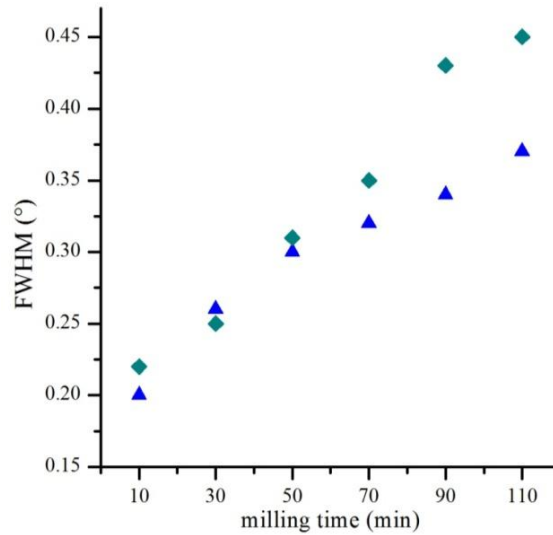


Fig 9. Influence of two different grinding media sizes, GM₁ and GM₂ [(▲) 1.4-1.6 mm, and (◆) 0.6-0.8 mm] on the evolution of FWHM values with milling time for a 30 wt% dispersion of Mg-fluorohectorite.

While the initial increase of FWHM values was similar for both ball sizes, at elongated milling times the smaller grinding media GM₂ exfoliated the synthetic clay more efficiently as indicated by the larger FWHM observed. The evolution of the particle size distributions with time also showed a crucial influence on the ball size (Fig. 10). Interestingly, on one hand using smaller grinding media led to a much narrower particle size distribution after milling as compared to the bigger grinding media GM₁ (Fig. 10).

On the other hand, the particle size dropped significantly quicker during early stages of milling with smaller grinding media (after 30 min.: $X_{50} = 14.8 \mu\text{m}$ and $X_{50} = 9.3 \mu\text{m}$ for GM₁ and GM₂, respectively). For the smaller grinding media, the particle size quickly approached a plateau already after 70 min. of milling, while for the larger grinding media anything up to 130 min. were required.

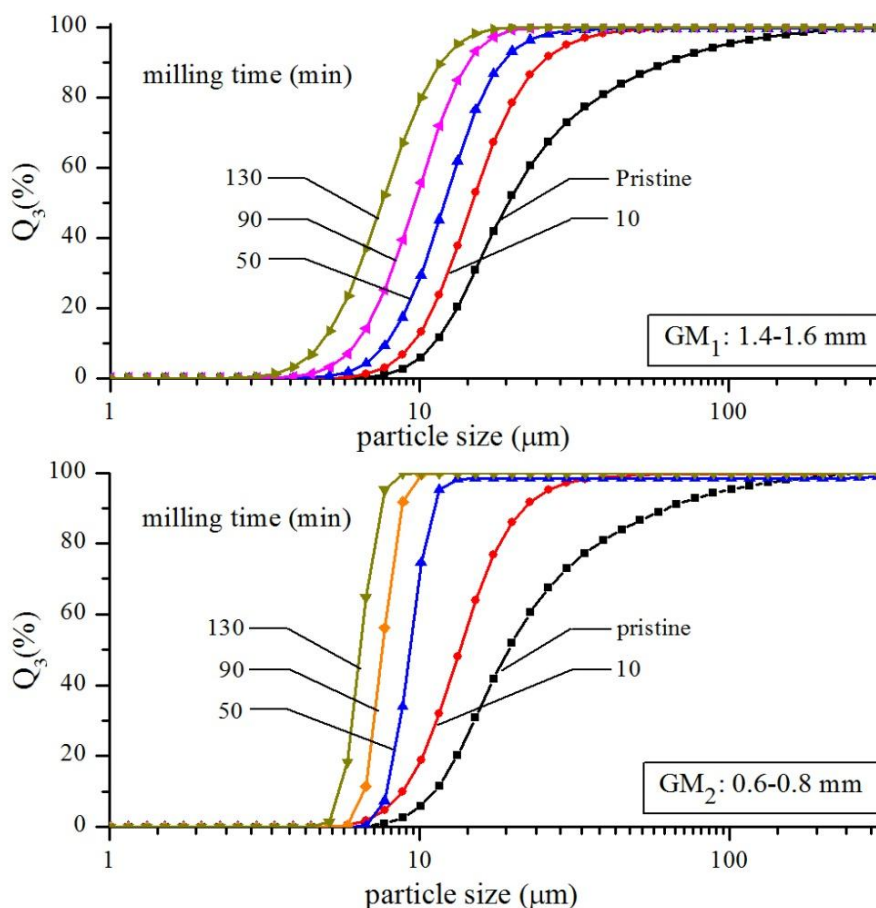


Fig 10. Cumulative, volume weighted particle size distribution (Q_3) curves obtained by SLS showing the effect of two different grinding media (GM_1 and GM_2) on a 30 wt% dispersion of Mg-fluorohectorite in respect to the milling time: [(■) initial, (●) 10, (▲) 50, (◆) 90, (▼) 130 min].

Although the difference in median particle sizes seen with the two different grinding media sizes became smaller with increasing milling time, even after 130 min., larger grinding media gave larger particle sizes ($X_{50} = 7.5 \mu\text{m}$ and $X_{50} = 6.4 \mu\text{m}$ for GM_1 and GM_2 , respectively). The assessment of the surface characteristics between the two grinding media showed higher values for both, the CEC of external surfaces and the BET surface areas, for smaller grinding media independent of milling time as is illustrated in Fig. 11. These observations were consistent with the evolution of FWHM of the basal reflection with milling time and indicated on one hand more efficient exfoliation of clay platelets with smaller grinding media.

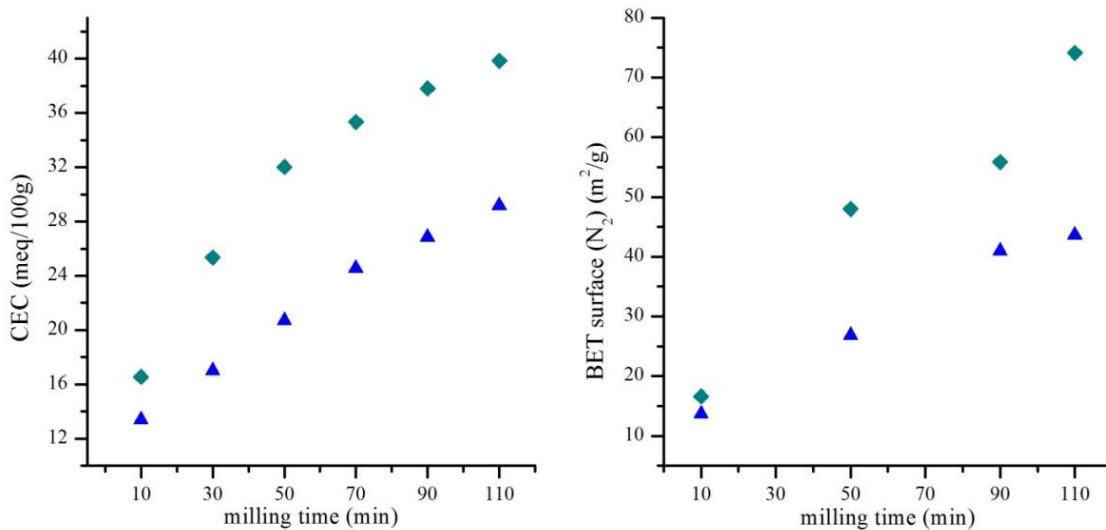


Fig 11. CEC values (left) of external surfaces and the corresponding BET values (right) for two sets of K-fluorohectorite produced by milling with two different grinding media [(▲) 1.4-1.6 mm, and (◆) 0.6-0.8 mm].

On the other hand, the evolution of particle sizes with milling (Fig. 10) showed that smaller grinding media caused more breakage of platelets and therefore the effect on the on maximum aspect ratio achievable was unclear at this stage. However, applying equation (3) allowed estimating the aspect ratio (Fig. 12) and it became apparent that for smaller grinding media efficiency of exfoliation still won over more pronounced breakage resulting in larger aspect ratios. A possible explanation for the counterintuitive higher efficiency of larger GM as compared to smaller GM in respect to exfoliation might possibly be related to the grossly differing specific surface area of the two GM ($6.54 \cdot 10^{-4} \text{ m}^2\text{g}^{-1}$ and $25.65 \cdot 10^{-4} \text{ m}^2\text{g}^{-1}$ for GM₁ and GM₂, respectively). Higher surface area will increase the probability of beads interacting directly with fluorohectorite triggering breakage. This would also explain why the particle size distribution at the same was getting narrower with smaller GM.

In summary, the data collected varying the concentration of dispersions and the grinding media size suggested that both, the average height of the tactoids and the distribution of lateral sizes of clay tactoids could be controlled to a certain degree by adjusting the parameters of the milling process in combination with the process duration.

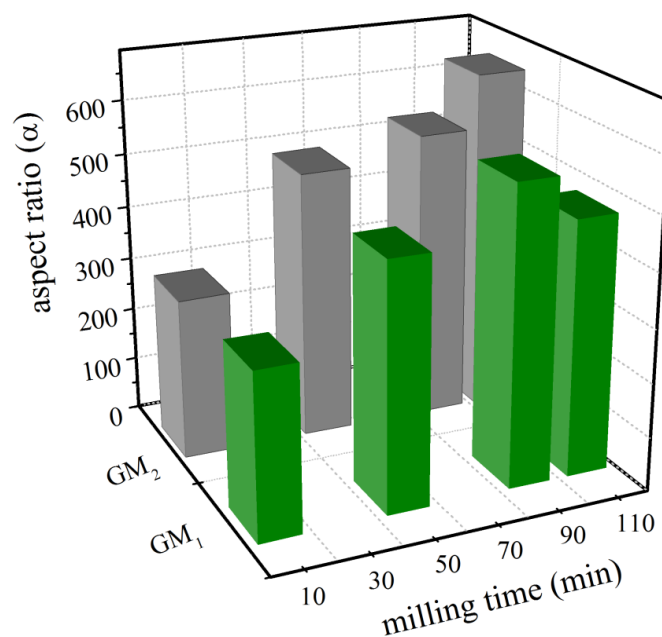


Fig 12. Evolution of estimated aspect ratio (α) values for 30 wt% clay dispersions treated with two different grinding media (GM₁ and GM₂) in respect to milling time.

4. CONCLUSION

Stirred media milling was proven as a very efficient and scalable method to significantly increase the aspect ratio of 'shear-labile' synthetic Mg-fluorohectorite. The efficiency was, however, crucially dependant on experimental parameters. Two different parameters, the clay content of dispersions and the grinding media diameter were studied and evaluated thoroughly and optimal parameters for maximizing aspect ratios could be identified: Clearly, the combination of high clay contents and small grinding media favoured exfoliation. In respect to grinding times, the aspect ratio passed through maxima which consequently must be identified for any particular material in order to obtain the best possible aspect ratios. Being a common industrial milling technique, up-scaling to mass production will be straight forward.

ACKNOWLEDGEMENTS

The authors acknowledge the Deutsche Forschungsgemeinschaft (SFB 840) for financial support. We would like to thank Dr. Peter Uhlík and the second anonymous reviewer for valuable comments that helped improving the manuscript.

REFERENCES

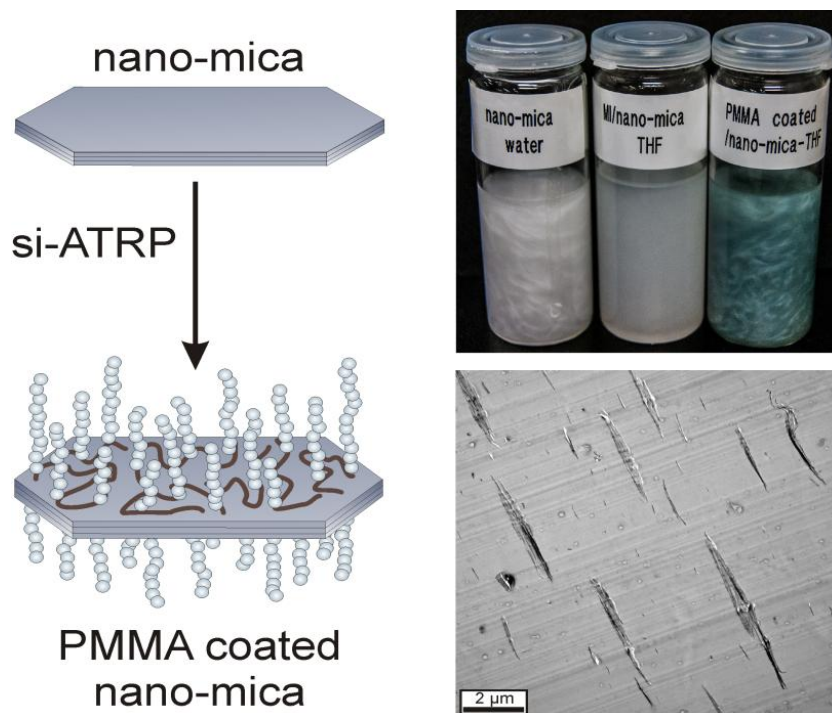
- Ammann L., Bergaya F. & Lagaly G. (2005) Determination of the cation exchange capacity of clays with copper complexes revisited. *Clay Minerals*, **40**, 441-453.
- Bowen P. (2002) Particle size distribution measurement from millimeters to nanometers, and from rods to platelets. *Journal of Dispersion Science and Technology*, **23**, 631-662.
- Burton A.W., Ong K., Rea T. & Chan I.Y. (2009) On the estimation of average crystallite size of zeolites from the Scherrer equation: A critical evaluation of its application to zeolites with one-dimensional pore systems. *Microporous and Mesoporous Materials*, **117**, 75-90.
- Chevigny C., Jouault N., Dalmas F., Boue F. & Jestin J. (2011) Tuning the mechanical properties in model nanocomposites: Influence of the polymer-filler interfacial interactions. *Journal of Polymer Science Part B: Polymer Physics*, **49**, 781-791.
- Dennis H.R., Hunter D.L., Chang D., Kim S., White J.L., Cho J.W. & Paul D.R. (2001) Effect of melt processing conditions on the extent of exfoliation in organoclay-based nanocomposites. *Polymer*, **42**, 9513-9522.
- Gardolinski J.E.F.C. & Lagaly G. (2005) Grafted organic derivatives of kaolinite: II. Intercalation of primary n-alkylamines and delamination. *Clay Minerals*, **40**, 547-556.
- Inam M.A., Ouattara S. & Frances C. (2011) Effects of concentration of dispersions on particle sizing during production of fine particles in wet grinding process. *Powder Technology*, **208**, 329-336.
- Kalo H., Möller M.W., Ziadeh M., Dolejs D. & Breu J. (2010) Large scale melt synthesis in an open crucible of Na-fluorohectorite with superb charge homogeneity and particle size. *Applied Clay Science*, **48**, 39-45.
- Kumar A.P., Depan D., Singh Tomer N. & Singh R.P. (2009) Nanoscale particles for polymer degradation and stabilization—Trends and future perspectives. *Progress in Polymer Science*, **34**, 479-515.
- Kwade A. (2003) A stressing model for the description and optimization of grinding processes. *Chemical Engineering & Technology*, **26**, 199-205.
- Kwade A. & Schwedes J. (2007) Wet Grinding in Stirred Media Mills. Pp. 251-382 in: *Handbook of Powder Technology - Particle Breakage* (A. D. Salman, M. Ghadiri & M. J. Hounslow, editors). Elsevier Science B.V., Amsterdam.

- Meier L.P. & Kahr G. (1999) Determination of the cation exchange capacity (CEC) of clay minerals using the complexes of copper(II) ion with triethylenetetramine and tetraethylenepentamine. *Clays and Clay Minerals*, **47**, 386-388.
- Mittal V. (2008) Mechanical and gas permeation properties of compatibilized polypropylene-layered silicate nanocomposites. *Journal of Applied Polymer Science*, **107**, 1350-1361.
- Möller M.W., Handge U.A., Kunz D.A., Lunkenbein T., Altstädt V. & Breu J. (2010a) Tailoring Shear-Stiff, Mica-like Nanoplatelets. *ACS Nano*, **4**, 717-724.
- Möller M.W., Lunkenbein T., Kalo H., Schieder M., Kunz D.A. & Breu J. (2010b) Barrier Properties of Synthetic Clay with a Kilo-Aspect Ratio. *Advanced Materials*, **22**, 5245-5249.
- Rutherford D.W., Chiou C.T. & Eberl D.D. (1997) Effects of exchanged cation on the microporosity of montmorillonite. *Clays and Clay Minerals*, **45**, 534-543.
- Scherrer P. (1918) Bestimmung der Grösse und der inneren Struktur von Kolloidteilchen mittels Röntgenstrahlen. *Nachrichten von der Gesellschaft der Wissenschaften zu Göttingen*, **2**, 98-100.
- Schmidt D., Shah D. & Giannelis E.P. (2002) New advances in polymer/layered silicate nanocomposites. *Current Opinion In Solid State & Materials Science*, **6**, 205-212.
- Schütz M.R., Kalo H., Lunkenbein T., Groschel A.H., Müller A.H.E., Wilkie C.A. & Breu J. (2011) Shear stiff, surface modified, mica-like nanoplatelets: a novel filler for polymer nanocomposites. *Journal of Materials Chemistry*, **21**, 12110-12116.
- Tamura K., Yokoyama S., Pascua C.S. & Yamada H. (2008) New age of polymer nanocomposites containing dispersed high-aspect-ratio silicate nanolayers. *Chemistry Of Materials*, **20**, 2242-2246.
- Vdovic N., Jurina I., Skapin S.D. & Sondi I. (2010) The surface properties of clay minerals modified by intensive dry milling -- revisited. *Appl. Clay Sci.*, **48**, 575-580.
- Zanetti M., Camino G., Thomann R. & Mülhaupt R. (2001) Synthesis and thermal behaviour of layered silicate-EVA nanocomposites. *Polymer*, **42**, 4501-4507.
- Zartman G.D., Liu H., Akdim B., Pachter R. & Heinz H. (2010) Nanoscale Tensile, Shear, and Failure Properties of Layered Silicates as a Function of Cation Density and Stress. *Journal Of Physical Chemistry B*, **114**, 1763-1772.

4.2. Towards completely miscible PMMA nanocomposites reinforced by shear-stiff, nano-mica

Mazen Ziakeh^a, Stephan Weiss^b, Bianca Fischer^c, Stephan Förster^d, Volker Altstädt^c, Axel H. E. Müller^d, Josef Breu^{a}*

Published in: Journal of Colloid and Interface Science (2014), 425, 143-151



^aLehrstuhl für Anorganische Chemie I, ^bLehrstuhl für Makromolekulare Chemie II, ^cLehrstuhl für Polymere Werkstoffe, and ^dLehrstuhl für Physikalische Chemie I, Universität Bayreuth, Universitätstrasse 30, 95440 Bayreuth, Germany ^eInstitute of Organic Chemistry, Johannes Gutenberg University Mainz, 55099 Mainz, Germany

*Corresponding Author: josef.breu@uni-bayreuth.de (J. Breu)

Author's individual contributions:

My contribution to this publication was focused on enhancing the adhesion of hybrid nanofiller based on high aspect ratio nano-mica platelets (**Chapter 2.1**) in a PMMA matrix. This was done by selective surface modification and a subsequent surface initiated controlled radical polymerization in a “grafting-from” approach. The modification was done using a macro-initiator provided by *Stephan Weiss* (Macromolecular Chem. II).

I have done all the experimental investigations and preparation of the nanocomposites which included: titration experiments, modification and phase transfer, polymerization and stability measurements. In addition, solution blending of nanocomposites and the subsequent melt compounding and preparation of specimen were carried out by me as well.

Bianca Fischer (Polymer Engineering) contributed the mechanical measurements. The academic writing was done mainly by me with the help of Prof. Dr. *Josef Brey* and some contributions of the other authors. The results regarding the polymerization kinetics and discussion were reviewed by Prof. Dr. *Axel H. E. Müller* (Macromolecular Chem. II) and the results related to the mechanical testing were reviewed by Prof. Dr. Ing.- *Volker Altstädt*.

A feedback was much appreciated from Prof. Dr. *Stephan Förster* regarding the surface conformation of the polymer brushes grafted from the external surfaces.

The manuscript is published in the **Journal of Colloid and Interface Science**.

My contribution to this publication is 70%.

Towards Completely Miscible PMMA Nanocomposites Reinforced by Shear-Stiff, Nano-Mica

Mazen Ziadeh^a, Stephan Weiss^b, Bianca Fischer^c, Stephan Förster^d, Volker Altstädt^c,
Axel H. E. Müller^e, Josef Breu^{a,*}

^aLehrstuhl für Anorganische Chemie I, ^bLehrstuhl für Makromolekulare Chemie II,
^cLehrstuhl für Polymere Werkstoffe, and ^dLehrstuhl für Physikalische Chemie I, Universität
Bayreuth, Universitätstrasse 30, 95440 Bayreuth, Germany ^eInstitute of
Organic Chemistry, Johannes Gutenberg University Mainz, 55099 Mainz, Germany

* Corresponding author. Tel.: + 49 921 552530; fax: + 49 921 552788.
E-mail address: josef.breu@uni-bayreuth.de (Prof. Dr. J. Breu)

ABSTRACT

Optimizing the reinforcement of polymers with nanoplatelets requires optimization of the aspect ratio and the moduli of the filler while providing a complete stress transfer. Employing a novel shear-stiff, nano-mica with large aspect ratio, we focus on maximizing the interfacial interaction between filler and matrix. External surfaces of the nano-mica were selectively modified by a polycationic macro-initiator and two PMMA-polymer brushes of length below and above critical entanglement length, respectively, and the mechanical properties of the three PMMA composites were measured.

The multiple electrostatic anchoring groups of the macro-initiator not only provide reliable adhesion but at the same time allow the variation of the degree of protonation providing a local match between the charge densities of the clay surface and the adsorbed macro-initiator. PMMA-coating of the nano-mica yielded long-term stable suspensions in THF that showed birefringence of a nematic phase. Solution blending of the PMMA coated nano-mica allows for dispersing single tactoids in the translucent PMMA-composites at 5 wt% clay content as determined by transmission electron microscopy (TEM). Although significantly improved mechanical properties could be achieved as compared to nanocomposites made with conventional clay fillers, the full potential, as expressed by Halpin-Tsai equations, of the PMMA coated nano-mica can still not be utilized.

This is attributed to the non-wetting character of the densely packed PMMA brushes attached to planar nanoplatelets.

Keywords: nano-mica, PMMA composites, ATRP, colloidal stability, nematic phase, non-wetting

1. INTRODUCTION

Incorporation of two-dimensional nanomaterials, in particularly anisotropic platelet-like layered compounds such as layered silicates [1-3] and layered double hydroxides [4,5], paved the way for cutting-edge composite materials. The incorporation of such nanomaterials into polymeric matrices created new and various fields of nanotechnological applications; for instance superb gas barrier diffusion for packaging [6-8], flame retardancy through intumescent-like behaviour [9], and mechanical reinforcement were described [10] for such polymer layered silicate nanocomposites (PLSN). Nevertheless, there are still fundamental challenges limiting the progress in all areas which leave room for further major improvements. These limitations range from the tendency of such nanoparticles to aggregate in polymeric matrices [11], the dimensions and properties of the dispersed nanoparticles [1,12], and inefficient interface management between the dispersed nanoparticles and the matrix [13].

Over the years, natural montmorillonite (MMT), completely ion exchanged with alkylammonium cations, has emerged as the conventional nanofiller. However, natural clays have major drawbacks such as the inherent small lateral extension (L) < 250 nm which limits their average aspect ratios (α) to typically less than 100. Furthermore, natural MMT suffers from heterogeneity in surface charge which consequently leads to non-uniform interlayer reactivity hampering control over the nanoplatelets stiffness. Moreover, amorphous materials like iron- and aluminium-oxihydroxides acting as binders render these fillers difficult to be disaggregated and even more so to be completely delaminated into individual silicate layers delivering the maximum possible aspect ratio for a given platelet diameter [14-16]. The aspect ratio (α) is expressed by the lateral extension (L) of the platelet divided by its thickness h which is ~ 1 nm for singular 2:1-layer.

Furthermore, incomplete delamination of clay tactoids in the polymer matrix has a detrimental effect on the mechanical efficiency because the remaining interlayer

spaces may act as inner shear planes inducing failure when introducing shear stress [17].

The shear stiffness may however be increased by collapsing the interlayer space producing mica-like platelets. In mica, the interlayer space is bridged by non-hydrated potassium ions protruding into cavities of the 2:1 silicate layer on both sides of the interlayer space. By adjusting the charge density to the hydration enthalpy of different interlayer cations, the synthetic fluorohectorite even allows for switching between a highly hydrated, shear-labile state with Mg^{2+} as interlayer cations and a completely nonhydrated, nonswelling, mica-like, shear-stiff state with K^+ as interlayer cations [18]. The shear stiffness is, in turn, related to the flexural rigidity of the reinforcing nanoplatelet, which increases with $\sim h^3$ and the strength of the interaction along the stacking direction [19]. Therefore, using mica-like synthetic clay with high inner shear plane stiffness, which allows high dispersion quality in the polymer matrix would be advantageous [20].

This synthetic layered silicate is characterized by an extraordinary lateral extension (L) of typically 5-7 μm and layer charge homogeneity. We have already reported that the incorporation of such high aspect ratio, shear-stiff, nano-mica platelets by melt compounding enhanced the mechanical properties of PMMA nanocomposite significantly [10]. However, the exploitation of the full potential of this novel nanomaterial has been hindered by suboptimal dispersion in the polymeric matrix. We now report on composite materials with improved interfacial interaction between the nanoplatelets and matrix leading to a homogeneous distribution of nanofiller.

It has already been reported that coating spherical iron oxide nanoparticles with a polymer brush layer provides perfect miscibility in a polyethylene matrix [21]. Moreover, coating the external basal surfaces of the nanoplatelets with polymer brushes of the same polarity as the matrix is expected to minimize surface tension and to provide the largest possible stress transfer from matrix to nanoplatelets.

When a "grafting-from" approach is taken for coating the nanoplatelets with a polymer brush *via* living polymerization techniques such as atom transfer radical polymerization (ATRP) are applied, the length of the brush may be controlled [22].

This allows checking for a possible further improvement of stress transfer for brushes longer than the critical entanglement length.

In this line, MMT has been modified with molecular cationic ATRP initiators to graft n-butyl acrylate (BA) and methyl methacrylate (MMA) from the clay surfaces [23,24]. While these molecular initiators occupy both, internal and external surface, the novel nano-mica allows selective attachment of a polycationic macro-initiator (MI^{n+}) to external surfaces. It is expected that the higher shear stiffness of the modified nano-mica provides improved reinforcement while the optimized interfacial interaction allows for a better stress transfer in these novel PMMA composites as compared to conventional MMT fillers.

2. EXPERIMENTAL AND CHARACTERIZATION METHODS

2.1. Materials and chemicals

The starting material for the preparation of the nanofiller is a synthetic Na-fluorohectorite with the chemical formula $Na_{0.5}[Mg_{2.5}Li_{0.5}]Si_4O_{10}F_2$ and a CEC of 110 meq./100 g. The aspect ratio was tuned to an average of 500 by exfoliation of the highly hydrated state, represented by the presence of Mg^{2+} cations in the interlayer space, in a stirred media mill. Subsequent cation exchange with K^+ cations yields a collapsed non-swollen and 'shear-stiff' nano-mica with no intracrystalline reactivity [18,25].

2-Cyano-2-propyl benzodithioate (CPBT) (97%, Aldrich), 2-bromoisobutyryl bromide (98%, Alfa-Aesar), triethylamine (min. 99%, Aldrich), 2-hydroxyethyl methacrylate (HEMA) (97% Aldrich) and N,N,N',N'',N'' -pentamethyldiethylenetriamine (PMDETA) (97%, Aldrich) were used as received without further purification. Ethyl 2-bromoisobutyrate (EBiB) (99%, Aldrich) was used as free sacrificial initiator. Azobisisobutyronitrile (AIBN) (98%, Aldrich) was used after recrystallization twice from methanol. Solvents such as THF (p.a.), DMSO (p.a.), Dimethylacetamide (DMAc) and anisole (p.a.) were purchased from Aldrich and used as received unless stated. Dichloromethane (p.a. Aldrich) was stored over molecular sieves (3\AA) to remove water traces. 2-Dimethylaminoethyl methacrylate (DMAEMA) (98% Aldrich) and methyl methacrylate (MMA) (99% Aldrich) were passed over a basic alumina column to remove stabilizer prior to polymerisation.

2-(2-Bromoisobutyryloxy)ethyl methacrylate (BIEM) was synthesized according to literature [24]. A commercial PMMA (Plexiglas POQ62 supplied by Evonik Industries) was used as matrix. PMMA has a molecular weight (M_w) of 73 kg/mol with a polydispersity index of 1.63.

2.2. Synthesis of poly (2-(2-bromoisobutyryloxy) ethyl methacrylate)-stat-(2-(dimethylamino) ethyl methacrylate) (MI^{n+})

To a 100 ml round bottom flask, equipped with rubber septum, BIEM (1.7 g; 6.1 mmol), DMAEMA (6.7 g; 42.8 mmol), 2-Cyano-2-propyl benzodithioate (CPBT), (270 mg; 1.2 mmol), AIBN (100 mg; 0.6 mmol) and 40 ml of DMSO as solvent in addition to 2 ml of anisole as internal standard were added. After three freeze-pump-thaw cycles the reaction was placed into an oil bath at 70 °C for 4 h to reach a conversion of 54% as determined by 1H NMR spectroscopy. The resulting polymer solution was cooled, exposed to air and dialysed against dioxane until no monomer related peaks at 5.8-6.4 ppm were detected by 1H NMR spectroscopy. $M_n = 9000$ g/mol and $M_w = 14000$ g/mol was determined via SEC with DMAc as eluent and a DMAEMA calibration. 1H NMR (300 MHz, $CDCl_3$, δ in ppm): 4.4 – 4.1 (R-C(-CH₃)-COO-CH₂-CH₂-OOC-C(CH₃)₂-Br), 4.0 (R-C(-CH₃)-COO-CH₂-CH₂-N-(CH₃)₂), 2.6 (R-C(-CH₃)-COO-CH₂-CH₂-N-(CH₃)₂), 2.2 (R-C(-CH₃)-COO-CH₂-CH₂-N-(CH₃)₂), 1.9 (R-C(-CH₃)-COO-CH₂-CH₂-OOC-C(CH₃)₂-Br), 1.8 (R-C(-CH₃)-COO-CH₂-CH₂-N-(CH₃)₂).

2.3. Organophilization and surface initiated (SI)-ATRP of PMMA brushes

The external surface of K-nano-mica (10 g) was flocculated with a solution of MI (330 mg) in DI water at pH=7.2. Subsequently, the flocculated hydrophobic nanoplatelets (MI/nano-mica) were centrifuged and redispersed in THF for few times. The grafting of MMA was initiated from MI/nano-mica *via* a copper mediated ATRP in the presence of EBiB as a free sacrificial initiator. All experiments were performed under inert atmosphere in a conventional run procedure [22,27]; A dispersion of the MI/nano-mica (10 g; calculated 370 μ mol of initiating sites) in 400 ml THF, MMA (164.5 g; 1.462 mol) and EBiB (19 mg; 97.5 μ mol) were added to a flask and sealed with a rubber septum.

The reaction mixture was degassed three times by freeze-pump-thaw cycles and filled with argon. In a separate flask a stock solution of PMDETA, Cu(I)Cl and

Cu(II)Cl₂ (338 mg; 975 μmol, 115.8 mg; 1.17 mmol and 39.2 mg; 292.5 μmol) in 20 ml anisole was degassed for 30 min under argon. Finally, 10 ml of the stock solution was introduced to the reaction flask by a syringe. The reaction flask was immersed in an oil bath at 80°C. Samples were withdrawn at various times to monitor the reaction kinetics by determining the monomer conversion from the integration of the residual monomer peaks by ¹H NMR spectroscopy with anisole as an internal standard. Average molecular weights and molecular weight distribution were measured by size exclusion chromatography (SEC) for the free polymer initiated from the sacrificial initiator.

The free polymer was recovered after passing over a basic alumina column to separate the clay nanoplatelets. The reaction was stopped after 300 min by cooling and exposing to air. The same procedure was repeated and the reaction was stopped after 30 min for shorter PMMA brushes. The final hybrids of PMMA coated nano-mica were centrifuged and washed few times with THF to remove the free PMMA chains and finally redispersed in THF.

2.4. Preparation of PMMA/nano-mica composites

A solution blending route was applied for optimum dispersion of the modified nano-mica in the matrix. Nano-mica suspension in THF was mixed with a solution of PMMA in THF (5 wt% clay content) and placed in an overhead shaker for 18 hr for homogenization. Subsequently, the suspension was film casted and dried in an oven under vacuum at 90 °C for 18 hours and at 140 °C for another 8 hours. The dried composite materials were cryo-grinded to fine powder prior to melt compounding. The compounding was done in a discontinuous counter-rotating twin-screw micro-compounder (DSM Xplore, 15 ml micro-compounder) at a temperature of 200 °C, a mixing speed of 210 rpm and a mixing time of 3 min. The material was added batch wise to the running micro-compounder and during each cycle a batch of 11 g was processed. After extrusion, the melt was injection-moulded with a microinjector (DSM Xplore 12 ml injection moulding machine; melt temperature: 190 °C; mould temperature: 40 °C; injection pressure: 8 bar) into dumbbell specimens (75 mm × 5 mm × 2 mm) for tensile testing.

2.5. Instrumentation and characterization

Determination of point of zero charge of the external basal surface was done using charge titration stability analyzer (Stabisizer[®], Particle Metrix GmbH). Aqueous dispersion of K-nano-mica (30 mg) was titrated with MI solution (1g/L) at different pH values. The transmittance absorption spectra were recorded on a Nicolet FTIR 460 (Thermo Nicolet Corp.) using 64 scans at 4 cm⁻¹ spectral resolution at room temperature. The specific surface area of a freeze-dried K-nano-mica sample was calculated from the N₂ adsorption/desorption isotherms (Quantachrome Nova 2000e analyzer) applying the Brunauer-Emmett-Teller (BET) equation. In the non-swollen K-nano-mica, the interlamellar space is no longer accessible and the CEC and BET values are attributed solely to the external basal planes of the tactoids. Furthermore, due to the high aspect ratio observed for the synthetic fluorohectorite, the contribution of the edges to the specific surface area can be safely ignored.

Monomer conversion was determined from the integration of the residual monomer peaks by ¹H NMR spectroscopy with anisole as an internal standard. The ¹H NMR spectroscopy was performed on a Bruker Avance 300 spectrometer. Average molecular weights and molecular weight distribution were measured by conventional size exclusion chromatography (SEC). Column set: 5 μm SDV[®] gel, 102, 103, 104, and 105 Å, 30 cm each (PSS, Mainz). Detectors used are refractive index (RI) and UV operated at 254 nm. The number-average (M_n) and weight-average (M_w) molecular weights were calculated by using a calibration curve which was constructed using PMMA with low dispersity as standard (PMMA standards series, PSS, Mainz). DMAc or THF was used as eluent at a flow rate of 1 ml/min.

Thermal gravimetric analysis (TGA) was conducted on a Mettler TG 50/TA 3000 thermobalance. Samples were heated at a heating rate of 20 K/min from 30 to 600°C under oxidative atmosphere. The morphology of the surface was examined by scanning electron microscope (SEM) using a Zeiss EM 922 EFTEM (Carl Zeiss GmbH) with an acceleration voltage of 200 kV.

The stability measurements were performed in a LUMiFuge[®] 114 (LUM) with a variable rotation frequency of 300, 600, 900 rpm and different time intervals of

200 and 400 s, respectively. Clay suspensions (0.5 wt%) in THF and water were placed in tubes in horizontal positions on the disc of the LUMiFuge®. During the horizontal rotation of this disc the transparencies of the suspensions were measured in the area between the menisci and the sediment. The mean transparency of the whole area was determined. The transparency was measured in time intervals of 10 s while increasing rotation speed stepwise.

The optical parameters transmittance, haze, and clarity of the PMMA/nano-mica composites were measured on a BYK Gardner haze-gard plus in accordance with ASTM D1003 “Standard Test Method for Haze and Luminous Transmittance of Transparent Plastics”.

Transmission electron microscope (TEM) measurements were carried out on a Zeiss CEM 902 EFTEM with an acceleration voltage of 200 kV. Specimens were microtomed to obtain 30–50 nm thick pieces, which were placed on a lacey carbon copper grid. Tensile modulus, tensile strength and elongation at break were measured using a Universal Tensile Tester according to ISO 527 applying a strain rate of 1 mm/min. For each material at least 6 samples were tested. The elongation was determined by a macro-displacement-transducer.

3. RESULTS AND DISCUSSION

3.1. Preparation of PMMA coated nano-mica nanofiller

3.1.1. Tailoring of high aspect ratio K-nano-mica

As previously shown [18], with synthetic Na-fluorohectorite the subtle balance between layer charge and hydration enthalpy of different interlayer cations allows for controlled transformation between a highly hydrated and a non-hydrated state by simple cation exchange. This transition between hydration states cannot be observed for natural MMT due to both heterogeneity of charge density and lower average layer charge. The highly hydrated and therefore ‘shear-labile’ state, in which Mg^{2+} cations occupy the interlayer space (basal spacing: $d = 18.6 \text{ \AA}$), enables an efficient exfoliation to increase the aspect ratio by applying shear forces in a stirred media mill [25].

Subsequent cation exchange with K^+ cations yields a collapsed non-swollen and ‘shear-stiff’ mica-like nanofiller (nano-mica, $d = 9.9 \text{ \AA}$) (Fig. 1a). A rough estimate

of the average aspect ratio can be calculated using a previously introduced method which correlates the tactoid thickness as determined by the Scherrer equation with the value of the total specific surface area [18]. Thus, by having a median particle size distribution, $X_{50} = 6.4 \mu\text{m}$ as determined by static light scattering and a large external specific surface area of $60 \text{ m}^2/\text{g}$ as obtained via N_2 adsorption/desorption measurement applying the BET equation, we can estimate an average aspect ratio of 500 for the K-nano-mica used here. This nanofiller combines the best of two worlds, the stiffness of the mica-sandwich and an aspect ratio significantly larger than what can be obtained with natural MMT.

3.1.2. Selective surface modification

The pristine K-nano-mica obtained still carries hydrated inorganic K^+ on the outer surface. To transfer it into a hydrophobic polymer matrix its surface tension has to be lowered to improve the matrix-filler interaction and to prevent aggregation of the filler. Any aggregation (see discussion below for details) will lower the specific interface in the composite and such reduce the potential improvements of composite properties. A polycationic macro-initiator (MI^{n+}) was employed for modification of the nano-mica. The MI^{n+} consists of a statistical copolymer of DMAEMA and BIEM in a 3:1 ratio with an average degree of polymerization (DP) of 40 units (Fig. S1). This polymeric modifier is unable to intercalate between the silicate layers and the cation exchange is restricted to outer basal surfaces leaving the basal spacing unchanged. Moreover, the multiple electrostatic anchoring by ammonium groups incorporated in the backbone of the MI^{n+} allow for a more reliable adhesion to the nano-mica as compared to single charged molecular anchoring groups.

The successful modification was confirmed qualitatively by FT-IR (Fig. S2). MI^{n+} not only is firmly anchored but at the same time the degree of protonation can be varied and by this the charge density of the macro-initiator can be adjusted to the charge density of the clay surface. Furthermore, each MI^{n+} chain bears an average of ten potential initiator groups for a surface-initiated (SI)-ATRP, subsequently enabling a controlled grafting of polymeric brushes from the surface of the modified nano-mica.

The charge ($n+$) of the macro-initiator, MI^{n+} , can be tuned by adjusting the pH and therefore the degree of protonation of the amine groups of the DMAEMA. The influence of charge variation on the adsorbed polycationic MI^{n+} on the external basal surface of nano-mica and its effect on stability has been investigated. The charged DMAEMA groups can be anchored onto the surface by a cation exchange with the K^+ cations and the uncharged amine groups act as neutral spacer (Fig. 1b).

To attain different degrees of protonation of the amine function of DMAEMA, the pH of the solution was adjusted using acetic acid [28]. The charge titration curves at different pH solutions with the same amount of K-nano-mica are shown in Fig. 2. The amount of MI^{n+} anchored on the external basal surface at the point of zero charge as expected increases with decreasing degree of protonation.

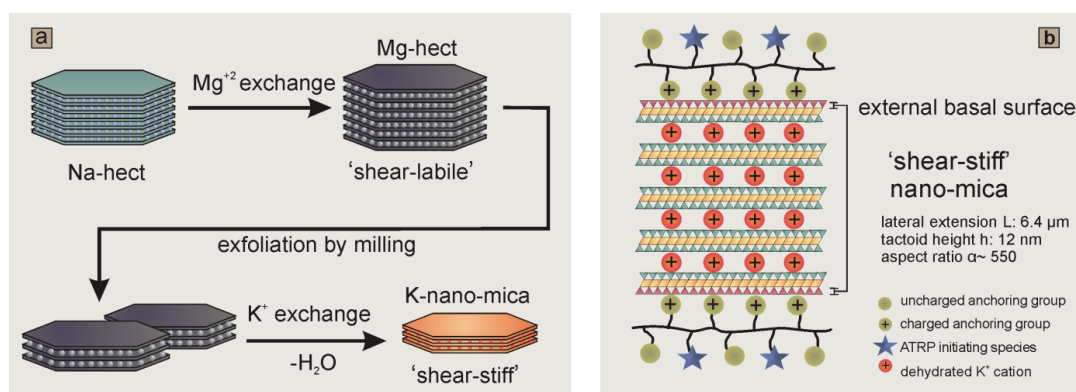


Fig. 1. a) A schematic representation of tailoring high aspect ratio 'shear-stiff', K-nano-mica nanoplatelets after exfoliation and exchanging the interlayer cations and b) selective modification of only the external basal surface using MI^{n+} .

Concomitantly with annihilation of the surface charge, the modification of K-nano-mica with MI^{n+} leads to organophilization of the clay altering its state from hydrophilic to hydrophobic and leading to flocculation of nanoplatelets in aqueous solution.

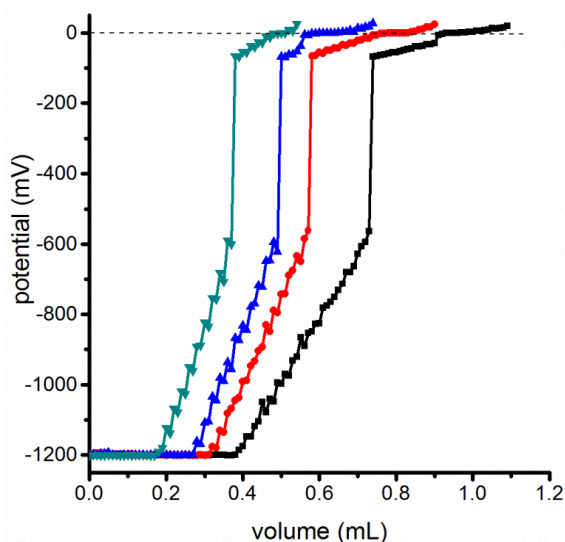


Fig. 2. Charge titration of K-nano-mica (30 mg in 10 ml DI water) with MI^{n+} solution (1 g/l) until point of zero charge as a function of pH, related to the degree of protonation (θ): (\blacktriangledown) pH= 4.6; θ = 100%, (\blacktriangle) pH= 5.5; θ = 75%, (\bullet) pH= 6.4; θ = 50% and (\blacksquare) pH= 7.2; θ = 25%.

The quality of the dispersion in THF after organophilization with MI^{n+} is significantly influenced by the loading of MI^{n+} . As a semi-quantitative measurement of dispersion stability, forced sedimentation experiments were performed applying a LUMiFuge[®] 114 (Fig. S3). The integrated transparency of a 0.5 wt% suspensions in THF of K-nano-mica modified with MI^{n+} at pH= 7.2; θ = 25% is significantly higher as compared to all other samples suggesting that this packing density of MI^{n+} gives the most stable dispersion in organophilic environments. Consequently, controlled polymerizations were focused on the K-nano-mica modified with MI^{n+} at pH= 7.2 (θ : 25%) and this material will be referred to as MI/nano-mica hereafter.

3.1.3. Surface initiated (SI)-ATRP of PMMA brushes

The grafting-from process of planar PMMA brushes was initiated from the basal planes of the MI/nano-mica. The determination of the molecular weight of grafted polymer was facilitated by analysis of free chains formed in solution using a sacrificial-initiator. EBiB was used as initiator from free chains due to its structural similarity to the incorporated BIEM in the MI^{n+} .

A good correlation between the molecular weights of these loose polymer chains grown in solution and the molecular weights of polymer brushes anchored to a

surface has been shown before [29,30]. The ATRP technique allows the grafted chains to grow slowly and simultaneously. Therefore, it is possible to obtain brushes with narrow molecular weight distribution and polydispersity. Table 1 lists the number and weight average molecular weights M_n and M_w of the free PMMA grown in solution determined by SEC as a function of reaction time. The differences between theoretical and experimental values can be assigned to an initiation efficiency of less than 100%.

Table 2. Molecular weights of the free PMMA chains as a function of polymerization time in THF

time (min)	Conv. ^a (%)	DP ^a	M_n^a (kg/mol)	DP ^b	M_n^b (kg/mol)	M_w^b (kg/mol)	PDI ^b
10	1	36	3.5	84	8.4	10.0	1.2
20	2	72	7.2	100	10.0	13.0	1.3
30	4	120	12.0	150	15.0	17.0	1.1
60	5	143	14.3	190	19.0	23.0	1.2
120	7	203	20.3	310	31.0	36.0	1.2
300	9	263	26.3	380	38.0	50.0	1.3

^adetermined by ¹H NMR spectroscopy. ^bdetermined by SEC with THF as eluent and PMMA calibration

The reaction shows a controlled character with polydispersity index close to 1. Fig. 3 (left) shows the evaluation of $\ln[M]_0/[M]$ vs. time where, polymerization rate slows down after 120 min. This indicates that the number of the initiating species remains approximately constant up to 120 min reaction time and then starts to decrease. Furthermore, by plotting the molecular weight versus conversion as in Fig. 3 (right), a linear increase ascertained the controlled behaviour of the reaction.

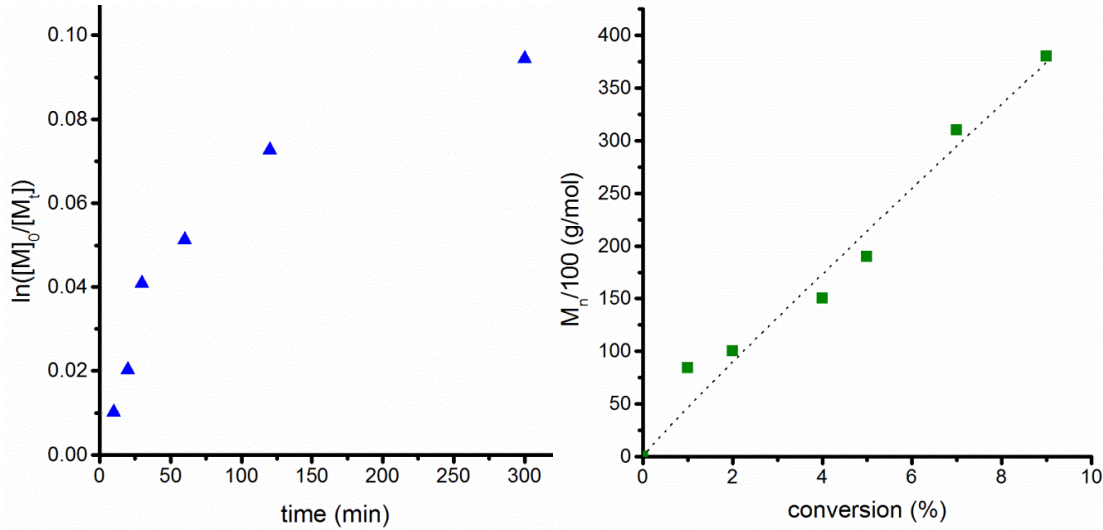


Fig. 3. (▲) Plots of $\ln[M]_0/[M]$ vs. time for the solution polymerization of free PMMA. (■) evolution of molecular weight with conversion of MMA monomers.

The amount of surface grafted PMMA was examined by TGA (Fig. 4). As expected, the PMMA coated nano-mica with longer polymer chains showed a higher weight loss of organic material. Weight losses observed below 100 °C are assigned to remaining solvent and are neglected in the calculation. MI/nano-mica was found to have 3.1 % loss of volatile materials after heating to 400 °C. The grafted PMMA coated nano-mica showed a weight loss of 13.0% and 32.5% for grafted PMMA chains with a DP of 150 (short PMMA) and 380 (long PMMA), respectively.

The grafting density and initiation efficiency represented by the number of chains per nm^2 can be calculated from the TGA and SEC data.

All calculations of grafting density were based on the following formulas:

$$\sigma = \frac{M_I \times N_A}{SA} \quad (1)$$

$$\sigma' = \frac{M_P \times N_A}{SA} \quad (2)$$

Where σ is the grafting density (initiator per nm^2), σ' is the grafting density (chain per nm^2), M_I is molar amount of the initiating species per g of MI/nano-mica, M_P is the molar amount of PMMA chains, N_A is the Avogadro constant and SA is the specific surface area of the K-nano-mica.

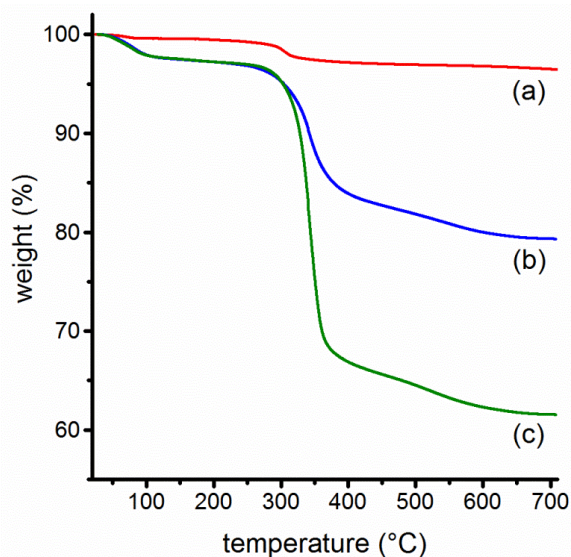


Fig. 4. TGA measurements of a) MI/nano-mica, b) short PMMA coated nano-mica (DP 150) and of c) long PMMA coated nano-mica (DP 380).

A grafting density of 0.3 ATRP initiator functions per nm^2 was calculated from (1). For the PMMA coated nano-mica calculations, (2) gave a grafting density of 0.09 and 0.085 chains per nm^2 corresponding to an initiation efficiency of 30% and 28% for DP 150 and DP 380, respectively. The relatively low efficiency can be attributed to certain issues in the applied polymerization system: whereas, copper-complexes used as catalysts can adsorb/ion-exchange onto the surface of the nanoplatelets. Indeed the PMMA coated nano-micas have a deep blue colour due to adsorbed catalyst (Fig. 6) and thus, reduction of the concentration of free catalyst will slow down kinetics of the polymerization.

The morphological changes of external surfaces of the nano-mica before and after polymerization were analyzed using SEM. The K-nano-mica after exfoliation has a large lateral extension and a smooth surface (Fig. 5a) when compared to the rough surface of MI/nano-mica (Fig. 5b). The grafted PMMA brushes gives a rougher and coarse surface with pattern typical for collapsed PMMA chains in a dried state forming mushroom-like structures (Fig. 5c), as expected for the achieved high grafting density [31].

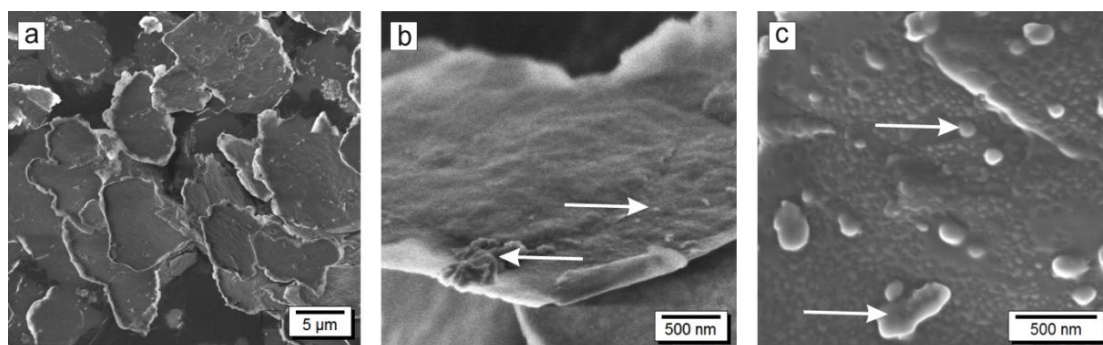


Fig. 5. SEM images of a) exfoliated K-nano-mica, b) surface morphology of MI/nano-mica and c) surface of PMMA coated nano-mica (DP 380) indicating collapsed polymer chains (Arrows indicate clay fragments from the milling treatment).

3.2. Dispersion quality and stability in solvents

3.2.1. Shear induced birefringence

Typically, particles in colloidal suspension are randomly oriented. When anisotropy comes into play, like with K-nano-mica nanoplatelets of 500 aspect ratio, the particles might no longer be able to move independently, in particular when objected to lamellar flows [32-34]. In Fig. 6 (left) a dispersion of unmodified K-nano-mica in water is compared to dispersions of MI/nano-mica and PMMA coated nano-mica in THF. As already mentioned the blue colour of the latter is due to adsorbed/ion exchanged copper-complexes used as a catalyst for ATRP.



Fig. 6. Dispersions (1 wt%) of unmodified K-nano-mica in water (left), MI/nano-mica in THF (middle) and PMMA coated nano-mica (DP 380) (right).

A gentle movement of the containers induces a vivid birefringence of a nematic phase in both unmodified K-nano-mica in water and PMMA coated nano-mica (DP

380) in THF (Fig. 6 left and right). However, the dispersion of MI/nano-mica in THF (Fig. 6 middle) is not stable enough to observe this birefringence. Stirring generates a lamellar flow, causing the clay platelets to orient parallel in the shear field. Platelets in the stack can no longer rotate freely and the distance of the platelets is fixed by lateral extension of the platelets which is in the range of visible light allowing birefringence to be observed with the naked eye. Observation and evidence of optical birefringence which demonstrates the existence of a liquid crystalline order of the platelet-like particles has already been reported for aqueous smectite suspensions [34-36]. The nematic phase displays a threaded Schlieren pattern resulting from the orientation of individual particles with high aspect ratio [37]. Interestingly, the occurrence of birefringence seems to be a first optical indication of the quality of dispersion as will be discussed next.

3.2.2. Stability of dispersion

The stability of the colloidal dispersions was investigated in a semi-quantitative way by forced sedimentation experiments applying a LUMiFuge® 114. Fig. 7 compares the integrated transparency of unmodified K-nano-mica in an aqueous dispersion with MI/nano-mica and two PMMA coated nano-micas in THF.

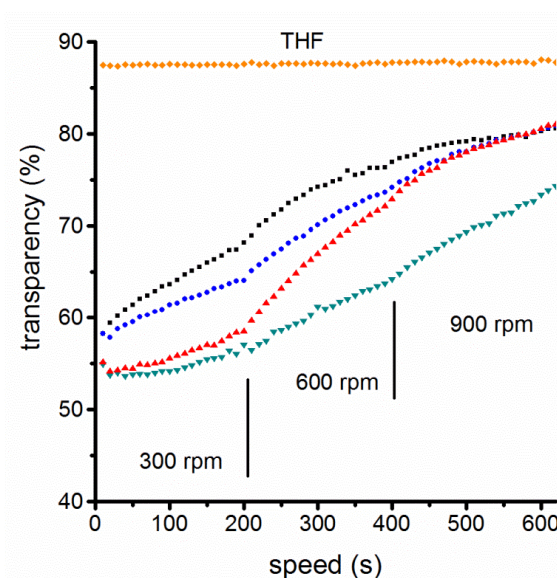


Fig. 7. Integrated transparency of 0.5 wt% dispersions under time dependent centrifugal forces of 300, 600 and 900 rpm; (■) MI/nano-mica in THF, (●) PMMA coated nano-micas in THF (DP 150), (▲) PMMA coated nano-micas in THF (DP 380) and (▼) unmodified K-nano-mica in water.

The K-nano-mica suspension in water is highly hydrophilic and carries a high negative surface potential resulting in the most stable suspension. Due to the large lateral dimension of platelets it still sediments. All organophilized samples in THF are less stable as compared to K-nano-mica in an aqueous dispersion. The fact that THF is a good solvent for PMMA explains the greatly enhanced stability of the PMMA coated nano-mica which improves with increasing chain length. DP 380 at low centrifugal forces (300 rpm) even matches the stability of K-nano-mica in an aqueous dispersion. Please note that these two samples also are the ones for which optical birefringence could be observed contrary to the less stable MI/nano-mica suspension in THF.

3.3. PMMA/nano-mica nanocomposites

3.3.1. Optical characteristic

The optical properties of PMMA/nano-mica nanocomposites at 5 wt% clay content were characterized by measuring the total optical transmittance, clarity, and haze (Fig. 8) using flat samples (1 mm thick). Neat PMMA is almost transparent, its total transmittance is very high, but some diffuse scattering appears.

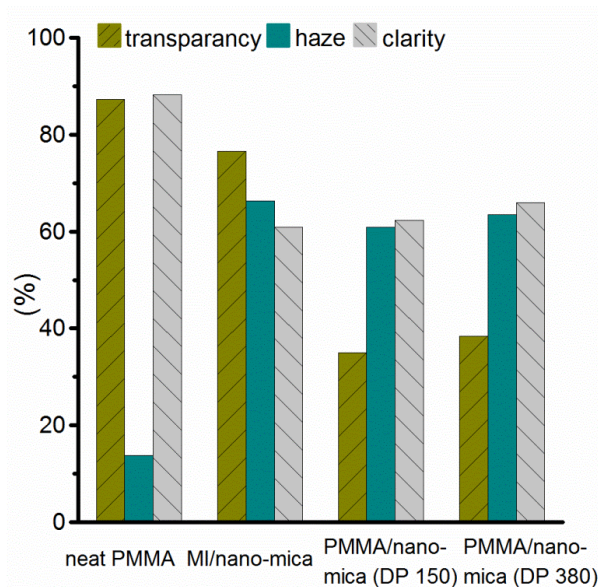


Fig. 8. Values of optical transmittance (ratio of transmitted to incident light), haze (wide angle scattering) and clarity (narrow angle scattering) of neat PMMA and three different PMMA/nano-mica nanocomposites at 5 wt% clay content.

MI/nano-mica exhibit high optical transmittance similar to PMMA even at this high clay content. In case of PMMA coated nano-mica, optical transmittance is

significantly reduced. This is attributed to the colour of the adsorbed/ion exchanged copper complexes onto the surface of the nanoplatelets. All nanocomposite samples show high levels of haze because random orientation, despite the limited thickness of the nanoplatelets, nevertheless leads to scattering due to typical diameters in the micron range. It is noteworthy to mention that all PMMA/nano-mica composites yield translucent samples with at least 60% clarity.

3.3.2. Morphology and mechanical properties

Whereas, an efficient dispersion is a key factor affecting the mechanical properties of nanocomposites [11], homogenous dispersion of such high aspect ratio nano-mica in a polymeric matrix is a challenging task. As already reported, the dispersion of MI/nano-mica as powder dispersed by an industrial relevant melt compounding process showed a good dispersion on a macroscopic level, however, on microscopic level some agglomerates were observed [10]. MI/nano-mica can be dispersed in THF-suspensions (3.2.2). Upon complete removal of solvent, however, due to the large aspect ratio, inevitably texture is induced with MI/nano-mica nanoplatelets becoming arranged parallel and eventually forming aggregates with band-like structure (Fig. 11a). The overlapping areas in these aggregates are too large to allow shear forces as generated during melt compounding to accomplish complete disaggregation. In order to avoid formation of band-like structures, here we choose solution blending to achieve an optimal dispersion prior to melt compounding.

Investigation of the dispersion quality for three different modified nano-micas incorporated in PMMA matrix after compounding is evaluated using TEM micrographs (Fig. 9).

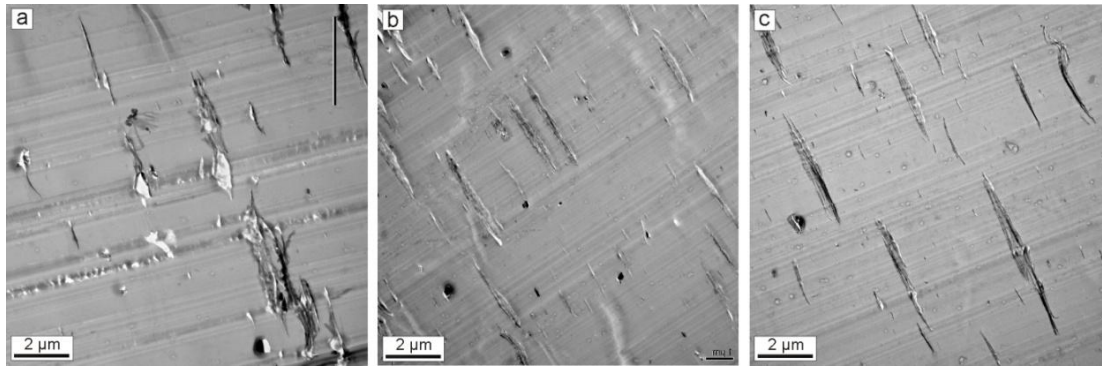


Fig. 9. TEM micrographs of PMMA/nanocomposite with incorporated a) MI/nano-mica, b) PMMA coated nano-mica (DP150), and c) PMMA coated nano-mica (DP380) at 5 wt% clay content.

As anticipated, a simple surface modification as in case of the MI/nano-mica is insufficient to achieve optimal dispersion (Fig. 9a) and consequently some aggregates are visible in the TEM. The quality of dispersion is, however, considerably enhanced by having a PMMA coating on the surface (Fig. 9b and c). In these nanocomposites the nano-mica is homogeneously dispersed as single tactoids. Surface modification with MI^{n+} already renders the K-nano-mica more hydrophobic. A subsequent grafting process of brushes chemically identical to the matrix reduces the interfacial tension close to zero as indicated by a much improved dispersion.

The Optimization of the adhesion between the matrix and the filler surface is essential to attain an effective load transfer from the polymer matrix into the filler by shear forces allowing the utilization of the full potential of the nano-mica reinforcement. In this line, longer chains are more capable of interpenetrate and consequently might show better mechanical properties as compared to shorter chains. With incorporation of the various modified types of nano-mica, the Young's modulus improves compared to neat PMMA (Fig. 10 left).

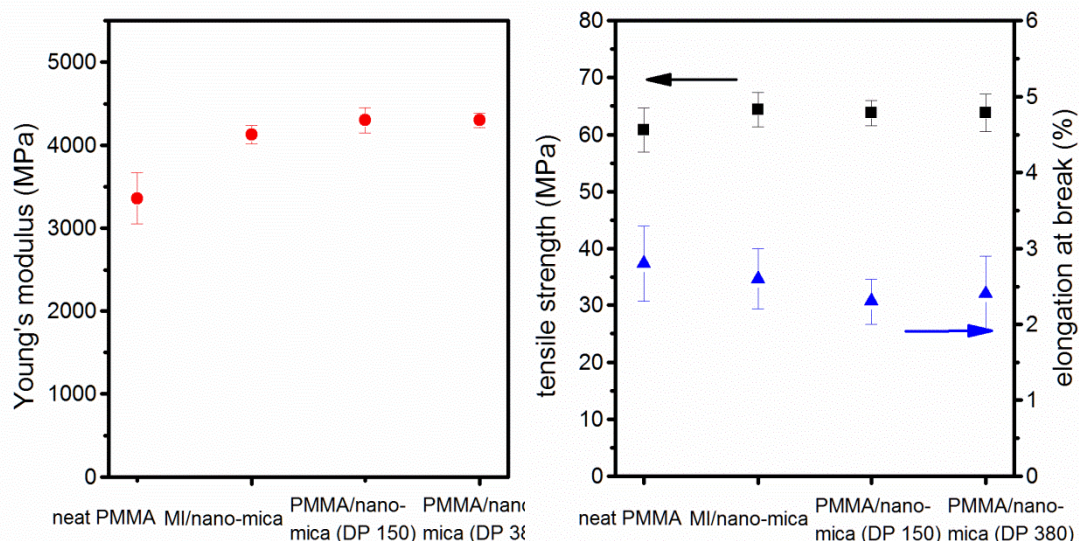


Fig. 10. (Left). (●) Young's modulus and (right). (■) tensile strength and (▲) elongation at break for neat PMMA and three different PMMA nano-mica filled nanocomposites.

The improvement for MI/nano-mica filled is already 24% and the two nanocomposites filled with PMMA coated nano-micas (DP 150) and (DP 380) lead to an improvement of 32%. Investigation of the mechanical properties of PMMA nanocomposites with conventional organo-MMT by Tiwari, R. R. et al. showed an increase in the Young's modulus of 25% at 4 wt% clay content whereas the impact strength was reduced by 64% [38].

Furthermore, a similar behaviour was observed for commercial Bentone 38® in PMMA nanocomposites prepared by melt blending at 4 wt%, whereas an increase in modulus of 28% was observed alongside a reduction in the tensile strength by 16% and reduce fracture toughness by 22% [10]. Contrary to most of the literature reports on composites made with conventional clay nanofillers, the addition of the nano-mica triggers no embrittlement, whereas using conventional natural clay based fillers in a brittle matrix leads to an increase in modulus at the expense of strength, strain and fracture toughness [39,40]. In respect to tensile strength no significant differences could be observed for the different coatings (Figure 10), while elongation at break is only slightly reduced by adding the various nano-micas. The reduction is smaller with the DP380-nano-mica filled nanocomposite.

In summary the mechanical data suggest that significant improvements were achieved in comparison to nanocomposites made with conventional clay

nanofillers, the PMMA coating still fails to meet expectations according to e.g. Halpin-Tsai model. As has been recently shown, the elastic modules of smectites are somewhat lower but in the range of micas [41,42]. Moreover, the anisotropy in the bending and the in-plane moduli is quite pronounced with the latter being approximately three times larger. Taking the bending modulus (C_{33}) of approximately 60 GPa [42] and the in-plane modulus (C_{11}) of 150 GPa [41] of mica, improvements of Young's modulus of the nanocomposite, as calculated by the Halpin-Tsai equation of 26% and 62% are expected, respectively. Clearly, the fillers are oriented more or less randomly in the composites manufactured and some kind of weighted average would have to be applied. Nevertheless, despite some uncertainties in the effective aspect ratio and despite the disregard of the anisotropy of filler moduli and possible preferred orientation, deviations from expectations remain. This deviation suggests that the stress transfer from the matrix to the nanofiller might still be suboptimal, even for DP380 nano-mica filled nanocomposites.

This in turn might be related to the lack of chain interpenetration (wetting) between the polymer matrix chains and the grafted polymer brush chains of the DP380 nano-mica filler. For brushes attached to a flat clay surface, the packing density does not decrease with distance from the surface as for spheres but stays constant (Fig. 11). With grafting densities of 0.085 chains per nm^2 for DP 380 a rather dense packing with stretched chains is expected [43] that inhibits penetration of polymer chains into the matrix (Fig. 11b).

The wettability of a brush layer depends on the polymer segment density at the periphery of the brush, which is determined by the grafting density, but also by the degree of polymerization of the grafted polymer. Brushes consisting of long polymer chains, as in the present case (DP = 380, contour length ca. 100 nm) with a ratio of contour length/grafting distance 10:1 are in the moderate-to-dense brush regime with a rather high segment density [44]. Fery et al. have for instance recently studied the influence of different polymeric glassfiber coatings on the interfacial shear strength of epoxy resin based composites [45]. They presented evidence that the grafting density is the most crucial parameter to attain high interfacial adhesion and they found the highest interfacial shear strength for

grafting densities below 0.05 chains per nm^2 . The surface roughness seen in the SEM images (Fig. 5c) is induced by heterogeneities in the grafting density resulting from non-equilibrium structures of adsorbed MI^{n+} . While these heterogeneities trigger segment density variations at the periphery of the coating, this will not allow chain interdigitation needed for good wetting.

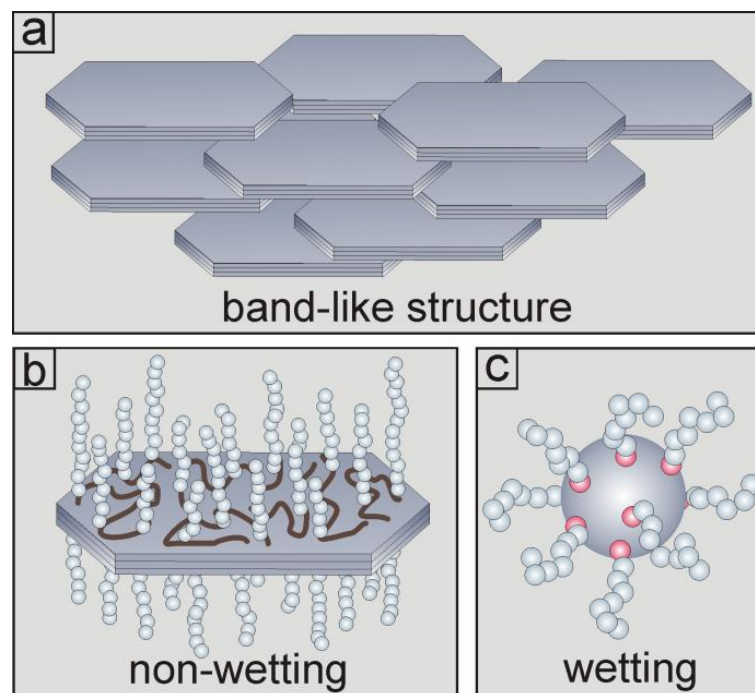


Fig. 11. Schematic representation showing a) drying effect on tactoid resulting in band-like structure agglomerates, b) non-wetting character of platelet-like exhibiting heterogeneities in polymer length and grafting density and c) wetting character of spherical nanoparticles having a high density of grafted polymer brushes from the surface.

This wetting behaviour is quite different from spherical nanoparticles coated by polymer brushes that are wettable even at high grafting density. This is because the density of brushes attached to a spherical particle declines quickly from a dense regime close to the core towards a loose regime at the periphery of the brush layer segment (Fig. 11c). Even at high grafting density, there is a sufficient conformational freedom allowing to interpenetrate with the matrix polymer chains [46]. Therefore, such spherical nanoparticles exhibit a wetting character leading to completely miscible nanofiller.

4. CONCLUSION

Hydrophilic K-nano-mica can be rendered hydrophobic without sacrificing aspect ratio by agglomeration by grafting PMMA brushes from external surfaces modified with a macro-initiator (MI^{n+}). Moreover, for this synthetic clay modification can be restricted to the external basal plans while dehydrated K-ions crosslink interlayers yielding shear-stiff nano-mica. Subsequently, (SI)-ATRP enables a controlled grafting of PMMA brushes propagated from the modified MI/nano-mica surface. For these PMMA coated nano-micas, a vivid birefringence of a nematic phase may be observed with the naked eye alongside a remarkable stability of suspensions in THF. Solution blending yields well dispersed single tactoids in the translucent PMMA-composites. Although significantly improved mechanical properties could be achieved as compared to nanocomposites made with conventional clay fillers, the full potential, as expressed by Halpin-Tsai equations, of the PMMA coated nano-mica can still not be utilized. This is attributed to the non-wetting character of the densely packed PMMA brushes attached to planar nanoplatelets.

ACKNOWLEDGEMENTS

The authors would like to thank Lena Geiling for here help in the compounding experiments and for SEM images. The financial support from the Deutsche Forschungsgemeinschaft in the frame of the Collaborative Research Centre (SFB) 840 is highly acknowledged.

REFERENCES

- [1]. H. Fischer, *Mater. Sci. Eng.*, C 23 (2003) 763-772.
- [2] P.C. LeBaron, Z. Wang, T.J. Pinnavaia, *Appl. Clay Sci.* 15 (1999) 11-29.
- [3] K. Tamura, S. Yokoyama, C.S. Pascua, H. Yamada, *Chem. Mater.* 20 (2008) 2242-2246.
- [4] L.A. Utracki, M. Sepéhr, E. Boccaleri, *Polym. Adv. Technol.* 18 (2007) 1-37.
- [5] Q. Wang, X. Zhang, J. Zhu, Z. Guo, D. O'Hare, *Chem. Commun.* 48 (2012) 7450-7452.
- [6] D.A. Kunz, J. Schmid, P. Feicht, J. Erath, A. Fery, J. Breu, *ACS Nano* 7 (2013) 4275-4280.
- [7] K.S. Triantafyllidis, P.C. LeBaron, I. Park, T.J. Pinnavaia, *Chem. Mater.* 18 (2006) 4393-4398.
- [8] M.W. Möller, D.A. Kunz, T. Lunkenbein, S. Sommer, A. Nennemann, J. Breu, *Adv. Mater.* 24 (2012) 2142-2147.
- [9] M.R. Schütz, H. Kalo, T. Lunkenbein, J. Breu, C.A. Wilkie, *Polymer* 52 (2011) 3288-3294.
- [10] B. Fischer, M. Ziadeh, A. Pfaff, J. Breu, V. Altstädt, *Polymer* 53 (2012) 3230-3237.
- [11] R.A. Vaia and H.D. Wagner, *Mater. Today* 7 (2004) 32-37.
- [12] E. Manias, *Nature Mater.* 6 (2007) 9-11.
- [13] M. Si, T. Araki, H. Ade, A.L.D. Kilcoyne, R. Fisher, J.C. Sokolov, M.H. Rafailovich, *Macromolecules* 39 (2006) 4793-4801.
- [14] J. Breu, K.J. Range, E.E. Kohler, U. Wagner, *Appl. Clay Sci.* 8 (1993) 313-320.
- [15] H.M. Köster, *Clay Miner.* 31 (1996) 417-422.
- [16] K. Vogt and H.M. Köster, *Clay Miner.* 13 (1978) 25-43.
- [17] D.A. Brune and J. Bicerano, *Polymer* 43 (2002) 369-387.
- [18] M.W. Möller, U.A. Handge, D.A. Kunz, T. Lunkenbein, V. Altstädt, J. Breu, *ACS Nano* 4 (2010) 717-724.
- [19] N. Sheng, M.C. Boyce, D.M. Parks, G.C. Rutledge, J.I. Abes, R.E. Cohen, *Polymer* 45 (2004) 487-506.
- [20] M. Bieligmeyer, S.M. Taheri, I. German, C. Boisson, C. Probst, W. Milius, V. Altstädt, J. Breu, H.W. Schmidt, F. D'Agosto, S. Förster, *J. Am. Chem. Soc.* 134 (2012) 18157-18160.
- [21] K. Matyjaszewski, P.J. Miller, N. Shukla, B. Immaraporn, A. Gelman, B.B. Luokala, T.M. Siclovan, G. Kickelbick, T. Vallant, H. Hoffmann, T. Pakula, *Macromolecules* 32 (1999) 8716-8724.
- [22] D. Lerari, S. Peeterbroeck, S. Benali, A. Benaboura, P. Dubois, *J. Appl. Polym. Sci.* 121 (2011) 1355-1364.
- [23] H. Zhao, S.D. Argoti, B.P. Farrell, D.A. Shipp, *J. Polym. Sci. A Polym. Chem.* 42 (2004) 916-924.

- [24] H. Kalo, M.W. Möller, M. Ziadeh, D. Dolejs, J. Breu, *Appl. Clay Sci.* 48 (2010) 39-45.
- [25] M. Ziadeh, B. Chwalka, H. Kalo, M.R. Schütz, J. Breu, *Clay Miner.* 47 (2012) 341-353.
- [26] Y. Cai and S.P. Armes, *Macromolecules* 38 (2004) 271-279.
- [27] H. Bottcher, M.L. Hallensleben, S. Nuß, H. Wurm, J. Bauer, P. Behrens, *J. Mater. Chem.* 12 (2002) 1351-1354.
- [28] F.A. Plamper, M. Ruppel, A. Schmalz, O. Borisov, M. Ballauff, A.H.E. Müller, *Macromolecules* 40 (2007) 8361-8366.
- [29] M. Ejaz, Y. Tsujii, T. Fukuda, *Polymer* 42 (2001) 6811-6815.
- [30] M. Husseman, E.E. Malmström, M. McNamara, M. Mate, D. Mecerreyes, D.G. Benoit, J.L. Hedrick, P. Mansky, E. Huang, T.P. Russell, C.J. Hawker, *Macromolecules* 32 (1999) 1424-1431.
- [31] T. Wu, K. Efimenko, P. Vlcek, V. Šubr, J. Genzer, *Macromolecules* 36 (2003) 2448-2453.
- [32] I. Langmuir, *J. Chem. Phys* 6 (1938) 873-896.
- [33] L. Onsager, *Ann. N. Y. Acad. Sci.* 51 (1949) 627-659.
- [34] E. DiMasi, J.O. Fossum, T. Gog, C. Venkataraman, *Phys. Rev.* 64 (2001).
- [35] H. Hemmen, N.I. Ringdal, E.N. De Azevedo, M. Engelsberg, E.L. Hansen, Y. Méheust, J.O. Fossum, K.D. Knudsen, *Langmuir* 25 (2009) 12507-12515.
- [36] J.C. Gabriel, C. Sanchez, P. Davidson, *J. Phys. Chem.* 100 (1996) 11139-11143.
- [37] P. Davidson and J.C. Gabriel, *Curr. Opin. Colloid Interface Sci.* 9 (2005) 377-383.
- [38] R.R. Tiwari and U. Natarajan, *Polym. Int.* 57 (2008) 738-743.
- [39] P. Meneghetti and S. Qutubuddin, *Thermochim. Acta* 442 (2006) 74-77.
- [40] J.H. Liaw, T.Y. Hsueh, T.S. Tan, Y. Wang, S.M. Chiao, *Polym. Int.* 56 (2007) 1045-1052.
- [41] D.A. Kunz, J. Erath, D. Kluge, H. Thurn, B. Putz, A. Fery, J. Breu, *ACS Appl. Mater. Interfaces* 5 (2013) 5851-5855.
- [42] D.A. Kunz, E. Max, R. Weinkamer, T. Lunkenbein, J. Breu, A. Fery, *Small* 5 (2009) 1816-1820.
- [43] S. Yamamoto, M. Ejaz, Y. Tsujii, T. Fukuda, *Macromolecules* 33 (2000) 5608-5612.
- [44] L.C.H. Moh, M.D. Losego, P.V. Braun, *Langmuir* 27 (2011) 3698-3702.
- [45] C. Kuttner, A. Hanisch, H. Schmalz, M. Eder, H. Schlaad, I. Burgert, A. Fery, *ACS Appl. Mater. Interfaces* 5 (2013) 2469-2478.
- [46] S. Fischer, A. Salcher, A. Kornowski, H. Weller, S. Förster, *Angew. Chem. Int. Ed.* 50 (2011) 7811-7814

Supporting Information

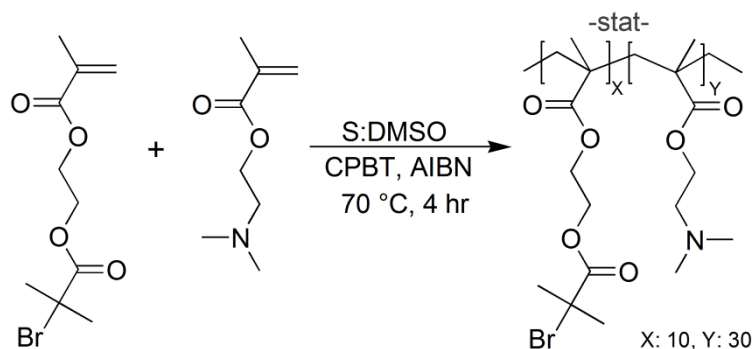


Fig. S1. Synthesis of the statistical copolymer poly(2-(2-(bromoisobutyryloxy) ethyl methacrylate)-stat-(2-(dimethylamino) ethyl methacrylate) (MIⁿ⁺).

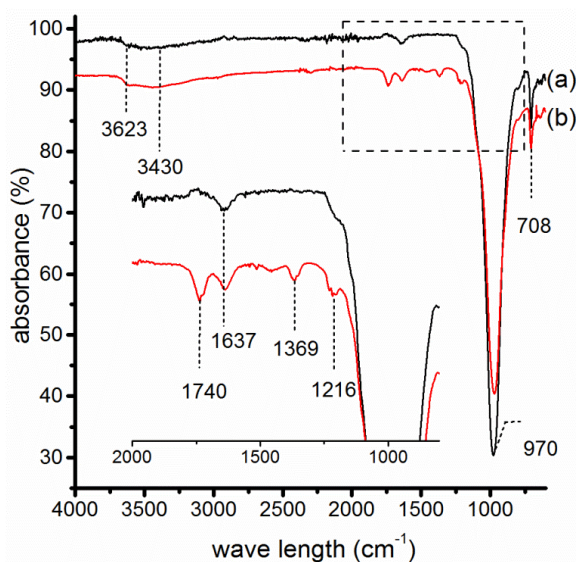


Fig. S2. FT-IR spectra of a) nano-mica and b) MI/nano-mica (modified at pH= 7.2). The nano-mica spectrum exhibits peaks for Si–O out-of-plane bending at 708 cm⁻¹ and the Si–O stretching band at 970 cm⁻¹. The HOH bending at 1637 cm⁻¹ and the wide vibration of OH stretching band in the range 3600-3100 cm⁻¹ are observed [1]. After modification with MI distinguished peaks are assigned to the CO and C–O vibrations at 1740 and 1216 cm⁻¹, respectively. Peak at 1370 cm⁻¹ is associated with the CH₃ groups in DMAEMA and BIEM.

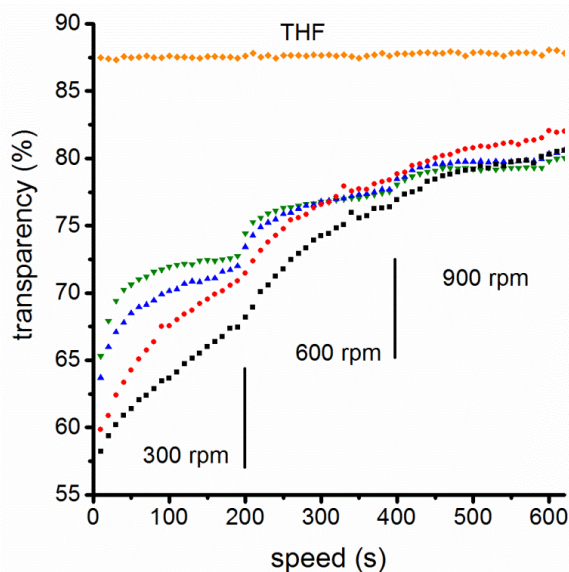


Fig. S3. Integrated transparency of 0.5 wt% dispersions of MI/nano-mica in THF under time dependent centrifugal forces of 300, 600 and 900 rpm. Modification with MI is dependent on pH which is related to the degree of protonation (θ) [2]. (∇) pH= 4.6; θ = 100%, (\blacktriangle) pH= 5.5; θ = 75%, (\bullet) pH= 6.4; θ = 50% and (\blacksquare) pH= 7.2; θ = 25%.

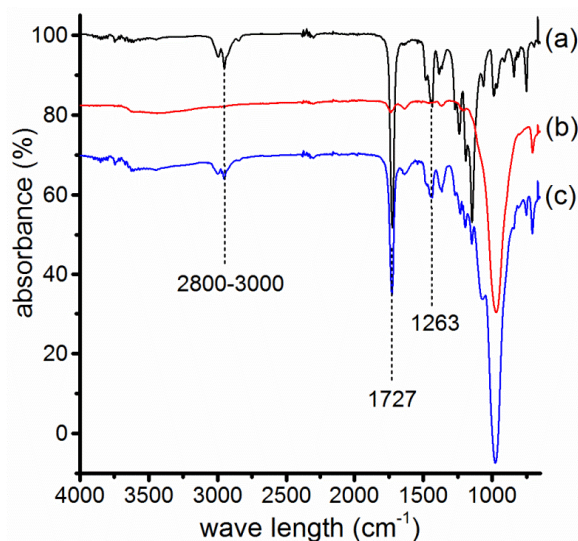


Fig. S4. FT-IR spectra of a) neat PMMA, b) surface modified MI/nano-mica and c) long PMMA coated nano-mica. Characteristic CH vibrations ($2800\text{-}3000\text{ cm}^{-1}$), C=O vibration (1727 cm^{-1}) and C–O vibration (1263 cm^{-1}) confirm the presence of PMMA on the surface even after extensive washing with THF.

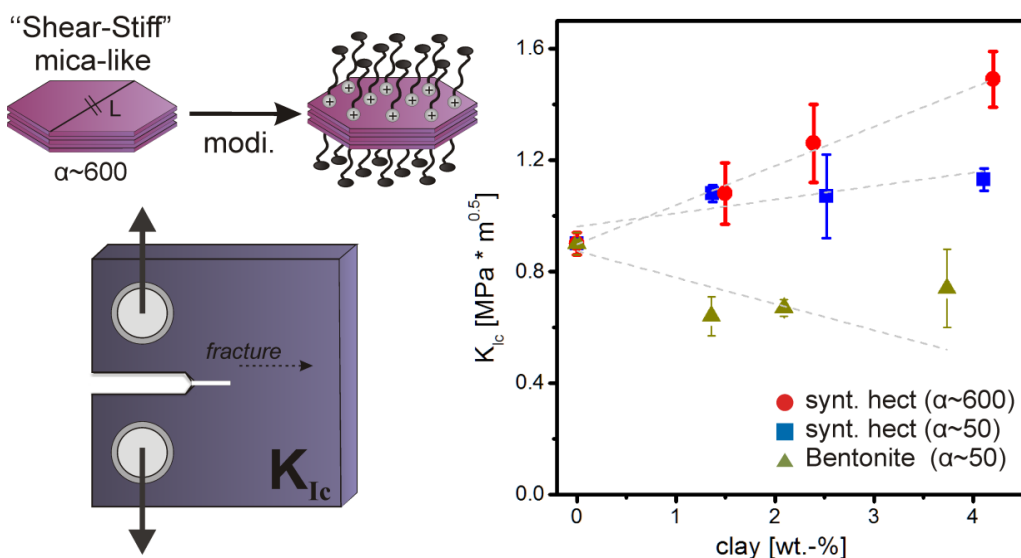
1. P.Komadel, J.Madejova, M.Janek, W.P.Gates, R.J.Kirkpatrick and J.W.Stucki, *Clays Clay Miner.* 44 (1996) 228-236.
2. F.A.Plamper, M.Ruppel, A.Schmalz, O.Borisov, M.Ballauff and A.H.E.Müller, *Macromolecules* 40 (2007) 8361-8366.

4.3. Impact of large aspect ratio, shear-stiff, mica-like clay on mechanical behaviour of PMMA/clay nanocomposites

Bianca Fischer^{a*}, Mazen Ziadeh^{b*}, Andre Pfaff^b, Josef Breu^a, Volker Altstädt^{b*}

*these authors contributed equally to this publication

Published in: Polymer (2012), 53 (15), 3230-3237



^aLehrstuhl für Polymere Werkstoffe and ^bLehrstuhl für Anorganische Chemie I Universität Bayreuth, Universitätstr. 30, 95447 Bayreuth

*Corresponding Author: altstaedt@uni-bayreuth.de (V. Altstädt)

Author's individual contributions:

This publication was in collaboration with the department of polymer engineering of Prof. Dr. Ing.- Volker Altstädt at Bayreuth University.

Preparation of nanoplatelets with two aspect ratios (~55 and 600) was done by me using a stirred media mill to exfoliate highly hydrated Mg-fluorohectorite nanoplatelets (**Chapter 2.1**). I have carried out the synthesis of the polycationic macro-initiator, the selective modification, and the freeze-drying of the nanofillers prior to melt compounding. All the characterizations of the employed nanofillers were done by me as well including FT-IR, PXRD, BET and SLS.

The melt compounding of the various nanofillers in a PMMA matrix using the twin-screw micro extruder was done by Florian Billing (Polymer Engineering).

Mechanical testing and the evaluation of the mechanical properties were done by *Bicana Fischer* (Polymer Engineering).

The academic writing related to the preparation and characterization of the employed nanofillers was done mainly by me and Prof. Dr. *Josef Breu*. The academic writing of the section related to, mechanical testing and evaluation of the PMMA/clay nanocomposites was done by Prof. Dr. Ing.- *Volker Altstädt, Bianca Fischer and André Pfaff*.

The manuscript is published in **Polymer**.

My contribution to this publication is 50%.

Impact of Large Aspect Ratio, Shear-Stiff, Mica-Like Clay on Mechanical Behaviour of PMMA/Clay Nanocomposites

Bianca Fischer^a, Mazen Ziadeh^b, André Pfaff^a, Josef Breu^b, Volker Altstädt^{a*}

Department of Polymer Engineering¹ and Inorganic Chemistry I²
University of Bayreuth, Universitaetsstr. 30, 95447 Bayreuth, Germany

* Corresponding author. Tel.: þ49 921557471; fax: þ49 921557473.
E-mail address: altstaedt@uni-bayreuth.de (V. Altstädt).

(Received 14 March 2012 accepted 28 April 2012 and available online 11 May 2012)

ABSTRACT

For the first time poly(methyl methacrylate) (PMMA) nanocomposites based on a synthetic shear-stiff, mica-like K-fluorohectorite clay were prepared by melt-compounding. Besides stiffness, this new synthetic type of clay offers very high aspect ratios above 600 after exfoliation, whereas a tailored surface modification of the clay yielded a good compatibility to the matrix material. The influence of different clay content (0 – 4 wt.-%) on mechanical behaviour of PMMA/clay nanocomposites were studied for two aspect ratios (≈ 55 and ≈ 620), set into correlation with morphology and compared to natural montmorillonite (MMT) clay, which has an aspect ratio of ≈ 50 . It was found, that the use of these novel nanoplatelets leads to a significantly increased fracture toughness of about 25 and 70% in the case of an aspect ratio of 55 and 620, respectively, in comparison to neat PMMA, without sacrificing tensile strength. Scanning electron microscopy (SEM) analysis of the corresponding fracture surfaces and μ -computer tomography (μ -CT) revealed a high dispersion quality of the synthetic organo-clay in PMMA. Different fracture mechanisms could be identified. The presence of the nanofiller varies the local stress state in the matrix and promotes additional energy dissipating mechanisms like crack deflection, crack pinning as well as debonding effects with platelets pull-out leading to enhanced fracture toughness.

Keywords: Mica-like nanofiller, large aspect ratio, poly(methyl methacrylate), nanocomposites, melt-compounding, mechanical properties

1. INTRODUCTION

Since the first studies performed by researchers from Toyota in 1985, the rapid development of polymer/clay nanocomposites brings continuous improvement of the overall properties of such materials along [1-8]. Besides the mechanical properties of the filler itself, the key issues that significantly influence the resulting properties are the aspect ratio and the quality of the surface modification of the nanofiller. Commercially available organically modified clays have the drawback that they have limited aspect ratios < 100 and a high heterogeneity of surface charge. Furthermore, during melt compounding the delamination of tactoids is hardly ever complete, which reduces the maximal possible aspect ratios and therefore the desired properties. So it is an important step to use synthetic clay, which allows higher dispersion quality in the polymer matrix together with much higher aspect ratios as compared to natural clay.

PMMA is a glassy polymer, which offers excellent properties for the packaging industry [9] and optical [10] or biomedical [11] sector due to its high strength, optical clarity, desirable dimensional stability and weatherability. However, due to its high stiffness, PMMA shows a high brittleness that limits the potential application areas. Therefore it is predominantly of interest to improve the toughness of this material without sacrificing optical or mechanical properties. Blending or copolymerisation with rubber implies the drawback of a decreased stiffness and strength [12]. Due to the high surface area and the small interparticle distances, nanoparticles can alter the local stress state in the matrix polymer and promote additional forms of energy dissipation, e.g. multiple crazing, crack deflection, crack pinning and particle / matrix debonding, leading to a tougher material [13].

Despite melt processing is the relevant method for many industrial applications of nanocomposites, relatively few studies exist on the processing of PMMA/clay nanocomposites. It is reported that the use of commercially available organo-clay for melt-compounding increases the stiffness for PMMA while embrittlement takes place, caused by unsatisfactory dispersion quality of the nanoclay in the PMMA matrix [14]. Therefore, it is very challenging to incorporate synthetic organo-clay with a large platelets diameter to thickness ratio (L/h) and to achieve a high

dispersion quality. In this study, novel synthetic modified, mica-like, shear-stiff K-fluorohectorite (K-lect) clay is used. In order to improve the dispersion of the nanofiller a strategy was applied with no need for exfoliation and intercalation. In addition to the better dispersion, by achieving a high aspect ratio beside an increased E-modulus also an increased fracture toughness of PMMA is expected.

The preparation method applied for the clay allowed for adjusting aspect ratios in a controlled way, whereas, a subsequent surface modification should guarantee the compatibility between nanofiller and polymer matrix. This novel synthetic nanofiller is dispersed in the matrix during melt compounding but no further desagglomeration and exfoliation is necessary or intended during compounding. The tailored surface modification is based on anchoring of polymer chains bearing multiple quaternized amino groups on the external basal planes of the synthetic K-lect, which yielded a synthetic organo-clay (O-lect) and assured a high quality of dispersion.

A series of PMMA/clay nanocomposites was prepared by melt compounding with various clay concentrations and two different aspect ratios, i. e. 55 and 620. The low aspect ratio of the synthetic clay (55) is roughly the same as in the commercial Bentone, which allows for a commendable comparison and highlights the advantages of the novel synthetic clay. The microstructure and mechanical properties were investigated and the micromechanics of the observed deformation behaviour was analysed in detail.

2. EXPERIMENTAL

2.1. Materials

A commercial PMMA (Plexiglas POQ62 supplied by Evonik Industries) has been used as matrix material. To detect possible degradation during processing the molecular weight and polydispersity index were determined before and after processing of the material via gel permeation chromatography. Before and after processing a molecular weight (M_w) of 73 kg/mol and a polydispersity index of 1.63 were determined. The commercial clay Bentone 38 modified with alkyl-ammonium chains was supplied by Elementis Specialties, which has a CEC of 70 mequiv. / 100g. The starting material for the preparation of the novel nanofiller is

a synthetic Na-fluorohectorite with the chemical formula $\text{Na}_{0.5}[\text{Mg}_{2.5}\text{Li}_{0.5}]\text{Si}_4\text{O}_{10}\text{F}_2$ and a CEC of 110 mequiv./ 100g [15].

2.2. Tuning of large aspect ratio and functionalization of the filler

The synthetic Na-fluorohectorite (Na-hect) was suspended in deionized water and then processed in a stirred media mill in order to exfoliate the tactoid stacks by applying shear forces. The degree of exfoliation was controlled by the number of milling passages [16]. This was done using a highly hydrated 'shear-labile' state, represented by the presence of Mg^{2+} cations (Mg-hect) in the interlayer space (Fig. 1). Subsequent to the exfoliation process the clay samples were exchanged with K^+ cations which transformed the clay to a non-swollen 'shear-stiff', mica-like state with no intracrystalline reactivity [17].

Due to the inertness of the interlayer space, this mica-like material allows for a selective cation exchange limited to the external basal planes of the clay. Consequently, the hydrophilic nanoplatelets can be converted to hydrophobic fillers compatible with the organic matrix by applying polycations in the cation exchange. The surface modifier chosen by us was a polycationic statistical copolymer, poly(2-(2-bromoisobutyryloxy)ethyl methacrylate)-stat-(2-dimethyl-aminoethyl methacrylate) (PBD, Fig. 1). Moreover, the surface modification concomitantly triggered flocculation of K-hect. PBD (1gL^{-1}) was quaternized and dissolved in water by adding equimolar amounts of concentrated acetic acid and this solution was added to the aqueous dispersions of K-hect obtained after milling until the clay was fully flocculated. Subsequently, the surface modified shear-stiff, mica-like O-hect was washed several times with deionized water and finally freeze-dried.

2.3. Preparation of the PMMA/clay nanocomposites

The commercial Bentone and the synthetic O-hect with two different aspect ratios were melt-compounded at various concentrations with PMMA in a discontinuous counter-rotating twin-screw microcompounder (DSM Xplore, 15 ml microcompounder) at a temperature of 190 °C, a mixing speed of 210 rpm and a mixing time of 3 min. The material was added stepwise to the running microcompounder and during each cycle a batch of 7.3 g was processed. After extrusion, the extruded flakes were compression-moulded with a Hot-Plate-Press

(190 °C, under vacuum) into CT (compact-tension) specimens to determine the critical stress intensity factor K_{Ic} or injection-moulded with a microinjector (DSM Xplore 12 ml injection moulding machine; melt temperature: 190 °C; mould temperature: 40 °C; injection pressure: 8 bar) into dumbbell specimens (75 mm x 5 mm x 2 mm) for tensile testing.

2.4. Characterisation of the clay

Powder X-ray diffraction (PXRD)

The degree of exfoliation of Mg-hect was determined by PXRD. The PXRD patterns were obtained in reflection mode using nickel filtered Cu-K α radiation $\lambda = 1.54187$ Å on a Bragg-Brentano-geometry diffractometer (PANalytical Xpert-Pro) equipped with an X'Celerator Scientific RTMS detector. The "Full Width at Half Maximum" (FWHM) of the 001 reflection was determined and related to the thickness of the platelets applying the Scherer equation [18-19].

Fourier transform infrared analysis (FTIR)

FTIR spectra were recorded on a Nicolet FTIR 460 spectrometer at a resolution of 4.0 cm⁻¹ at room temperature in a wave number range between 4000 and 550 cm⁻¹ and averaged over 12 scans.

Thermal gravimetric analysis (TGA)

The amount of modifier on external platelets was assessed by TGA and carried out with a TGA/STDA 851e from Mettler Toledo. The samples were heated up to 700 °C at a heating rate of 10 K/min under nitrogen atmosphere.

Specific surface (BET)

The specific surface areas of freeze-dried Bentone and K-hect samples were calculated using the BET equation from the adsorption/desorption isotherms. Measurements were carried out on a Quantachrome Nova 2000e analyzer. The specific surface area was determined using 5-points within the range of $0.09 < p/p_0 < 0.3$ using N₂ as adsorption gas. Prior to measurement, all samples were carefully degassed overnight at 150 °C under ultra high vacuum to remove adsorbed water.

Static Light Scattering (SLS)

The particle size distributions (PSD) curves were recorded from aqueous dispersions (~1% solid content) of milled Mg-hect on a Retsch Horiba LA-950 static light scattering instrument.

2.5. Nanocomposite characterisation

Scanning Electron Microscopy (SEM)

A scanning electron microscope Leo 1530 Gemini (Zeiss) was used to image the fracture surfaces of the PMMA/clay nanocomposites to analyse the dispersion quality of the nanofiller and the micromechanical reason for fracturing. For this purpose the specimens were spattered with 1.3 nm of platinum.

Micro-computer tomography (μ -CT)

Monitoring of agglomerates was carried out using a Skyscan X-Ray Microtomography 1072 with a maximum spot resolution of 5 μ m per pixel. The measurements were done at a voltage of 80 kV and a current of 94 μ A. The cylindrical specimens were 4 mm in diameter and height. The 3D-data is obtained by acquisitions every 0.23° with an exposure time of 1.5 s up to a complete rotation of 360°. 3-D volumetric images were digitally reconstructed by using the software “NRecon” from Skyscan.

Mechanical testing

Tensile modulus, tensile strength and elongation at break were measured with a Universal Tensile Tester according to ISO 527 with a strain rate of 1 mm/min. For each material at least 5 samples were tested. The elongation was determined with a macro-displacement-transducer.

Fracture toughness tests were performed according to ISO 13586 to obtain the mode-I critical stress intensity factor (K_{Ic}) of the PMMA/clay nanocomposites. At least 5 notched, compact tension specimens are tested with a strain rate of 10 mm/min. The thickness of the specimens was 4 mm.

3. RESULTS AND DISCUSSION

3.1. Tailoring of mica-like nanofiller

The remarkable characteristics of the synthetic Na-hect prepared by melt synthesis include large median particle sizes (D_{50} : 20 μm) and a homogenous charge distribution [15]. The latter is essential for allowing to switching between different states of hydration. If the charge density is homogeneous, fixing the right layer charge during synthesis makes it possible to transform the material from highly hydrated to non-swollen by simple cation exchange. Möller et.al. showed that Mg-hect is highly hydrated and this material consequently is 'shear-labile' and can be efficiently exfoliated by applying shear forces [17]. The degree of exfoliation can be controlled by adjusting various parameters, which control the total shear forces such as solid content, grinding media and time of the process [16]. Subsequently, by simple cation exchange with K^+ cations a collapsed non-swollen and thus shear-stiff, mica-like material can be obtained (Fig. 1).

In this collapsed state the interlayer is no longer accessible for cation exchange, allowing for selective modification, which is restricted solely to the external basal plans of the platelets. The modifier used to reduce the surface tension of the hydrophilic platelets is a polycationic statistical copolymer.

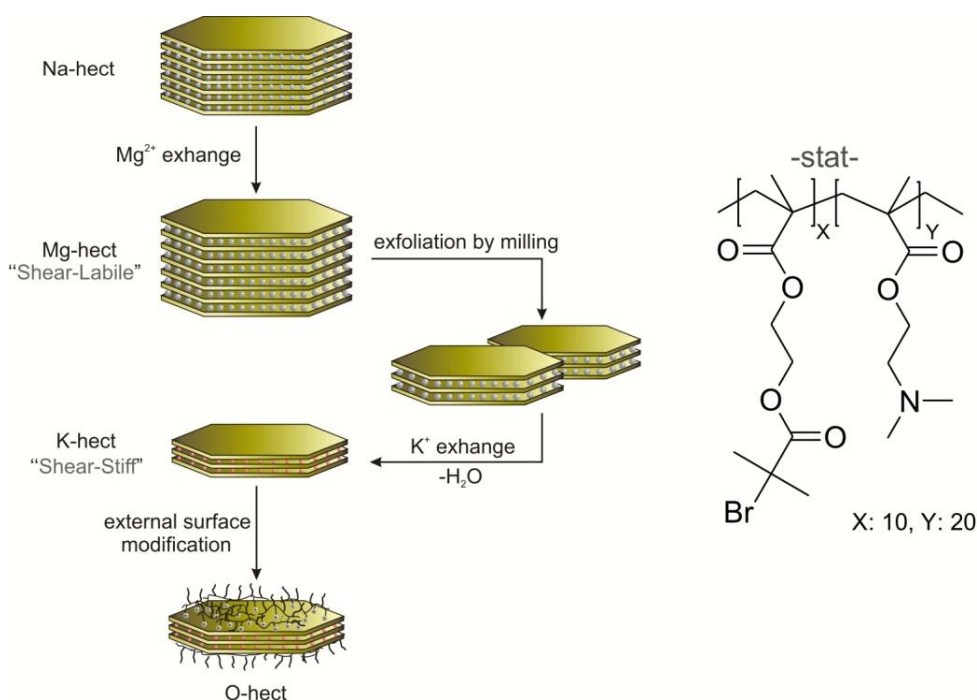


Fig. 1. (Left) synthetic pathway for preparation of O-hect; (Right) chemical structure of the polycationic macro-initiator.

The exchange procedure with the charged polycationic modifier leads to the organophilization of the platelets (hydrophobic state), which turned hydrous suspensions instable and allowed for easy recovery of the O-hect.

FTIR analysis in Fig. 2 compares the FTIR spectra of K-hect before and after surface modification (O-hect). The K-hect spectrum exhibits peaks for SiO out-of-plane bending at 708 cm^{-1} and also a SiO stretching band at 970 cm^{-1} . Furthermore, HOH bending at 1637 cm^{-1} and a wide vibration of OH stretching band in the range $3600\text{-}3100\text{ cm}^{-1}$ is observed. After modification with PBD distinguished peaks that can be assigned to the C=O and CO vibrations at 1735 and 1216 cm^{-1} , respectively, can be found.

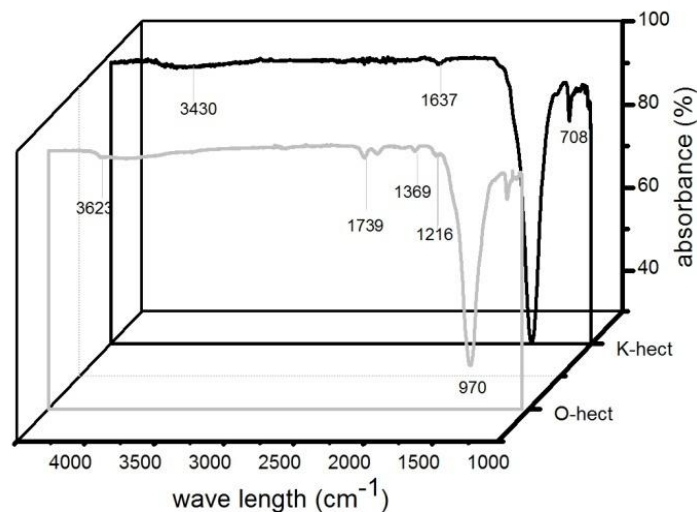


Fig. 2. FT-IR spectra of (a) K-hect and (b) O-hect (after organophilization).

PXRD patterns give a direct proof of the exclusive modification of external surfaces of the shear-stiff, mica-like K-hect and consequently of the organophilization. Comparing the two basal reflections of the K-hect before and after surface modification (Fig. 3), no shifts can be detected for the typical basal spacing of non-hydrated, mica-like 2:1 layered silicates at 6.12° (9.9 \AA).

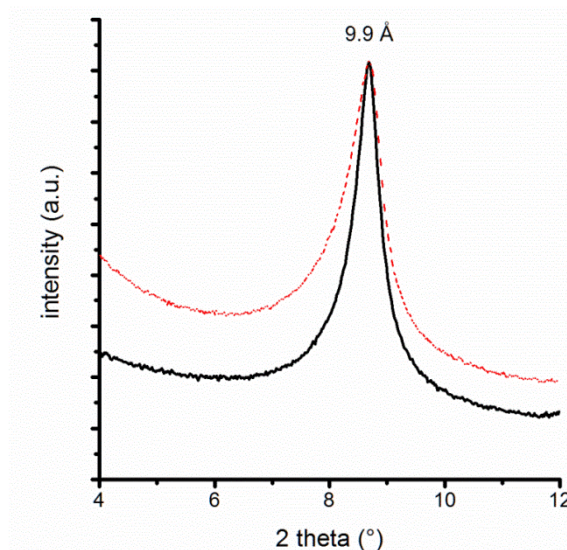


Fig. 3. PXRD patterns of K-hect (—) and O-hect (- - -).

Hence, the modifier does not intercalate into the interlayers of the mica-like platelets but is exclusively bound to the external surface of the platelets. As compared to natural clays, significantly less amount of modifier is needed by avoiding any intercalation of the organic modifier in the interlayer. While Bentone contains up to 30 wt.-% of modifier, the O-hect contains as little as 8 wt.-% as determined by the mass lost between 200 and 500 °C obtained by TGA measurements.

3.2. Characterization of the nanofiller

Determination of the average aspect ratio would indeed require the simultaneous measurement of both thickness and lateral extension of a statistical significant number of individual clay platelets. While AFM delivers height and extension of platelets concomitantly, measurement of large numbers is very time-consuming and thus impractical. Therefore, we have previously introduced a simple method that allows a rough estimation of an average aspect ratio [18]. The method correlates the tactoid thickness as determined by the Scherrer equation with the value of the total specific surface area. The contribution of the edges is accounted for by assuming a uniform and ideal hexagonal morphology of the platelets. The median particle size diameter (D_{50}) is used as the lateral extension of this uniform hexagonal platelet. Please note, that it has been shown by Goossens [21] that the lateral extensions of tactoids correlate well with the hydrodynamical radius obtained from SLS. For details see the supporting information of Möller et al [18].

Table 1 lists the derived aspect ratios together with the experimental data used for their derivation.

Table 1. Collected data of the synthetic clay and Bentone 38

Type	Average aspect ratio	Milling time [min]	FWHM [°]	BET surface (N ₂) [m ² /g]	D ₅₀ [μm]	D ₉₀ [μm]
K-hect ₅₀	55	-	0.08	2	20.12	58.92
K-hect ₆₀₀	620	130	0.44	69	6.80	8.62
Bentone	50	-	-	4	0.36	0.63

Assuming that no aggregation occurred during freeze-drying, the BET values would directly correlate to the external basal planes of the tactoids. As expected, BET areas increased significantly by exfoliation during milling. At the same time, the FWHM increased significantly again supporting efficient exfoliation of tactoids by milling. Not surprisingly, particle diameters also were reduced during milling. Two effects contributed to this reduction, some breakage of tactoids [22] along with the destruction of agglomerates obtained in the melt synthesis. After compounding of the clay with PMMA, the size distribution of the platelets was determined again. For this the compounds were dissolved in tetrahydrofuran (THF), the fillers were collected by centrifugation, redispersed in THF before the PSD were determined by SLS.

The median D₅₀ were in good agreement with the values cited in Table 1 (19.80 and 6.80 μm for O-hect₅₀ and O-hect₆₀₀, respectively). Clearly, processing did not change the PSD. The aspect ratio can be sustained during melt compounding as the clay has a very high shear-stiffness and no change in platelet size occurs. While from the raw data, it is not obvious how the competing mechanisms of particle exfoliation and breakage transform into aspect ratio, our method of estimation showed that it was indeed improved significantly from 55 to 620 by milling. To be consistent, the average aspect ratio of the commercial Bentone was also listed in Table 1. While the value appears sensible, the absolute value will be more severely affected by band-type aggregates and the influence of random interstratification on the FWHM as compared to the synthetic fluorohectorite samples.

3.3. Mechanical properties of the PMMA/clay nanocomposites

The mechanical properties of neat PMMA and PMMA/clay nanocomposites determined by tensile test and fracture mechanical investigations by K_{Ic} measurements are presented in Fig. 4-7 as a function of clay content. In each diagram the data points were fitted linearly. By the incorporation of the novel clay, the tensile modulus as well as the fracture toughness of PMMA/clay nanocomposites shows a significant enhancement compared to neat PMMA. The tensile strength is not negatively influenced by the addition of synthetic clay whereas the elongation at break is slightly reduced. The incorporation of Bentone leads to an increase in tensile modulus but the values for tensile strength, strain at break and fracture toughness are significantly reduced [9,23]. This can be explained by the presence of large agglomerates, due to inefficient incompatibility of the filler, acting as stress concentrators and reducing the aspect ratio dramatically.

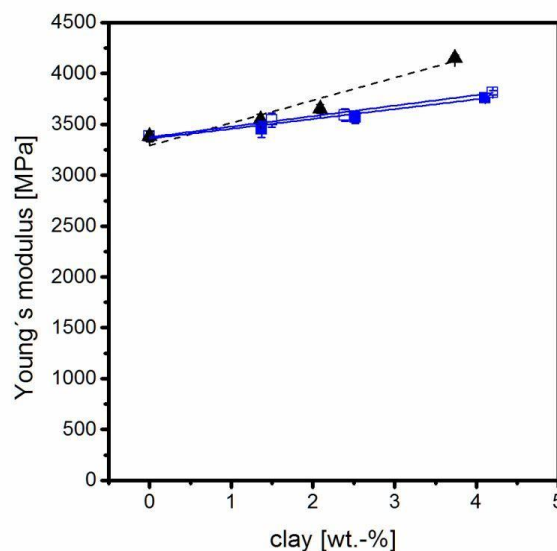


Fig. 4. Effect of clay content on Young's Modulus of PMMA/clay nanocomposites for (▲) Bentone ($\alpha \sim 50$), (□) O-hect ($\alpha \sim 50$) and (■) O-hect ($\alpha \sim 600$).

In general, the addition of rigid nanofillers to a brittle matrix leads to an increase in modulus at the expense of strength, strain and toughness as embrittlement takes place [9,23]. This phenomenon is also observed in this study for PMMA nanocomposites based on Bentone. For synthetic clay nanocomposites an increase of Young's modulus by 11% could be achieved at 4 wt.-% clay content as the clay platelets have a much higher stiffness (~ 50 GPa) than the polymer matrix, leading

to a reinforcing effect. By comparing the synthetic filler with two different aspect ratios, it can be seen that the Young's modulus is not significantly influenced by the aspect ratio. According to the Halpin-Tsai model, a difference in Young's modulus of about 2% between the two aspect ratios is expected for the investigated range of filler loading what is in good agreement with the experimental results. The theoretically possible improvement of Young's modulus, calculated by Halpin-Tsai equations for asymmetric fillers, could be exceeded by the incorporation of this novel clay. Park et al. prepared PMMA/organoclay nanocomposites with an intercalated structure by melt-blending and reported that the tensile modulus increased by 32% at a clay content of 3.8 wt.-% [9]. However, both the tensile strength and the impact toughness were significantly reduced by 50% and 9%, respectively. In addition, Tiwari et al. investigated the mechanical properties of PMMA/organo-modified montmorillonite and found an increase in Young's modulus of 25% at 4 wt.-% clay whereas the impact strength was reduced by 64% [24]. In contrast to these studies, the nanocomposites investigated here show a particularly interesting behaviour, namely constant strength combined with enhanced toughness.

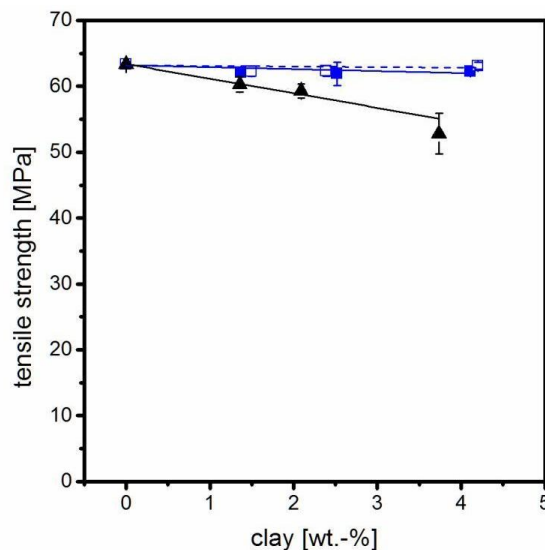


Fig. 5. Effect of clay content on tensile strength of PMMA/clay nanocomposites for (▲) Bentone ($\alpha\sim 50$), (□) O-hect ($\alpha\sim 50$) and (■) O-hect ($\alpha\sim 600$).

Concerning the tensile strength, the addition of the novel clay platelets does not show a significant influence. This phenomenon can be explained by the high dispersion quality of the nanofiller (as observed in scanning electron microscopy

(SEM) images which are presented hereafter). In general, large agglomerates lead to additional local stress concentrations and consequently to lower tensile strengths in the case of brittle polymer matrices [25-26]. The use of a commercial Bentone shows this typical behaviour and leads to a decrease of tensile strength by 16% at a clay amount of 4 wt.-% due to the presence of large agglomerates caused by inefficient dispersion. An increase of the tensile strength is expected to take place in the case of strong interfacial adhesion between the nanofiller and the matrix in order to generate effective stress transfer from the matrix to the filler. In this study it can be assumed that the adhesion between the novel clay platelets and PMMA chains is relatively weak as no change in T_g could be detected by DSC measurements. This behaviour is not unexpected as the modified clay exhibits only very short organic chains on the surface, which improve compatibilization, but are not long enough to entangle with the PMMA chains.

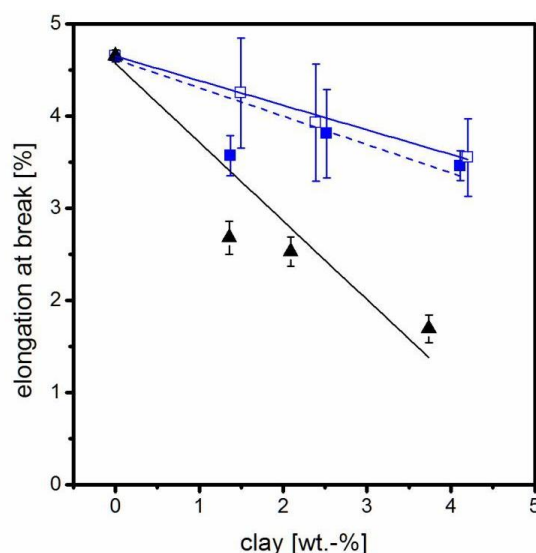


Fig. 6. Effect of clay amount on elongation at break of PMMA/clay nanocomposites (▲) Bentone ($\alpha \sim 50$), (□) O-hect ($\alpha \sim 50$) and (■) O-hect ($\alpha \sim 600$).

Furthermore, the elongation at break decreased with the incorporation of clay into PMMA (Fig. 6). For the synthetic clay nanocomposites it decreased slightly with increasing clay content whereas a reduction of almost 24% is observed at 4 wt.-% filler. However, the nanocomposites based on Bentone show a strong reduction in elongation at break of 65% at a clay amount of 4 wt.-%. This behaviour is reported in literature also for melt processed intercalated polystyrene- and polycarbonate-nanocomposites [26-27]. The presence of clay platelets restricts the sliding of

polymer chains among each other, which can be considered as the reason for lower elongation behaviour of the nanocomposites.

According to literature, a decrease in fracture toughness as expressed by K_{Ic} [9,24] could be expected due to the increasing modulus of PMMA with increasing clay content. This behaviour can be clearly observed in case of the incorporated Bentone composite (Fig. 7). Surprisingly, a significant improvement in K_{Ic} fracture toughness was observed by the incorporation of synthetic clay into PMMA. In the case of low aspect ratio clay, an improvement in fracture toughness of about 25% and in the case of high aspect ratio clay of about 66% at a clay content of 4 wt.-% was observed. However, in the case of low aspect ratio clay one can also observe a plateau-like behaviour above 1 wt.-% clay. This can be attributed to a worse dispersion of clay with increasing concentration, which is confirmed by SEM pictures and μ -CT measurements.

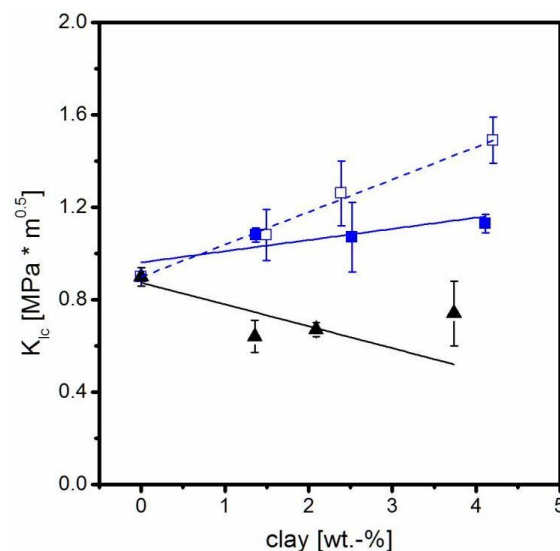


Fig. 7. Effect of clay amount on stress intensity factor of PMMA/clay nanocomposites (\blacktriangle) Bentone ($\alpha \sim 50$), (\square) O-hect ($\alpha \sim 50$) and (\blacksquare) O-hect ($\alpha \sim 600$).

It should be mentioned at this part that the unsatisfying dispersion quality is not related to aggregates in the lower micron size range as it is in the case of Bentone, which could lead to stress concentrations and subsequently to lower tensile strength [28]. However, the worse dispersion restricts most probably the amount of specific interfaces and interactions between filler and polymer chains. The use of clay with high aspect ratio led to an almost linear increase of toughness with clay content up to an improvement of 66% at 4 wt.-% of filler content. Here, the

dispersion quality is not significantly influenced by clay concentration leading to a higher amount of interfaces at high clay contents and more effective energy dissipation. These results demand consideration about the dominating toughening mechanisms.

3.4. Toughening mechanisms and nanocomposite morphology

Several energy-dissipating mechanisms are known for brittle polymers filled with rigid particles whereby mainly thermosetting polymers were investigated [13,24,29]. To analyse the occurring toughening mechanisms, the micromorphology of the fractured surfaces from the K_{Ic} tests of neat PMMA and nanocomposites were investigated via SEM. The crack-propagation direction in all images is from left to right. Fig. 8 shows the micrographs of neat PMMA taken from the centre of the fracture surface in the vicinity of the notched region.

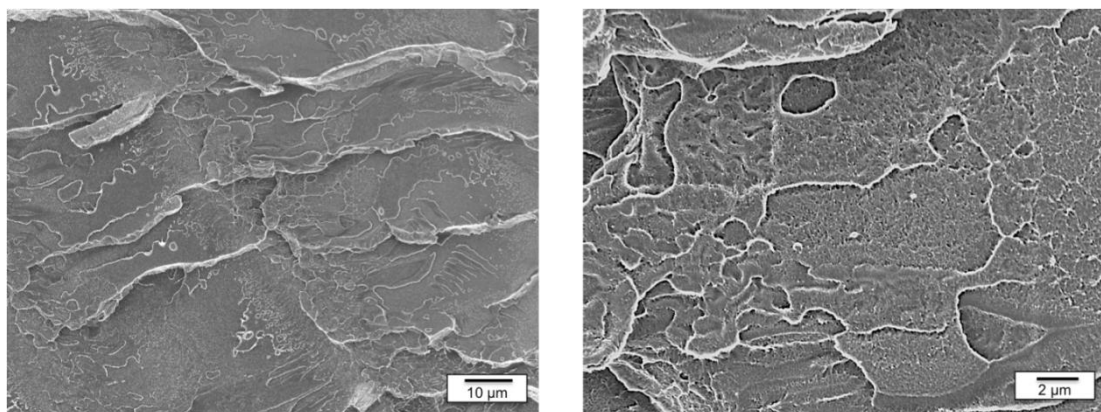


Fig. 8. SEM micrographs of the fracture surface of neat PMMA.

As can be seen neat PMMA possesses the typical smooth failure surface morphology formed by craze formation and growth. In Fig. 9 the fracture surfaces of PMMA/clay nanocomposites are shown.

One can clearly observe that in case of Bentone large agglomerates are formed whereas the synthetic O-hect is better dispersed in the matrix, which can be attributed to the good compatibility of the modified clay platelets and the PMMA matrix. Moreover the clay is tailored to the designated aspect ratios and a shear-stiff state, and consequently dispersion but no further exfoliation is expected to occur during compounding.

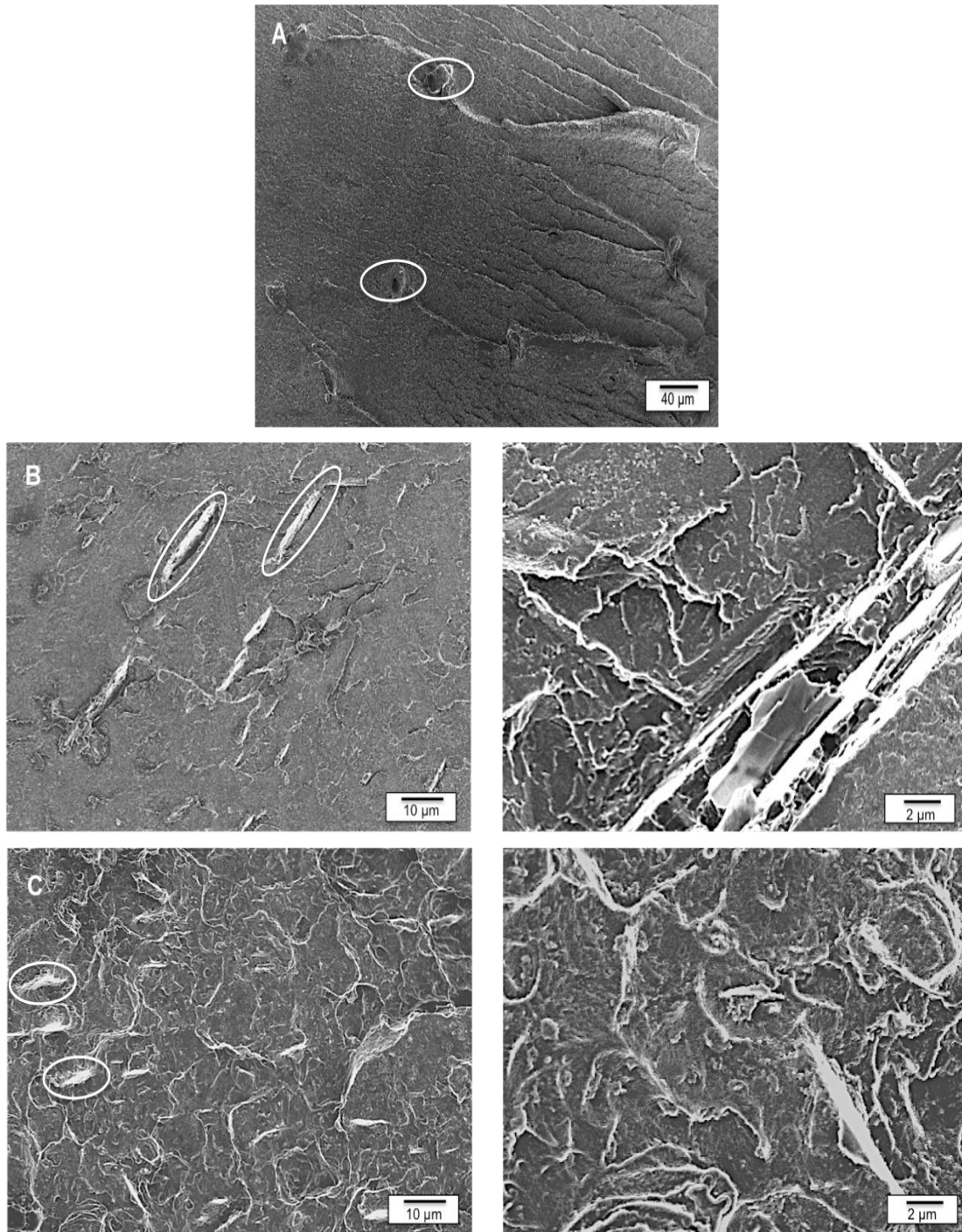


Fig. 9. SEM micrographs of fracture surfaces of PMMA/clay nanocomposites at a clay content of 4 wt.-%. A: Bentone; B: O-hect₅₀; C: O-hect₆₀₀ (crack growth is from left to right); the white cycles highlight selected agglomerates for Bentone and clay platelets for O-hect.

However, the clay with the lower aspect ratio shows a poorer dispersion quality at high concentrations, as seen in Fig. 9 B. This could be caused by agglomerates from melt synthesis. For further investigation of the nanocomposite morphology, μ -CT

measurements were performed in order to generate 3-dimensional representation of filler dispersion (Fig. 10) [30]. The μ -CT measurements support the previous statements regarding dispersion quality. In case of the high aspect ratio clay (620), almost no second phase could be detected indicating excellent dispersion of clay platelets. However, in case of O-hect₅₀ and Bentone, agglomerates were observed. It is worth mentioning that, in terms of O-hect₅₀ the primary particles range between 20 and 58 μm (Table 1) and therefore the detected phase represents both, primary particles and agglomerates. Nevertheless, Bentone particles range between 360 and 630 nm and consequently the entire detected phase is solely agglomerated particles.

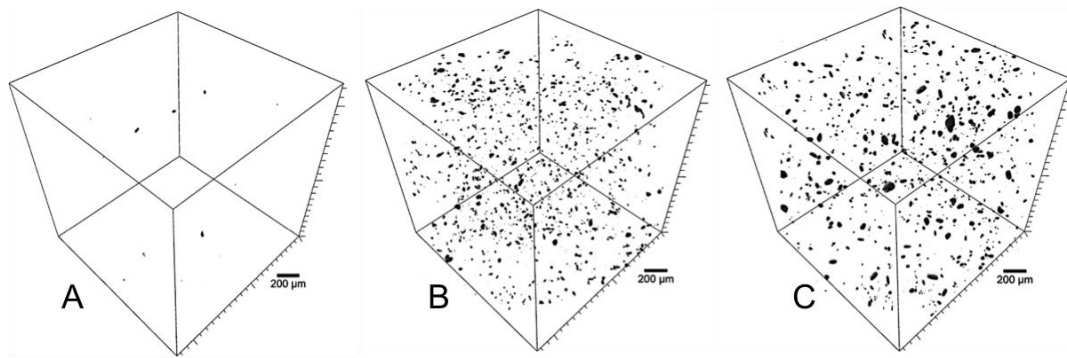


Fig. 10. Three-dimensional reconstruction exhibiting dispersion quality of different nanofillers: A: O-hect₆₀₀; B: O-hect₅₀; C: Bentone (μ - computer tomography).

The SEM images (Fig. 9) confirmed the size of the platelets, which were determined by SLS measurements. As the platelets are sticking out of the matrix, it reveals that during the fracture process, the layered silicates were debonded and pulled out of the PMMA matrix. The surface of the platelets is smooth, which indicates a weak adhesion between the nanofiller and the PMMA matrix. Furthermore, the fracture surfaces of the novel nanocomposites are rougher than neat PMMA, indicating the creation of additional surface area. Crazeing is a local restricted plastic deformation that appears mostly in amorphous polymers or by testing at low temperatures or high strain rates. In PMMA crazeing takes place if the crazeing strength is much lower than the yielding strength leading to craze initiation instead of shear yielding. Further load increase leads to the growth of the crazes due to lower required stress for further growth than for initiation of new crazes. As a result, the craze breaks down into a micro-crack, which leads at the

end to a catastrophic brittle failure of PMMA with a less efficient energy dissipation compared to shear yielding. In the case of PMMA nanocomposites based on Bentone, the incorporation of the filler leads to a reduction in fracture toughness due to the large agglomerates caused by unsatisfied dispersion of the clay in the matrix.

As a consequence of the extreme stress concentrations at these agglomerates, only a few but large crazes are initiated that break down into a micro-crack without much energy dissipating. To further improve the fracture toughness of PMMA, it must be ensured that massive crazes are initiated over a huge volume of material ahead of the main crack tip and hence more energy can be dissipated before fracture occurs. In the novel PMMA/clay nanocomposites, the highly dispersed rigid layered silicates act as stress concentrators that initiate a large number of crazes as indicated by the rough surface structure (Fig. 10). This results in a high amount of localized energy dissipation. Other important fracture events, which contribute to energy dissipation in nanocomposites are crack deflection and crack pinning.

During crack deflection, the crack is forced to alter the initial propagation plane by striking platelets leading to an increased total fracture surface (Fig. 11A). Pinning the surfaces of the cracks by the platelets slows down the development of crazes into microcracks and a higher stress level is needed for further craze growing (Fig. 11B). Additional stress loading leads to debonding along the PMMA/clay interface due to weak adhesion and subsequent to the formation of micro-voids and finally to platelets pull-out (Fig. 11C). The initiation of micro-voids consumes additional energy as well as the extension of the micro-voids and the pull-out of platelets. Debonding occurs, as the interfacial strength between PMMA and layered silicates is lower than the fracture strength of PMMA.

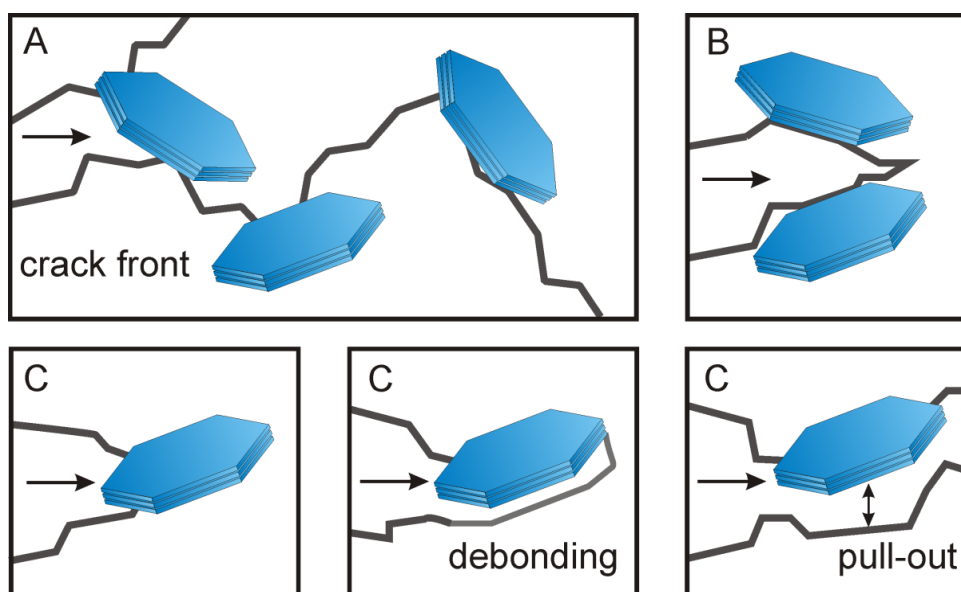


Fig. 11. Schematic representation of the above mentioned fracture mechanisms; A) crack deflection; B) crack pinning and C) filler/matrix debonding and platelets pull-out.

In summary, there are different toughening events occurring in the novel PMMA/clay nanocomposite and in each of the events a substantial amount of energy was dissipated. It must be emphasized here that the toughening mechanisms especially the crack pinning effect of PMMA/clay nanocomposites needs further investigation.

4. CONCLUSION

This study focused on the melt incorporation of tailored large aspect ratio, shear-stiff, mica-like nanoplatelets ($\alpha = 620$) in PMMA matrix and its impact on the mechanical behaviour. The prepared novel PMMA/clay nanocomposites offer improved toughness and stiffness over the neat PMMA without reduced strength. However, the incorporation of commercial natural clay leads to detrimental effects due to inefficient dispersion and the behaviour of the clay platelets. To the best of our knowledge, this is the first report on the preparation of PMMA/clay nanocomposites conducted by the industrial relevant melt compounding process that yielded a significantly improved toughness. Due to additional energy dissipating mechanisms an increase in fracture toughness of 66% could be detected in case of the large aspect ratio, mica-like clay.

ACKNOWLEDGEMENTS

The authors thank Hussein Kalo from the Department of Inorganic Chemistry I for producing the synthetic clay and Stephan Weiß from the Department of Macromolecular Chemistry II for synthesising the macroinitiator. Special thank goes to Florian Billing for his experimental contribution and Annelise Lang for the REM pictures. The financial support from the German Research Foundation, in the frame of the Collaborative Research Centre (SFB) 840: “From particulate nanosystems to mesotechnology” is highly acknowledged.

REFERENCES

- [1] Ajayan PM, Schadler LS, and Braun PV. *Nanocomposite Science and Technology*, Wiley- VCH Verlag, Germany 2003:77-154.
- [2] Bhattacharya SN, Gupta RK, and Kamal MR. *Polymeric Nanocomposites: theory and practice*, Hanser Gardner Publications Inc., USA 2008:35-144.
- [3] Hedicke K, Wittich H, Mehler C, Gruber F, and Altstädt V. *Composites Science and Technology* 2006;66(3-4):571-575.
- [4] Lietz S, Sandler JKW, Hedicke K, and Altstädt V. *16th European Conference of Fracture* 2006.
- [5] Lietz S, Yang J-L, Bosch E, Sandler JKW, Zhang Z, and Altstädt V. *Macromolecular Materials and Engineering* 2007;292(1):23-32.
- [6] Sandler J, Werner P, Shaffer MSP, Demchuk V, Altstädt V, and Windle AH. *Composites Part A: Applied Science and Manufacturing* 2002;33(8):1033-1039.
- [7] Sandler J, Windle AH, Werner P, Altstädt V, Es MV, and Shaffer MSP. *Journal of Materials Science* 2003;38(10):2135-2141.
- [8] Zeiler R, Handge UA, Dijkstra DJ, Meyer H, and Altstädt V. *Polymer* 2011;52(2):430-442.
- [9] Meneghetti P and Qutubuddin S. *Thermochimica Acta* 2006;442(1-2):74-77.
- [10] Abdelrazek EM. *Physica B: Condensed Matter* 2004;351(1-2):83-89.
- [11] Vega-González A, Subra-Paternault P, López-Periago AM, García-González CA, and Domingo C. *European Polymer Journal* 2008;44(4):1081-1094.
- [12] Cheng S-K and Chen C-Y. *European Polymer Journal* 2004;40(6):1239-1248.
- [13] Lin Y, Ng KM, Chan C-M, Sun G, and Wu J. *Journal of Colloid and Interface Science* 2011;358(2):423-429.
- [14] Su S, Jiang DD, and Wilkie CA. *Polymer Degradation and Stability* 2004;83(2):321-331.
- [15] Kalo H, Möller MW, Ziadeh M, Dolejš D, and Breu J. *Applied Clay Science* 2010;48(1-2):39-45.
- [16] Ziadeh M, Chwalka B, Kalo H, Schütz RM, and Breu J. accepted in *Clay minerals*.
- [17] Möller MW, Hirsemann D, Haarmann F, Senker Jr, and Breu J. *Chemistry of Materials* 2009;22(1):186-196.

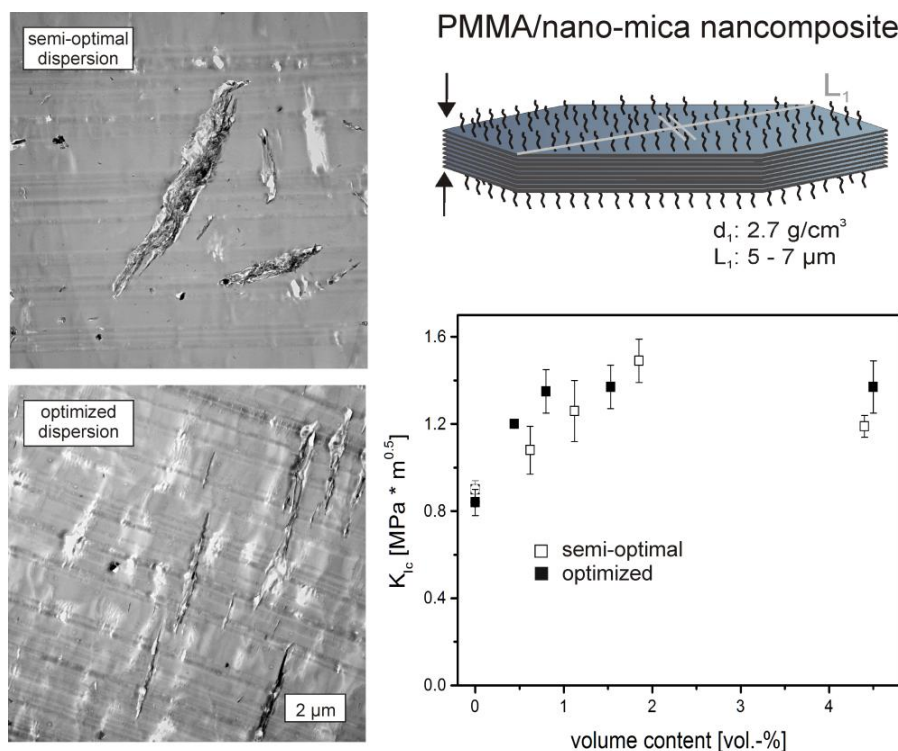
- [18] Burton AW, Ong K, Rea T, and Chan IY. *Microporous and Mesoporous Materials* 2009;117(1-2):75-90.
- [19] Scherrer P. *Nachr. Ges. Wiss. Goettingen* 1918;2:98-100.
- [20] Möller MW, Handge UA, Kunz DA, Lunkenbein T, Altstädt V, and Breu J. *ACS Nano* 2010;4(2):717-724.
- [21] Goossens D. *Sedimentology* 2008;55:65-96.
- [22] Cao T, Fasulo PD, and Rodgers WR. *App. Clay Science* 2010;49(1-2):21-28.
- [23] Liaw JH, Hsueh TY, Tan T-S, Wang Y, and Chiao S-M. *Polymer International* 2007;56(8):1045-1052.
- [24] Tiwari RR and Natarajan U. *Polymer International* 2008;57(5):738-743.
- [25] Fu S-Y, Feng X-Q, Lauke B, and Mai Y-W. *Composites Part B: Engineering* 2008;39(6):933-961.
- [26] Tanoue S, Utracki LA, Garcia-Rejon A, Tatibouët J, and Kamal MR. *Polymer Engineering & Science* 2005;45(6):827-837.
- [27] Yoon PJ, Hunter DL, and Paul DR. *Polymer* 2003;44(18):5323-5339.
- [28] Jiang L, Zhang J, and Wolcott MP. *Polymer* 2007;48(26):7632-7644.
- [29] Wetzels B, Rosso P, Hauptert F, and Friedrich K. *Engineering Fracture Mechanics* 2006;73(16):2375-2398.
- [30] Köppl T, Brehme S, Wolff-Fabris F, Altstädt V, Schartel B, and Döring M. *Journal of Applied Polymer Science* 2012; 124:9-18.

4.4. On the importance of specific interface area in clay nanocomposites of PMMA filled with synthetic nano-mica

Mazen Ziadeh^{a}, Bianca Fischer^{b*}, Jasmin Schmid^a, Volker Altstädt^b, Josef Breu^{a*}*

**these authors contributed equally to this publication*

Published in: Polymer (2014) DOI: 10.1016/j.polymer.2014.05.063



^aLehrstuhl für Anorganische Chemie I and ^bLehrstuhl für Polymere Werkstoffe, Universität Bayreuth, Universitätstrasse 30, 95440 Bayreuth, Germany

*Corresponding Author: josef.breu@uni-bayreuth.de (J. Breu)

Author's individual contributions:

My contribution to this publication was employing an appropriate blending method to achieve an optimum dispersion of high aspect ratio nanoplatelets in the PMMA matrix. This was achieved by a solution blending to prepare a 5 wt.-% masterbatch of efficiently dispersed nanoplatelets in the matrix.

My tasks included: (i) tuning of high aspect ratio nano-mica platelets, (ii) synthesis of modifier, modification and phase transfer into organic solvent, (iii) solution blending and preparation of the nanocomposites, and (iv) preparation of nanocomposites films for gas barrier measurements.

Jasmin Schmid provided technical help with the gas barrier measurements of the nanocomposites.

The melt compounding of the solution blended nanocomposites and the mechanical characterization were done by *Bianca Fischer* (Polymer Engineering). These included differential scanning calorimetry, tensile tests and fracture toughness.

The academic writing related to nanofiller preparation and characterization in addition to the gas barrier evaluation was done by me and Prof. Dr. *Josef Breu*. The academic writing related to the mechanical properties of the PMMA/clay nanocomposites was done by *Bianca Fischer* and *me with the help of* Prof. Dr. Ing.-*Volker Altstädt* and Prof. Dr. *Josef Breu*.

The manuscript is published in **Polymer**.

My contribution to this publication is 50%.

On the importance of specific interface area in clay nanocomposites of PMMA filled with synthetic nano-mica

Mazen Ziadeh^{a‡}, Bianca Fischer^{b‡}, Jasmin Schmid^a, Volker Altstädt^b, Josef Breu^{a*}

^aLehrstuhl für Anorganische Chemie I and ^bLehrstuhl für Polymere Werkstoffe, Universität Bayreuth, Universitätsstrasse 30, 95447 Bayreuth, Germany

[‡] Authors contributed equally to this work

* Corresponding author. E-mail address: josef.breu@uni-bayreuth.de (Prof. Dr. J. Breu)
Tel.: +49921552530; fax: +49921552788.

ABSTRACT

In clay nanocomposites, the specific interface area is the key factor determining potential improvements of properties. Nevertheless, in most systematic studies of nanocomposites little emphasis is put on assuring and characterizing dispersion quality. To probe the influence of dispersion quality, we compare nanocomposites filled with two layered silicates which were made by melt compounding and solution blending, respectively. Poly(methyl methacrylate) (PMMA) is chosen here as a thermoplastic model matrix which was compounded with a synthetic nano-mica (O-heck) and commercial Bentone with typical diameters of 5-7 μm and < 300 nm, respectively.

The dispersion quality was monitored by μ -computer tomography (μ -CT) and transmission electron microscopy (TEM). Moreover, gas barrier measurements proved to be an additional independent and very sensitive probe. Reductions of the oxygen permeation at ~4 wt.-% by 60% and 30% for solution blended and melt compounded samples directly evidence a mediocre dispersion in the latter.

Structure-property relationships were established by in-depth mechanical testing and the properties were correlated with the improved morphology. Significantly higher stiffness was achieved by enhanced dispersion quality for O-heck-filled nanocomposites without causing any embrittlement. Interestingly, a maximum increase of fracture toughness (63%) was obtained at filler content as low as 0.8 vol.-% for the solution blended sample. A similar improvement of fracture toughness for the melt compounded sample afforded more than twice the clay

content emphasising the crucial influence of specific surface area. This highlights the importance of the solution blending method to exploit the full potential of nanofillers and suggests that only samples with comparable dispersion quality may be compared.

Keywords: PMMA/clay nanocomposites, nano-mica, Bentone, solution blended masterbatch, gas barrier, mechanical properties

1. INTRODUCTION

Polymer clay nanocomposites have received an ever growing attention since Toyota central research laboratories reported the *in situ* preparation of nylon-6-montmorillonite composite in the late 1980's [1]. Clay nanoplatelets have a large surface-to-volume ratio allowing for enhancement of properties of neat polymers such as heat distortion temperature, gas barrier, and mechanical reinforcement [2,3]. Natural montmorillonite (MMT), completely ion exchanged with alkylammonium cations, has emerged as the conventional nanofiller for preparation of polymer clay nanocomposites. However, natural clays suffer of major drawbacks such as the inherent small lateral extension (L) < 300 nm which limits their average aspect ratios (α) [4]. Additionally, it suffers from heterogeneity in surface charge which consequently leads to non-uniform surface chemistry and interlayer reactivity which in turn affects bonding to the matrix and shear lability at a great deal. Moreover, the associated amorphous materials in natural MMT deposits (bentonites) like iron- and aluminium-oxihydroxides act as binders and render these fillers difficult to be disaggregated and even more to be delaminated in order to achieve maximum aspect ratio [5,6]. Incomplete delamination of clay tactoids in the polymer matrix in turn has a detrimental effect on the mechanical properties because the remaining interlayer spaces may act as inner shear planes inducing failure when introducing shear load [7].

Poly(methyl methacrylate) (PMMA) is chosen here as a thermoplastic model matrix for nanocomposite preparation due to its amorphous state and high stiffness; yet the relatively high brittleness causes poor resistance to crack initiation and propagation resulting in unsatisfying fracture toughness [8]. Therefore, improving the fracture toughness of such material without sacrificing its stiffness or strength is of great and general interest. For this purpose

compounding with nanofillers is promising as they can alter the local stress state in a polymer matrix and consequently promote additional forms of energy dissipation leading to a tougher material [9,10]. The number of reports dealing with the effect of nanofillers on the fracture toughness of amorphous polymers is, however, limited. In a recent study we have reported the preparation of PMMA/clay nanocomposites by melt compounding and compared a commercially available organo-clay (Bentone) and a modified synthetic shear-stiff, nano-mica (O-heck) with a focus on fracture toughness [10].

The synthetic nano-mica material is characterized by a large lateral extension of 5-7 μm (Figure S1) and a platelet thickness of 10-15 nm and thus a typical aspect ratio $\alpha \sim 500$. Contrary to MMT, the interlayer space of this nano-mica is not accessible but collapsed and consequently organophilization is restricted to external surfaces. This material therefore combines higher stiffness of the mica-sandwich and remarkable larger aspect ratio as compared to natural MMT. For the O-heck filler a significantly increase of fracture toughness by 66% was achieved for the nanocomposite in comparison to neat PMMA without sacrificing tensile strength. Additional energy dissipating mechanisms like crack deflection, crack pinning as well as debonding effects with platelets pull-out could be identified as occurring toughening mechanisms [10]. While melt compounding was found to provide a decent dispersion on a macroscopic level, on a microscopic level some smaller aggregates were detected. This suggested that melt compounding fails to maximize the specific interface area and consequently the full potential of the stiff, large- α nanofiller could not yet be exploited. Achieving a perfect dispersion for such huge nanoplatelets by conventional melt compounding proved to be impossible for reasons discussed in more detail later.

Therefore, in this study, an optimized processing method allowing for nearly perfect dispersion even of large- α nano-mica was applied and the nanocomposites obtained were characterized in terms of mechanical and gas barrier properties. The optimized process strictly avoids powdered samples that always suffer from band-like aggregation. Instead, a solution blended masterbatch was applied with homogeneously dispersed platelets. For comparison, the same processing was also applied to disperse commercial Bentone, an organically modified MMT. To probe

dispersion quality, oxygen transmission rates (OTR) of thin films were determined. Microstructure and mechanical properties were characterized in-depth to establish structure-property relationships.

2. EXPERIMENTAL

2.1. Materials

A commercial PMMA (Plexiglas POQ62 supplied by Evonik Industries) has been used as matrix material with a molecular weight (M_w) of 73 kg/mol and a polydispersity index of 1.63.

The starting material for the preparation of the nanofiller is a synthetic Na-fluorohectorite with the chemical formula $\text{Na}_{0.5}[\text{Mg}_{2.5}\text{Li}_{0.5}]\text{Si}_4\text{O}_{10}\text{F}_2$ and a CEC of 110 meq./100 g. In order to maximize the aspect ratio of the nanofiller, the interlayer Na^+ cations were exchanged with Mg^{2+} cations. These cations have a higher hydration of enthalpy leading to a highly hydrated 'shear-labile' state enabling a more efficient exfoliation of the tactoids under shearing. The suspension was processed in a stirred media mill and the degree of exfoliation was controlled by the number of milling passages [11]. Subsequent to the exfoliation process, the Mg^{2+} were exchanged with K^+ cations which due to their much reduced enthalpy of hydration as compared to Mg^{2+} transformed the clay to a non-swollen 'shear-stiff' nano-mica with no intracrystalline reactivity [12]. In nano-mica the interlayer space is collapsed and bridged by non-hydrated potassium ions protruding into cavities of the 2:1 silicate layer on both sides of the interlayer space. Please note that switching from 'shear-labile' to 'shear-stiff' by this simple ion-exchange requires a charge density of the clay which is significantly higher than observed for natural MMT. Moreover, the intracrystalline reactivity of all interlayers in a tactoid must be similar. This again is only the case for fluorohectorite synthesized at high temperatures from the melt but not for MMT. As a consequence of lower and heterogeneous charge density with MMT always external and internal interlayers will be accessible and modification cannot be restricted to external basal planes.

Contrary to MMT, the hydrophilic nano-mica platelets were converted to hydrophobic organo-clay (O-hect) compatible in the organic matrix using a polycationic modifier that selectively exchanges only for cations located at external basal planes. The surface modifier is a polycationic statistical copolymer, poly(2-

(2-bromoisobutyryloxy) ethyl methacrylate)-stat-(2-dimethyl-aminoethyl methacrylate) prepared as described in details by Ziadeh et al. [13]. Upon addition of the polycationic copolymer (1.65 g at pH=7.2) the nano-mica (50 g) flocculated. The modified flocculated nano-mica (O-hect) suspension was then centrifuged and finally redispersed in THF.

As a reference for a conventional organoclay, Bentone® 38 (L= 0.3 μm) was supplied by Elementis Specialties. This material is a natural swellable montmorillonite (MMT) which has been organophilized by cation exchange with highly selective alkylammonium cations of chain lengths varying from C14-C16. This cation exchange is not restricted to external basal planes but rather all, interlayer and external, cations are exchanged and consequently the organic content is high (38 wt.-%).

2.2. Nanocomposite Preparation

PMMA/clay nanocomposites containing 1, 2, and 4 wt.-% inorganic filler were prepared by two different methods: (i) melt compounding as already reported [10] and (ii) dilution via melt compounding of a masterbatch produced by solution blending, referred to as solution blending. The preparation sequence of the latter is schematically shown in Figure 1. After modification in an aqueous solution the modified nanofiller (O-hect) was phase transferred and redispersed in THF. As the Bentone powder was already organically modified, it was dispersed in THF. From this step onwards both clays suspensions in THF were processed the same way. The two clay suspensions at 5 wt.-% clay content were then mixed with the PMMA solution in THF (20 wt.-%). The dispersions were placed on an overhead shaker for 24 hours for homogenization. Subsequently, the dispersions were film casted and dried under vacuum in an oven at 90 °C for 18 hours and at 140°C for 8 hours to ensure complete removal of THF. The two dried nanocomposite masterbatches (O-hect and Bentone in PMMA) were then cryo-grinded to a fine powder for better feeding for melt compounding.

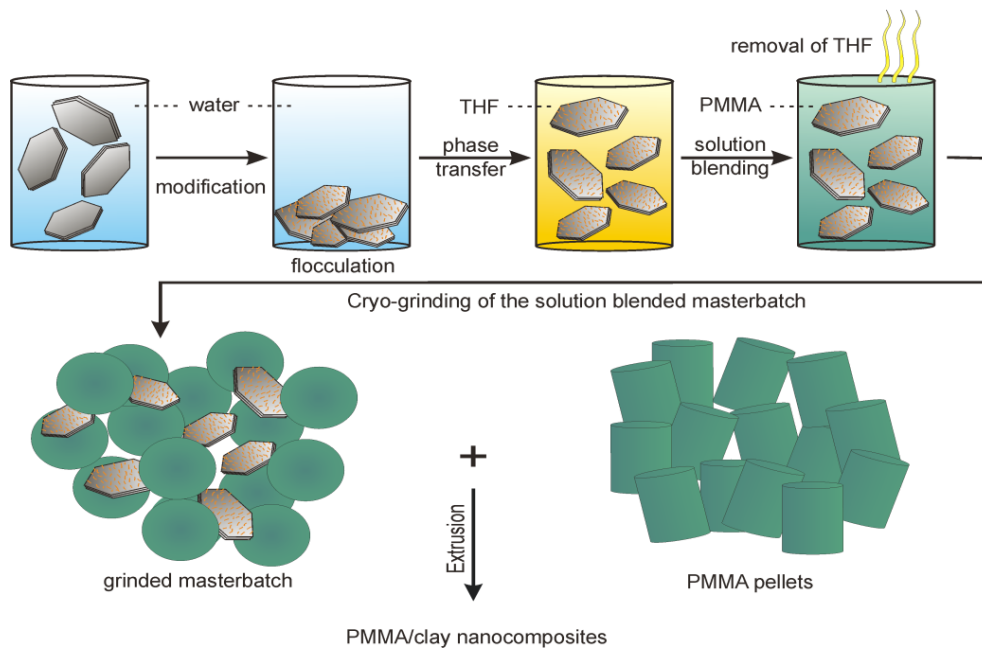


Figure 1. Schematic representation of the solution blending route after selective surface modification of large- α nano-mica for the preparation of PMMA/O-heckt nanocomposite.

Subsequently, both O-heckt and Bentone /PMMA masterbatches were melt compounded in two separate steps. In the first step, compounding in a continuous co-rotating twin-screw extruder (Brabender DSE 20/40) with a screw diameter of 20 mm and a length to diameter ratio $L/D = 40$ was done. This compounding step brings enough shear energy for dispersion and allows the complete removal of residual THF. Screw speed was fixed at 70 rpm and the temperature profile ranged from 90 °C to 210 °C near the nozzle. Pure PMMA was processed in the same way. The extruded strand was solidified in a water bath and pelletized. In the following compounding the adjustment of various concentrations with PMMA was realised in a discontinuous counter-rotating twin-screw microcompounder (DSM Xplore, 15 ml microcompounder) at 200 °C, a mixing speed of 210 rpm and a mixing time of 3 min.

2.3. Specimen Preparation

The specimen required for characterisation were compression-moulded using a hot-plate-press (190 °C, under vacuum) into CT (compact-tension; thickness: 4 mm and width: 33 mm) specimens to determine the critical stress intensity factor K_{Ic} or injection-moulded with a microinjector (DSM Xplore 12 ml injection moulding

machine; melt temperature: 190 °C; mould temperature: 40 °C; injection pressure: 8 bar) into tensile bars (75 mm x 5 mm x 2 mm) for tensile testing.

For permeability measurements, thin films with an area of $\approx 50 \text{ cm}^2$ were melt pressed from the O-*hect*-filled nanocomposites compounded pellets using a hot-plate-press (210 °C under 50 KN for 2 min) and the exact thickness was determined from SEM cross-section micrographs.

2.4. Nanocomposite Characterisation

2.4.1. Micro-Computer Tomography (μ -CT)

Investigation of the dispersion quality on a macroscopic level was carried out using a Skyscan X-Ray Microtomograph 1072 with a maximum spot resolution of 5 μm per pixel. 4 mm long pieces of the extruded strand were used. The measurements were done at a voltage of 80 kV and a current of 94 μA . The 3D-data is obtained by acquisitions every 0.23° with an exposure time of 1.5 s up to a complete rotation of 360° . 3-dimensional volumetric images were digitally reconstructed by using the software “NRecon” from Skyscan.

2.4.2. Transmission Electron Microscope (TEM)

The dispersion quality of the nanofiller in PMMA on a microscopic level was investigated using a LEO 922 A EFTEM (Carl Zeiss AG) with an acceleration voltage of 200 kV. Specimens of the extruded strand were prepared on a Leica Ultracut microtome (Leica Biosystems GmbH) equipped with a diamond knife to obtain 30–50 nm thin sections, which were placed on a carbon copper grid. The average interparticle distance in the nanocomposites was determined using the image-processing program ImageJ. The distance was measured from centre to centre of the particles.

2.4.3 Gas Barrier Measurements

Oxygen transmission rates were acquired on a Mocon (Minneapolis, MN, USA) OX-TRAN MH 2/21 instrument at standard pressure (STP). The measurements were conducted at RT and 50% relative humidity. A mixture of 95% nitrogen and 5% hydrogen (Linde Formiergas 95/5) was used as carrier gas and pure oxygen (>99.95, Linde Sauerstoff 4.5) as permanent. All samples were conditioned at least 12 hr prior to measurement. The calculation of the normalized oxygen permeation P was derived from the OTR according to following equation:

$$P = OTR \cdot l = \frac{\Delta V \cdot l}{A \cdot \Delta p \cdot \Delta t} \quad (1)$$

(l : film thickness in μm , ΔV : transmitted volume of oxygen, Δp : pressure gradient, Δt : elapsed time, and A : area of the specimen).

2.4.4. Scanning Electron Microscopy (SEM)

A scanning electron microscope Leo Zeiss 1530 Gemini (Carl Zeiss AG) with a field emission cathode was used to image the fracture surfaces of the PMMA/clay nanocomposites to investigate the micromechanical reason for fracturing. For this purpose the specimens were sputtered with 1.3 nm of platinum.

2.4.5. Differential Scanning Calorimetry (DSC)

The glass transition temperatures (T_g) of neat PMMA and PMMA/clay nanocomposites were determined using a DSC/SDTA 821e from Mettler Toledo. The measurements were carried out in a range from 25-190 °C under nitrogen atmosphere (50 ml/min) at a heating rate of 10 K/min. The specimens consist of 8 ± 1 mg of the extruded material. For determination of T_g the second heating curve were taken. For each material three measurements were done and the average value was reported. The standard deviation of T_g is ± 1 °C.

2.4.6. Thermogravimetric Analysis (TGA)

Since the content and type of organic modifier differs for the two types of the compared fillers, filler contents were related to the pure inorganic mass. This inorganic weight content of the fillers was determined by TGA (TGA/STDA 851e from Mettler Toledo). Specimens with mass of 18 ± 1 mg of the compounds were heated up in the range from 25 to 600 °C at a heating rate of 10 K/min under nitrogen atmosphere. All samples were run three times and the average values are reported. The mass is reproducible to $\pm 0.3\%$.

For evaluation of mechanical properties, the volume fraction of the nanofiller is the relevant feature. The inorganic weight content as determined by TGA was therefore converted into volume fraction applying the two distinct densities of the different fillers:

$$V_f = \frac{\rho_m \cdot W_f}{\rho_f \cdot W_m + \rho_m \cdot W_f} \quad (2)$$

Where V_f is the volume fraction of the filler, ρ_m and ρ_f are the densities of the matrix (1.19 g/cm³) and the filler ($\rho_{Bentone} = 1.7$ g/cm³ and $\rho_{O-lect} = 2.7$ g/cm³), respectively. W_m and W_f are the weight of the matrix and the filler, respectively.

2.3.7. Mechanical Testing

Tensile modulus, tensile strength and elongation at break were measured at 25 °C with a Universal Testing machine Zwick 1455 (Zwick GmbH & Co. KG) according to EN ISO 527 with a crosshead speed of 1 mm/min. For each material at least 5 samples were tested. The elongation was determined with a macro-displacement-transducer.

Fracture toughness tests were performed according to ISO 13586 to obtain the mode-I critical stress intensity factor (K_{Ic}) of the PMMA/clay nanocomposites. The tests were carried out using a universal testing machine Zwick BZ2.5/TN1S (Zwick GmbH & Co. KG). At least 5 notched, compact tension specimens are tested with a strain rate of 10 mm/min. To generate the sharp crack into the V-notch, a razor blade was used. The crack opening displacement was measured by a clip extensometer (632.29F-30, MTS). The K_{Ic} was calculated using the following equation:

$$K_{Ic} = \frac{F_{max}}{d \cdot \sqrt{w}} \cdot \sqrt{a} Y \cdot (a/w) \quad (3)$$

Where: F_{max} represents the maximum force required for crack propagation, d is the thickness of the specimen, w is the specimen width, a is the initial crack length, and Y is a geometrical term.

For deeper understanding of occurring fracture mechanisms, the crack tip opening displacement (δ_{tc}) was calculated using equation (3) and the mechanical values obtained from tensile and K_{Ic} tests:

$$\delta_{tc} = \frac{K_{Ic}^2}{E \cdot \sigma_Y} (1 - \nu^2) \quad (4)$$

E represents the Young's modulus obtained from tensile tests and σ_Y the yield stress obtained from compression tests, and ν is the Poisson's ratio of the polymer, here taken to be 0.35.

3. RESULTS AND DISCUSSION

3.1. Morphology and Dispersion Quality

The specific interface area is the key factor affecting potential improvements of nanocomposite properties. Therefore, the quality of nanofiller dispersion in the polymeric matrix is a crucial feature. As a first indication, the overall dispersion and distribution of the nanofiller or aggregates on a macroscopic scale was monitored using μ -computer tomography (μ -CT) analyses. The maximum spatial resolution of the μ -CT is 5-10 μm and thus only particles bigger than 5-10 μm can be detected by this method. As mentioned before, the typical lateral extension of MMT platelets is < 300 nm (Figure S1). Consequently, for MMT only aggregates can be visualized with μ -CT. Synthetic fluorohectorite platelets typically have lateral extensions of 5-7 μm while the thickness typically is 10 – 15 nm. Depending on the orientation relative to the X-ray beam, for fluorohectorite not only larger aggregates but also some primary platelets might be detectable in μ -CT.

As already reported, after melt compounding many Bentone aggregates were detected by μ -CT (Figure S2a), which for this filler must be aggregates [10]. The aggregates are homogeneously distributed over the whole volume of the sample making roughly 40% of the filler content. Melt compounding of O-hect showed a good dispersion quality on macroscopic level compared to conventional Bentone-filled composites (Figure S2b). Only very few particles can be spotted in the specimen with μ -CT. For the reasons discussed above it remains unclear at this point whether these represent large primary platelets or few remaining aggregates. As expected, with solution blending a much better dispersion as indicated by μ -CT was achieved (Figure S2c and 2d). In this case, no aggregates can be detected for both PMMA/clay nanocomposites suggesting that even for the Bentone-filled composite the specific interface area could be significantly increased. Comparing Figure S2a and 2c it is obvious that the full potential of any particular filler can only be estimated after optimization of the interface area.

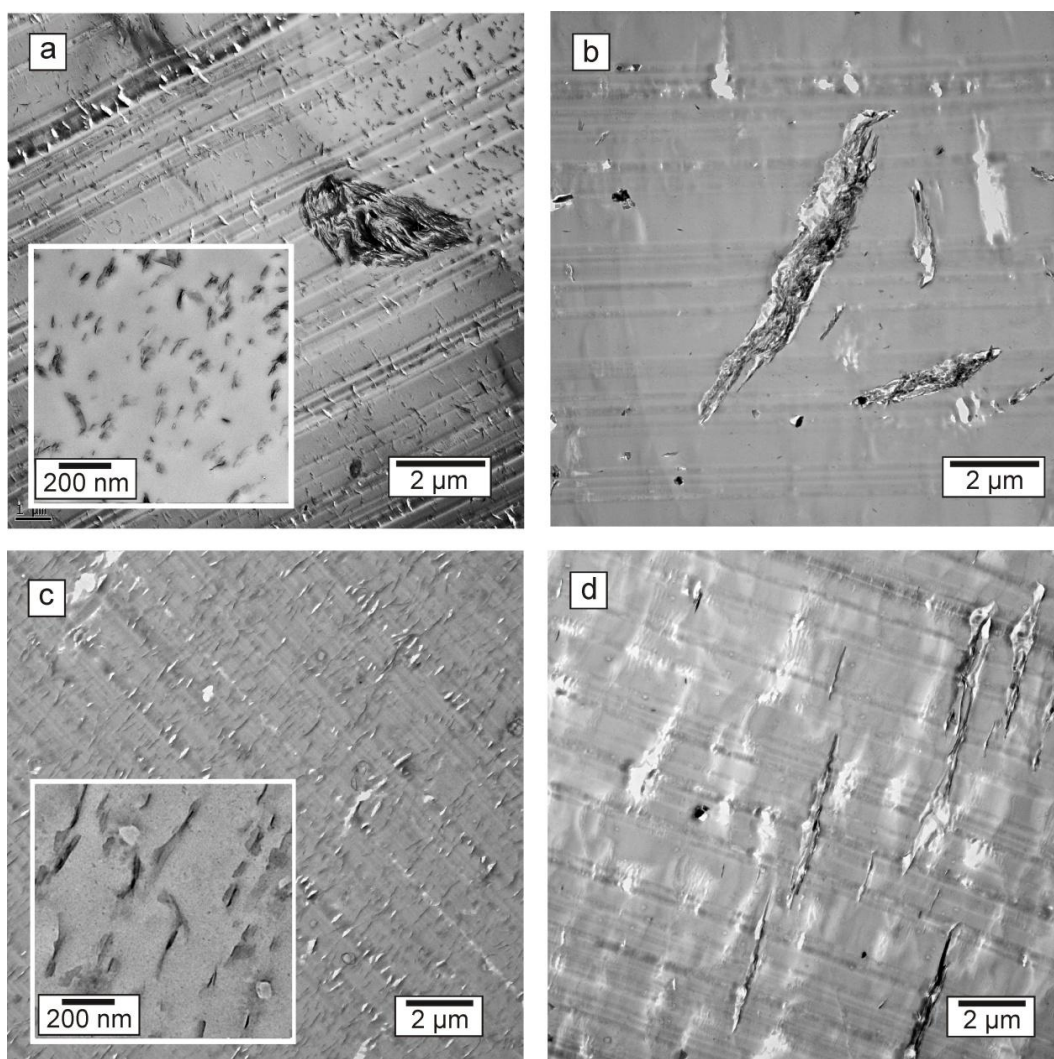


Figure 2. TEM micrographs of PMMA/clay nanocomposites; a) Bentone and b) O-heck prepared by melt compounding and c) Bentone and d) O-heck prepared by solution blending at 4 wt.-% clay content.

The dispersion quality of PMMA/clay nanocomposites on a microscopic level was monitored using TEM micrographs. TEM allows a qualitative understanding of the internal structure through direct visualization of the particle distribution in the matrix. Micrographs of PMMA/clay nanocomposites prepared by melt compounding are shown in Figure 2. As already indicated by μ -CT for Bentone-filled composites, huge aggregates exist in the specimen which reduces the effective specific interface area significantly (Figure 2a). Nevertheless, thin tactoids of Bentone were spotted alongside these huge aggregates. In case of O-heck-filled nanocomposites the microscopic dispersion is much better as compared to the Bentone sample (Figure 2b). Comparison with the sample obtained by the solution

blending (Figure 2d), however, clearly indicates that the dispersion can still be improved a great deal.

The advantage of solution blending was also noticeable for the Bentone-filled nanocomposite where aggregates were no longer observed but rather single clay tactoids (Figure 2c). The much improved dispersion quality as indicated by both μ -CT and TEM is expected to deliver improved properties due to the increase of specific interface area between the nanofiller and the matrix and the concomitant decrease of potential internal failure planes in the filler volume.

Due to the large α of O-hect platelets, inevitably texture is induced when clay suspensions are dried after modification and platelets are arranged parallel during drying. Upon complete removal of solvent, aggregates with band-like structure are formed. The large overlapping areas in these aggregates imply vdW forces of a magnitude that apparently cannot be overcome by shear forces generated during melt compounding to accomplish complete disaggregation. Contrary to this, the solution blending route avoids any drying steps for pure O-hect suspensions and thus avoids the formation of the band-like structures. For commercial Bentone powders, the overlapping areas are much smaller due to the smaller diameter and the absolute adhesion energy is much lower. Moreover, contrary to O-hect with Bentone, the modifier is exchanged at external and internal basal surfaces and a d-spacing of 25.5 Å (Figure S3) is observed for this intercalation compound. Therefore, the volume of the organic modifier amounts to as much as 68 vol.-% (see discussion in chapter 3.3) and this large volume swells in organic solvents assisting disaggregation by internal stress.

Quantitative analyses.

The number of particles per area in the nanocomposites as seen in the TEM micrographs represents quantitative information of the much improved dispersion quality (Figure 3). As a result of the improved dispersion quality, no longer aggregates were spotted and consequently, a higher number of nanoplatelets at any given area in the nanocomposites is observed. Due to their smaller lateral extension, the number of Bentone nanoplatelets per area (Figure 3a) is approximately two orders of magnitude higher than the number of O-hect nanoplatelets (Figure 3b).

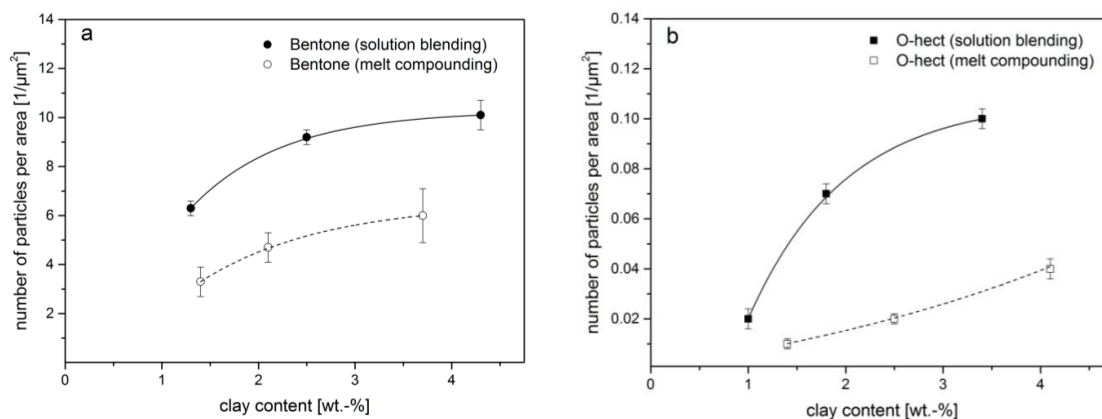


Figure 3. Effect of clay content and preparation method on number of particles per area for a) Bentone and b) O-hect-filled nanocomposites.

Moreover, the quantitative analysis provides details concerning the average interparticle distance (Table 1) which is a relevant parameter especially for interpretation of the mechanical behaviour [14].

As expected, the higher number of nanoplatelets obtained by a better dispersion reduces the interparticle distance significantly. Due to the large lateral extension of the nano-mica, the average interparticle distance in the O-hect-filled nanocomposites is one magnitude higher than in the Bentone-filled nanocomposites. It is worth to point out, that the interparticle distance is still in the same order of magnitude of the particle lateral extension, in respect to each nanofiller, which reduce the possibility to form any spatial-linked structures [15].

Table 1. Average interparticle distances for PMMA/Bentone and PMMA/O-hect nanocomposites in relation to preparation method as determined from TEM micrographs:

sample	weight content [%]	interparticle distance [nm]	
		<i>melt compounding</i>	<i>solution blending</i>
PMMA/Bentone	~ 1.3	483 ± 187	328 ± 145
PMMA/Bentone	~ 2.3	424 ± 154	261 ± 109
PMMA/Bentone	~ 4.0	350 ± 149	237 ± 109
PMMA/O-hect	~ 1.2	4836 ± 2137	3322 ± 1674
PMMA/O-hect	~ 2.2	3758 ± 1956	3013 ± 1401
PMMA/O-hect	~ 3.7	2936 ± 1563	1557 ± 727

Gas barrier measurements.

Gas barrier measurements were used as an additional independent indirect probe for dispersion quality of the nanofiller in the matrix at certain clay content. According to tortuous path models, for instance the Cussler model [16], the relative permeability of matrix and nanocomposite scale by α^2 . The permeability is therefore a sensitive measure for the effective aspect ratio. Since the effective aspect ratio will be reduced by band-like aggregation, permeability may also serve as indirect probe for dispersion quality. The nanocomposite films were prepared by melt pressing which probably induced an orientation of the nanoplatelets parallel to the melt flow. This texture will contribute to the reduction of permeability on top of the improvement of dispersion quality but the latter is expected to be the dominating effect.

At low filler content as applied here, MMT nanocomposites show little improvement, if any, in oxygen permeability due to the modest α as the aspect ratio of the filler is the key factor [17,18]. For instance, polystyrene/MMT-filled nanocomposites prepared via *in situ* polymerization of styrene showed a reduction of permeability by as little as 8% at a comparatively high filler content of 7 wt.-% [19]. Only for large aspect ratio fillers like O-hect a filler content of ~ 4 wt.-% as applied here, is expected to produce significant reductions in permeability. Therefore, the oxygen transmission rate (OTR) measurements were restricted to O-hect-filled nanocomposite films (Table 2). Since the thickness of functional films prepared varies to some degree, OTR values were normalized to permeabilities (P) of films with thickness of 100 μm for better comparability.

The translucent unfilled PMMA film showed a high permeability for oxygen ($P = 53 \text{ cm}^3 \text{ 100 } \mu\text{m m}^{-2} \text{ day}^{-1} \text{ bar}^{-1}$). A significant reduction (30% as compared to neat PMMA films) of the oxygen permeation to $37 \text{ cm}^3 \text{ 100 } \mu\text{m m}^{-2} \text{ day}^{-1} \text{ bar}^{-1}$ was observed for O-hect-filled nanocomposite films prepared by melt compounding. As anticipated, by a more efficient dispersion of O-hect by solution blending the permeation was reduced further (60% as compared to neat PMMA films) to $21 \text{ cm}^3 \text{ 100 } \mu\text{m m}^{-2} \text{ day}^{-1} \text{ bar}^{-1}$. In addition to aspect ratio, permeability is of course also dependant on filler content. The significantly better barrier for the solution blended nanocomposite (3.4 wt.-%) as compared to the melt compounded film

(4.1 wt.-%) was even achieved with lower filler content. Employing the Cussler model [16] to correct for the differing filler contents, the film prepared by solution blending at 4.1 wt.-% would be expected to show a reduction of permeability by 75% to a value as low as $14 \text{ cm}^3 \text{ 100 } \mu\text{m m}^{-2} \text{ day}^{-1} \text{ bar}^{-1}$. The superior performance of the solution blended over the melt compounded nanocomposite may be directly related to the reduction of effective aspect ratio by band-like aggregates in the latter and thus corroborates a superior dispersion quality achieved by solution blending.

Table 2. Oxygen transmission rates (OTR) and calculated permeations of PMMA/O-hect nanocomposites measured at 50% RH.

sample	method	content wt.-%	thickness (μm)	OTR ($\text{cm}^3 \text{ m}^{-2} \text{ day}^{-1} \text{ bar}^{-1}$)	Permeation ($100 \mu\text{m cm}^3 \text{ m}^{-2} \text{ day}^{-1} \text{ bar}^{-1}$)
neat PMMA	solution	-	230	23	53
PMMA/O-hect	melt	4.3	150	24	36
PMMA/O-hect	solution	3.6	120	18	21

3.3. Tensile Properties of PMMA/Clay Nanocomposites

Employing clay minerals as nanofillers to reinforce polymeric matrices generally leads to an increase in stiffness while concomitantly embrittlement takes place [20-22]. As it has been shown, dispersion quality is a key factor influencing the mechanical properties [23] and to probe the importance of the dispersion efficiency on mechanical performance, tensile tests were carried out. The larger accessible interfacial area, as indicated by TEM, μ -CT, and permeability, is expected to affect the mechanical properties of the nanocomposites significantly [24].

Tensile properties for different PMMA/clay nanocomposites and neat PMMA as a reference were compared as a function of volume content at 25 °C. The actual filler content was determined after complete thermal removal of organic matter (matrix and modifier). The remaining ceramic mass was converted to volume fractions of filler. The two types of fillers used differ, however, significantly in modifier content. For Bentone, the complete cation exchange capacity is neutralized by alkylammonium cations (Figure 4) and consequently the density of this filler is 1.7 g cm^{-3} . For O-hect, interlayer cations are non-exchangeable K-ions and thus the density of mica (2.7 g cm^{-3}) was used to convert mass into volume content.

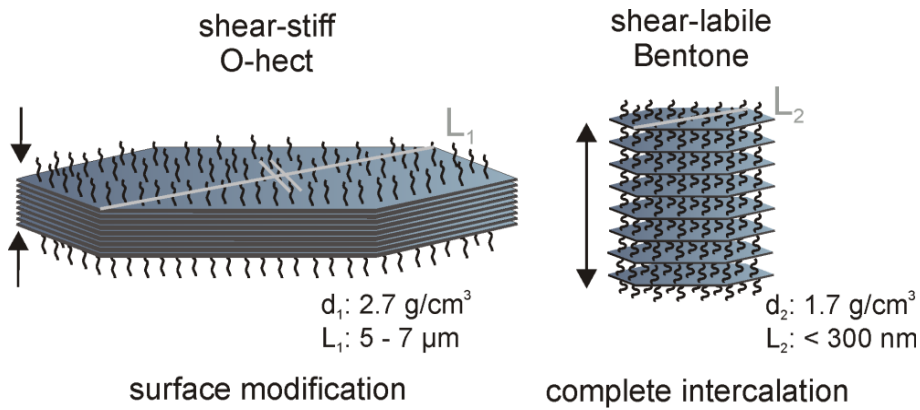


Figure 4. Schematic representation of (left) selective modification restricted to external basal surfaces in the shear-stiff O-hect and (right) complete ion exchange of both external and internal basal surfaces in Bentone leading to different densities of the two fillers.

The in-plane modulus of the platelets is the most relevant feature of the nanofiller in respect to reinforcement. The in-plane modulus of a single 2:1-layer has recently been determined experimentally by applying a sophisticated wrinkling method [25]. Interestingly, the in-plane module of such a delaminated, singular 2:1-silicate layer was found to significantly lower ($\sim 20\%$) than the corresponding value found for mica. This was attributed to the fact that non-hydrated interlayer K^+ cations protrude on both sides of the interlayer space into hexagonal cavities of the silicate surface. From a mechanical point of view, the stacks of silicate layers cross-linked by K^+ as found in the nano-mica filler therefore need to be treated as sandwich type reinforced nanoplatelets (for details see ref. [12]) which consist of a “soft” interlamellar region and a “strong” silicate lamella. Moreover, the “softness” of the interlamellar region correlates directly with the cohesion energy between adjacent silicate lamella which derives mainly from strong Coulomb interaction that diminishes with distance and hence basal spacing. For example, Heinz et al. calculated via MD-simulations a 3.3 times higher cleavage energy for K^+ -intercalated MMT as compared to its Octadecylammonium intercalated Bentone form [26]. And indeed, the TEM micrographs show that Bentone nanoplatelets exhibit some curvature in the structure as compared to the stiff nano-mica platelets (Figure 2c and d).

As expected, the incorporation of both nanofillers (Bentone or O-hect) into PMMA via melt compounding leads to an increase in Young's modulus (Figure 5) as the clay platelets promote a higher stiffness than the neat polymer matrix.

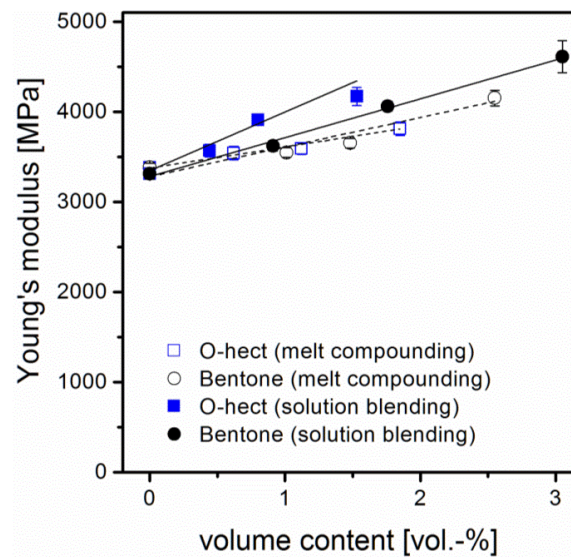


Figure 5. Effect of clay content and preparation method on Young's modulus of PMMA/clay nanocomposites.

The reinforcement model based on Halpin-Tsai [27,28] indicates that larger aspect ratios would promote a larger load carrying area. For instance experimentally, employing clay platelets with 100 and 200 aspect ratio in a rubbery matrix were found to increase Young's modulus by 167% and 298%, respectively [29].

Due to its much higher aspect ratio, O-hect would be expected to induce a larger increase of Young's modulus as compared to Bentone. For melt compounded nanocomposites we found, however, no significant difference in the performance of both fillers. Only when applying solution blending, O-hect nanocomposites outperform Bentone nanocomposites as expected. The effective aspect ratio improves with dispersion quality [30]. Even for melt compounded O-hect where little signs of aggregation were seen in μ -CT, apparently band-like aggregates reduce the effective aspect ratio as already indicated by permeability measurements. Interestingly even the solution blended Bentone nanocomposites outperform the melt compounded O-hect nanocomposites. This suggests that improvements in the properties of filler materials might easily be counterpoised by mediocre dispersion quality.

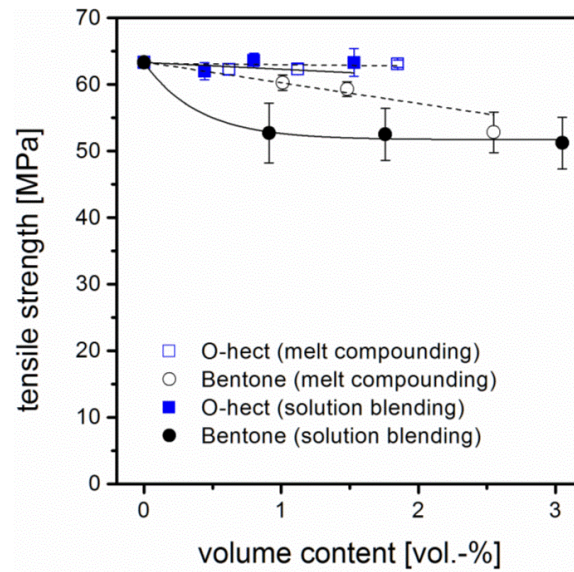


Figure 6. Effect of clay content and preparation method on tensile strength of PMMA/clay nanocomposites.

Incorporation of O-hect into PMMA has no detrimental effect on the tensile strength (Figure 6) and all nanocomposites showed a constant strength independently of clay content and dispersion quality. During tensile testing the applied external load leads to local stress concentrations at the edges of the platelets. However, no premature failure occurs due to the fact that the number of platelets at a given filler volume is relatively small for the huge O-hect platelets (Figure 3). Therefore the occurring deformation mechanisms of the PMMA matrix most likely will not be altered. This is confirmed on the nanoscale by SEM images of the fracture surfaces (Figure 7). Neat PMMA deforms by the formation of crazes that arise from stretching and failing of polymer chains (Figure 7a). In the presence of O-hect this craze formation is preserved as the dominant deformation mechanism taking place over large volumes (Figure 7b). Moreover pulled-out platelets can be seen with no visible debonded area indicating partial adhesion between platelets and PMMA matrix.

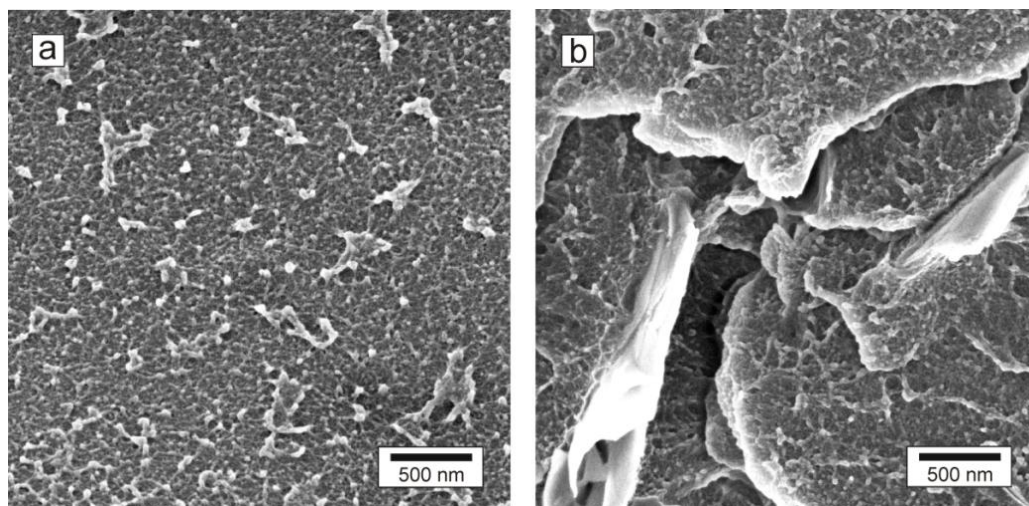


Figure 7. SEM micrographs of fracture surface of tensile bar for a) neat PMMA and b) O-hect filled nanocomposite prepared by solution blending were pulled-out platelets from the matrix can be observed.

An increase in tensile strength is expected to take place in the case of strong interfacial adhesion granted by effective stress transfer from the matrix to the filler during uniaxial tensile loading [31]. The load transfer between nanofiller and matrix can be realised via shear stress induced in the interface region. Information about the filler/matrix adhesion can be deduced from the glass transition temperature (T_g) which is highly sensitive to chain mobility. In case of a strong adhesion, T_g increases due to immobilisation of polymer chains in the surroundings of the platelets. A decrease in T_g indicates no interactions at all or a plasticizing effect of the organic modifier. We observe no change in T_g values of the nanocomposites (Table 3) as compared to unfilled neat PMMA, which has been processed in the same way as the nanocomposites. This suggests a partial interfacial bonding between clay and matrix leading to a limited load transfer and therefore to a matrix dominated failure. This partial interfacial bonding is not surprising as the modified clays exhibit only very short organic chains on the surface, which improve compatibilization but are too short to penetrate the PMMA matrix and to promote good adhesion. Although, the Bentone filler bears high organic loading, the glass transition temperature of Bentone-filled PMMA nanocomposites is not reduced disqualifying a potential contribution of the modifier as a plasticising agent. Consequently, we do not expect a significant influence of the different modifiers used for the two nanofillers. Such behaviour is

similar to previous observations in PMMA/clay nanocomposites prepared using conventional organoclay such as Cloisite 15A and 30B [32,33].

Contrary to O-*h*-ect nanocomposites, Bentone-filled nanocomposites failed at lower tensile strength compared to neat PMMA. In case of melt compounded nanocomposites the presence of huge aggregates (Figure 2a) most likely is responsible for premature failure. These micro-sized agglomerates led to stress concentrations and consequently to cracks with supercritical length resulting in premature failure [34,35].

Table 3. Glass transition temperatures (T_g) of neat PMMA and PMMA/clay nanocomposites at 4 wt.% clay content in respect to the preparation technique.

sample	glass transition temperature (T_g) [°C]	
	melt compounding	solution blending
neat PMMA	101 ± 1	103 ± 1
PMMA/O- <i>h</i> -ect	102 ± 1	103 ± 1
PMMA/Bentone	102 ± 1	101 ± 1

Surprisingly, improving the dispersion quality by solution blending led to an even more pronounced reduction in tensile strength for Bentone-filled nanocomposites even at low clay contents (1 vol.-%). As already mentioned, the external load applied during tensile testing leads to stress concentrations at the edges of the platelets. As the lateral extension of Bentone nanoplatelets is one order of magnitude smaller than of O-*h*-ect, the number of platelets and consequently the number of stress concentrators per volume is at least two orders of magnitude higher (Figure 3). Consequently, the matrix ligament thickness is comparatively small due to the tremendous reduction of interparticle distances by increasing the number of particles per filler volume (Table 1).

In case of an insufficient interfacial strength, the stress concentration promotes partial debonding and void initiation at a certain stress level. These phenomena appear first in the core region of the tensile bar, where the particle orientation in load direction is low [36]. The orientation is based on the assumption of a parabolic velocity distribution during the injection moulding process across the thickness of the mould.

Additional stress loading often leads to a distortion of stress fields in the matrix surrounding the particles which in turn induces local shear yielding with concomitant void growth in load direction [37]. Further stress loading will eventually promote coalescence of adjacent micro voids into macro voids that induces premature failure (Figure 8) [36].

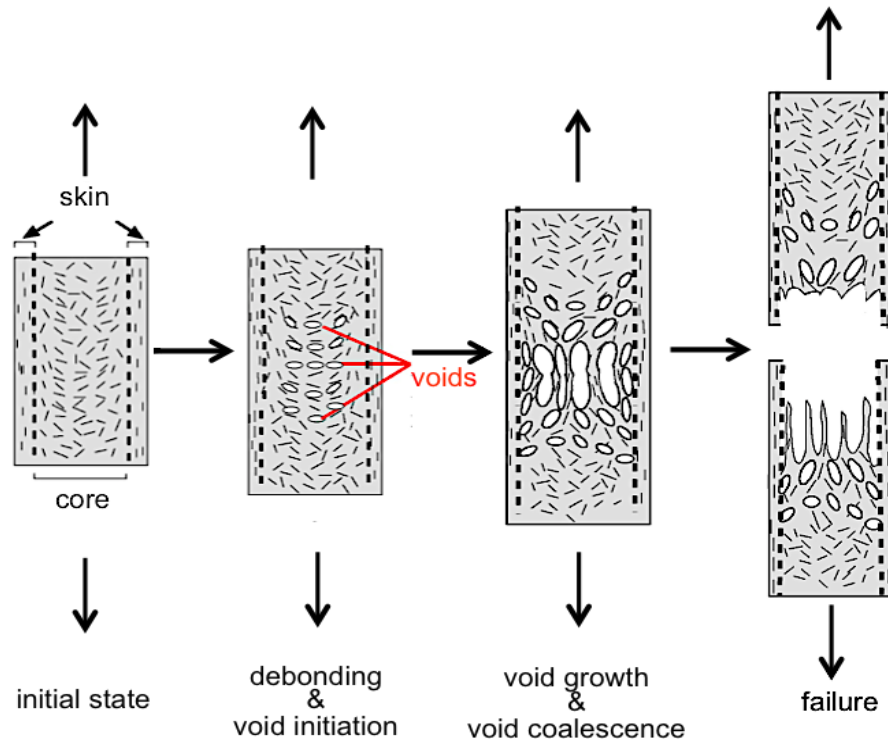


Figure 8. Schematic representation of the gradual deformation process in Bentone-filled nanocomposites with partial interfacial adhesion under uniaxial tensile loading (modelled after [36]).

The point when void coalescence occurs strongly depends on the interparticle distance. Increasing the number of particles by disaggregation reduces interparticle distances in case of solution blended Bentone-filled nanocomposites (Table 1). The resulting small ligament thickness fosters void growth at relatively low applied stress and therefore leads to premature failure. Compared to neat PMMA the fracture surface showed completely different deformation scenario. Local shear-yielding of PMMA and the presence of a huge number of voids can be observed (Figure 9). Nevertheless, in some areas with lower Bentone concentration the same deformation mechanisms as in neat PMMA could be identified.

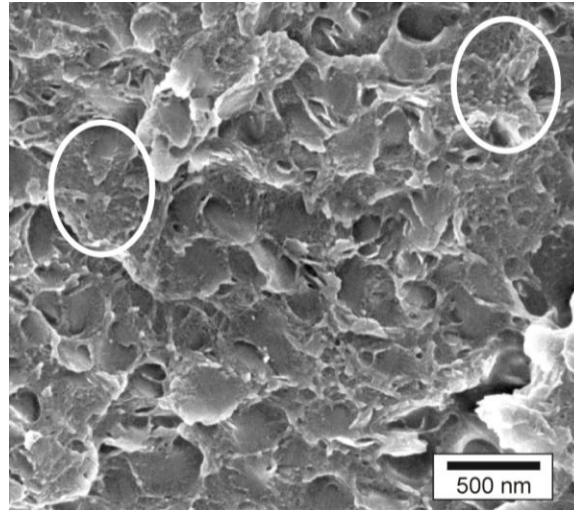


Figure 9. SEM micrographs of fracture surfaces of a tensile bar of Bentone-filled nanocomposite prepared by solution blending showing a huge number of voids; only in selected areas highlighted by circles craze formation is preserved.

In agreement with all previous literature reports [21,32,33], for all prepared PMMA/clay nanocomposites, the increase in stiffness was accompanied by a reduction of elongation at break (Figure 10). The reduction was found to be more pronounced for the Bentone-filled nanocomposites due to the much higher number of particles per volume and a consequently much smaller average interparticle distance.

In nanocomposites, the plastic deformation is limited by the ligament thickness between two particles. Therefore, in case of small interparticle distances, the deformation capability of the PMMA matrix during stretching is restricted to a greater degree. In line with this, improving the dispersion quality by solution blending led to an even more severe reduction in the elongation at break due to shorter average interparticle distances.

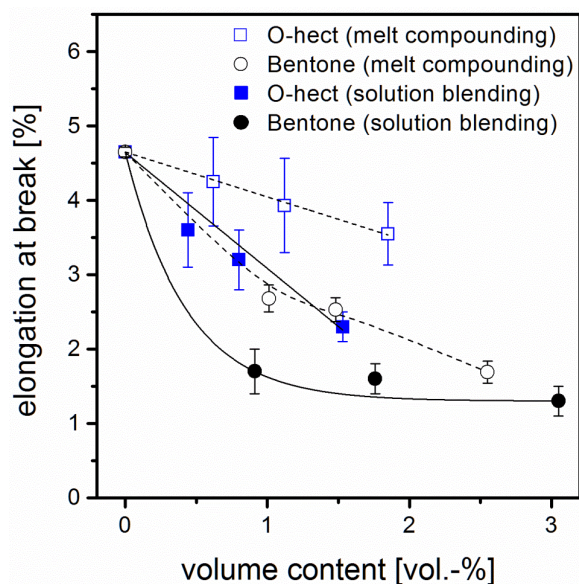


Figure 10. Effect of clay content and preparation method on elongation at break of PMMA/clay nanocomposites.

3.4. Fracture Toughness

In order to investigate the effect of dispersion efficiency on fracture toughness of PMMA/clay nanocomposites, K_{Ic} measurements were performed at 25 °C under mode I load (Figure 11).

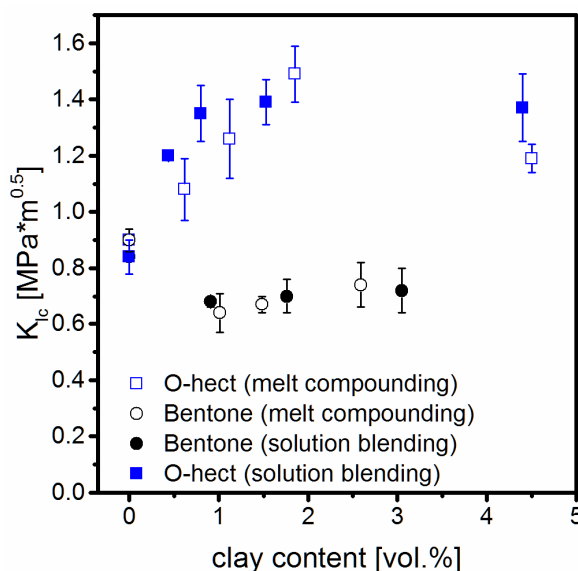


Figure 11. Effect of clay content and preparation method on K_{Ic} of PMMA/clay nanocomposites.

As already reported the incorporation of Bentone by melt compounding does not promote any toughening but on the contrary has a detrimental effect on the fracture toughness of PMMA [10]. For Bentone nanocomposites enhancing the

dispersion quality by solution blending also failed to improve the fracture toughness. The decrease of fracture toughness might be attributed to a significant restriction in average plastic deformation of the PMMA matrix by the presence of a large number of Bentone nanoplatelets [38]. Further evidence for a reduced plastic deformation comes from the drastically reduced elongation at break (Figure 10).

In contrast to Bentone nanocomposites, incorporation of O-heck by melt compounding considerably increases the fracture toughness up to 66% compared to neat PMMA (Figure 11). While optimizing the dispersion of O-heck by solution blending led to comparable maximum values, the initial increase with low filler volume is much more pronounced. At clay content as low as 0.8 vol.-% an increase in fracture toughness as high as 63% was achieved. Interestingly, toughening as a function of filler content quickly merges into a plateau. At a first glance, this seems irritating as additional particles in the nanocomposites would be expected to contribute to further toughening. With increasing filler volume, however, plastic deformation of the PMMA matrix is also increasingly restricted as indicated by the reductions seen in the elongation at break (Figure 10).

Toughening Mechanisms.

In order to provide a deeper understanding of the different fracture toughness behaviour of Bentone and O-heck-filled nanocomposites, the crack opening displacement (δ_{tc}) in compact tension specimens during K_{Ic} measurement can be calculated using Irwin's equation (eq. 4). δ_{tc} represents the expansion of the crack tip due to plastic yield of the matrix altering the crack shape and size. It has already been shown that the Irwin equation can be employed for nanocomposites based on spherical fillers to understand possible toughening mechanisms. For instance, δ_{tc} was calculated for epoxy nanocomposites filled with silica nanoparticles (~ 20 nm) and was in a micrometer range. However, to promote toughening mechanisms, in particular crack pinning and crack deflection, the filler must be at least as large as δ_{tc} . Therefore, the silica nanoparticles were not able to promote the aforementioned toughening mechanisms [33].

Table 4 gives an overview of the crack opening displacements for Bentone and O-heck-filled nanocomposites at different clay contents. Only the nanocomposites prepared by solution blending are considered.

Table 4. Crack tip opening displacement (δ_{tc}) calculated using the Irwin model for PMMA/clay nanocomposites.

filler type	solid content (vol.-%)	δ_{tc} - CTOD (μm)
neat PMMA	-	1.9
O-hect	0.44	3.6
O-hect	0.80	4.0
O-hect	1.53	3.9
Bentone	0.91	1.2
Bentone	1.76	1.1
Bentone	3.05	1.0

For the neat PMMA matrix the δ_{tc} is 1.9 μm and for Bentone and O-hect-filled nanocomposites the maximum δ_{tc} is 1.2 and 4.0 μm , respectively. Bentone typically has lateral extension < 300 nm whereas O-hect shows platelet diameters between 5-7 μm (Figure S1). Bentone thus is significantly smaller than the calculated δ_{tc} and therefore, the aforementioned toughening mechanisms are unlikely to occur [39,40]. On the contrary, O-hect platelets are much larger than δ_{tc} allowing for crack pinning and crack deflection as occurring toughening mechanisms.

To verify these considerations, the fracture surfaces of neat PMMA and PMMA/clay nanocomposites were investigated in detail. SEM micrographs of the fracture surface of neat PMMA show a relatively smooth fracture surface with slight plastic deformation on a macroscale and the typical nanoscale structure arises from craze initiation and growth (Figure 12).

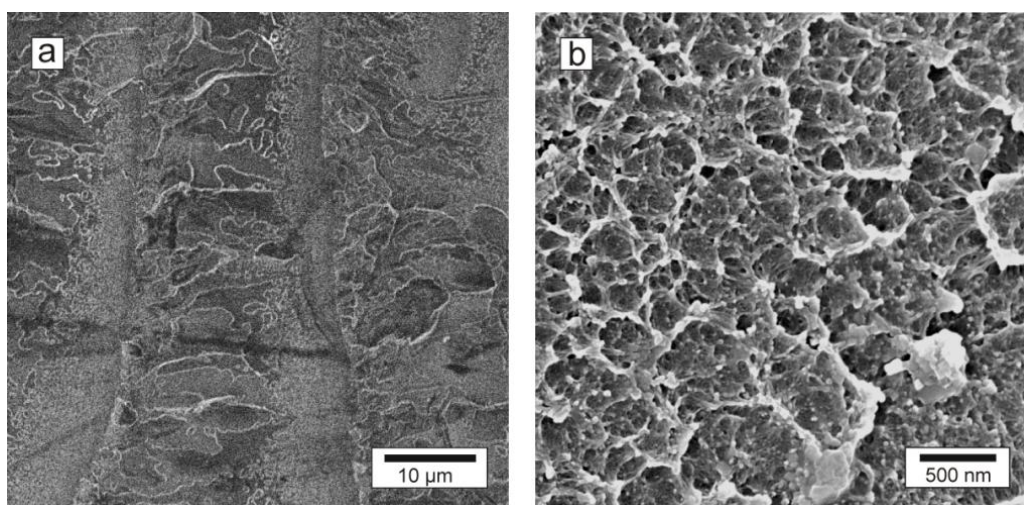


Figure 12. SEM micrographs of K_{Ic} fracture surface for neat PMMA.

The incorporation of O-hect alters the macroscopic deformation mechanism as the crack is caused to propagate along an extended tortuous path leading to higher energy dissipation during crack propagation (Figure 13 top). Moreover crack pinning and platelet pull-out occur in a similar fashion to what we have previously discussed in detail for O-hect-filled nanocomposites prepared by a melt compounding [10]. The nanoscale deformation mechanism is quite similar to neat PMMA.

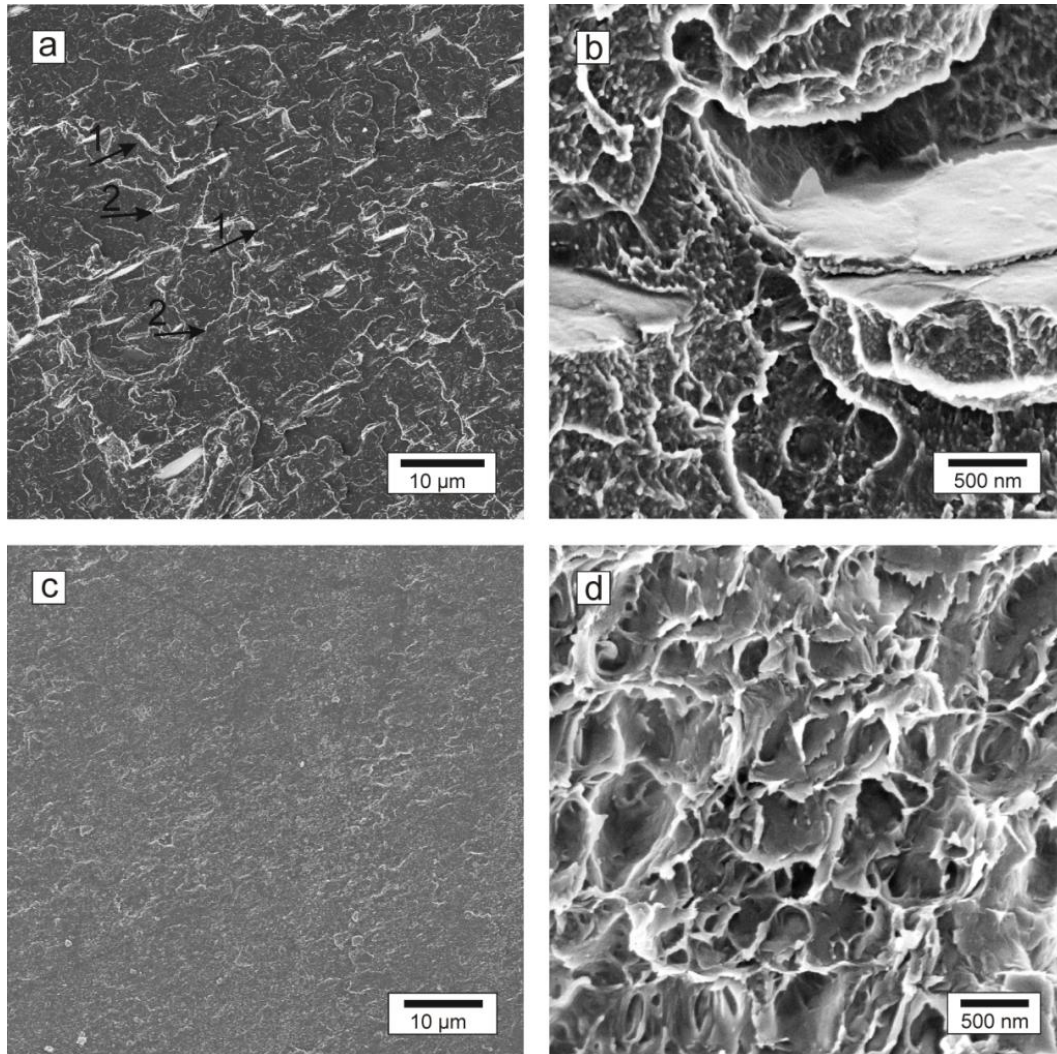


Figure 13. SEM micrographs of K_{Ic} fracture surfaces a,b) O-hect-filled and c,d) Bentone-filled nanocomposites prepared by solution blending; the crack propagation direction is from left to right. The arrows indicate (1) crack pinning and (2) crack deflection occurring mechanisms, respectively.

In case of Bentone-filled nanocomposites the macroscopic fracture surface shows no signs of the abovementioned toughening mechanisms and is much smoother

indicating less energy dissipation compared to neat PMMA (Figure 13 bottom). On the nanoscale, debonding of Bentone platelets and local shear-yielding of the PMMA matrix was observed as occurring deformation behaviour. Nevertheless, the macroscopic deformation capability of the matrix is significantly restricted as compared to the deformation of neat PMMA matrix.

4. CONCLUSION

The focus of this study was to maximize the specific interface area of large aspect ratio nano-mica (O-hect) in a PMMA matrix by an efficient dispersion. Melt compounding proved to be ineffective to achieve shear forces sufficient to break band-like aggregates of partially parallel overlapping nanoplatelets produced when drying suspensions. Consequently, masterbatches were produced by solution blending of suspensions of filler and matrix. This approach yielded a much improved dispersion of clay tactoids in the matrix as confirmed by μ -CT, TEM micrographs, and gas barrier measurements. The latter appears to be a sensitive probe as the barrier depends on the square of the aspect ratio and any reduction of effective aspect ratio by band-like aggregates may be immediately detected.

Characterization of the mechanical properties of the nanocomposites stressed the prime importance of the dispersion quality. The superiority of new filler materials can easily be masked by inferior dispersion processes. For instance, the solution blended Bentone nanocomposites outperform the melt compounded O-hect nanocomposites in respect to Young's modulus. Only when applying solution blending for both materials, the impact of the high aspect ratio of O-hect was realized. This suggests that improvements in the properties of filler materials might easily be counterpoised by mediocre dispersion quality.

The O-hect-filled nanocomposites offered significantly improved E-modulus (+30%) without reduced strength. Most notable, fracture toughness maybe increased by 63% at filler content as low as 0.80 vol.-% for solution blended O-hect nanocomposites. A comparable improvement in toughness required 1.85 vol.-% using melt compounding. This reduction of filler content by more than 50% to achieve a similar toughening effect again underlines the importance of dispersion quality assuring maximum specific interface area. The full potential of any

nanofiller can only be retrieved if the effective aspect ratio is maximized by a blending process capable of preventing aggregation.

By optimizing the dispersion of Bentone, surprisingly the tensile strength was significantly reduced. Due to insufficient interfacial strength, the stress concentration promotes partial debonding at a certain stress level eventually leading to void initiation. Premature failure is then induced by growth of these voids and eventually coalescence of adjacent micro voids into macro voids, an incidence which strongly depends on the interparticle distance. Increasing the number of particles by disaggregation will thus fosters void growth at relatively low applied stress and therefore is responsible for premature failure. In this context, it should be noted that the interparticle distance at any given filler content is of course also dependant on the platelet diameter. As the lateral extension of Bentone nanoplatelets is one order of magnitude smaller than of O-heckt, the number of platelets per volume is at least two orders of magnitude higher. Consequently, no premature failure was observed for the comparatively few huge O-heckt platelets and the strength was not reduced for this nanocomposite at any filler content.

ACKNOWLEDGEMENTS

The authors would like to thank Bernd Putz (Inorganic Chemistry I) for the synthesis of Na-fluorohectorite and Melanie Förtsch and Anneliese Lang for the electron microscopy pictures. The financial support from the German Research Foundation, in the frame of the Collaborative Research Centre (SFB) 840: "From particulate nanosystems to mesotechnology" is highly acknowledged.

REFERENCES

- [1] Usuki A, Kojima Y, Kawasumi M, Okada A, Fukushima Y, Kurauchi T, Kamigaito O. *J Mater Res* 1993;8(5):1179-1184.
- [2] Paul DR, Robeson LM. *Polymer* 2008;49(15):3187-3204.
- [3] Thostenson ET, Li C, Chou TW. *Compos Sci Technol* 2005;65(3-4):491-516.
- [4] Cadene A, Durand-Vidal S, Turq P, Brendle J. *J Colloid Interface Sci* 2005;285(2):719-730.
- [5] Breu J, Range KJ, Kohler EE, Wagner U. *Appl Clay Sci* 1993;8(4):313-320.
- [6] Köster HM. *Clay Miner* 1996;31(3):417-422.
- [7] Brune DA, Bicerano J. *Polymer* 2002;43(2):369-387.
- [8] Dasari A, Lim H, Yu Z, Mai W. *Fracture Properties and Mechanisms of Polyamide/Clay Nanocomposites*, editors. *Nano- and Micromechanics of Polymer Blends and Composites* Carl Hanser Verlag GmbH & Co. KG, 2009, pp. 377-423.
- [9] Lin Y, Ng KM, Chan CM, Sun G, Wu J. *J Colloid Interface Sci* 2011;358(2):423-429.
- [10] Fischer B, Ziadeh M, Pfaff A, Breu J, Altstädt V. *Polymer* 2012;53(15):3230-3237.
- [11] Ziadeh M, Chwalka B, Kalo H, Schütz MR, Breu J. *Clay Miner* 2012;47(3):341-353.
- [12] Möller MW, Handge UA, Kunz DA, Lunkenbein T, Altstädt V, Breu J. *ACS Nano* 2010;4(2):717-724.
- [13] Ziadeh M, Weiss S, Fischer B, Förster S, Altstädt V, Müller AH, Breu J. *J Colloid Interface Sci* 2014;425:143-151.
- [14] Mizuno C, John B, Okamoto M. *Macromol Mater Eng* 2013;298(4):400-411.
- [15] Sinha Ray S, Yamada K, Okamoto M, Ueda K. *Polymer* 2003;44(3):857-866.
- [16] DeRocher JP, Gettelfinger BT, Wang J, Nuxoll EE, Cussler EL. *J Membr Sci* 2005;254(1-2):21-30.
- [17] Möller MW, Lunkenbein T, Kalo H, Schieder M, Kunz DA, Breu J. *Adv Mater* 2010;22(46):5245-5249.
- [18] Priolo MA, Gamboa D, Grunlan JC. *ACS Appl Mater Interfaces* 2009;2(1):312-320.
- [19] Nazarenko S, Meneghetti P, Julmon P, Olson BG, Qutubuddin S. *J Polym Sci B Polym Phys* 2007;45(13):1733-1753.

- [20] Liaw JH, Hsueh TY, Tan TS, Wang Y, Chiao SM. *Polym Int* 2007;56(8):1045-1052.
- [21] Tiwari RR, Natarajan U. *Polym Int* 2008;57(5):738-743.
- [22] Shah D, Maiti P, Jiang DD, Batt CA, Giannelis EG. *Adv Mater* 2005;17(5):525-528.
- [23] Vaia RA, Wagner HD. *Mater Today* 2004;7(11):32-37.
- [24] Dhibar AK, Mallick S, Rath T, Khatua BB. *J Appl Polym Sci* 2009;113(5):3012-3018.
- [25] Kunz DA, Erath J, Kluge D, Thurn H, Putz B, Fery A, Breu J. *ACS Appl Mater Interfaces* 2013;5(12):5851-5855.
- [26] Heinz H, Vaia RA, Farmer BL. *J Chem Phys* 2006;124(22).
- [27] Halpin JC, Kardos JL. *Polym Eng Sci* 1976;16(5):344-352.
- [28] Mori T, Tanaka K. *Acta Metallurgica* 1973;21(5):571-574.
- [29] Gatos KG, Karger-Kocsis J. *Eur Polym J* 2007;43(4):1097-1104.
- [30] Panwar A, Choudhary V, Sharma DK. *J Reinf Plast Compos* 2013;32(10):740-757.
- [31] Hsueh CH. *J Am Ceram Soc* 1989;72(2):344-347.
- [32] Unnikrishnan L, Mohanty S, Nayak SK, Singh N. *J Appl Polym Sci* 2012;124(1):309-318.
- [33] Tiwari RR, Natarajan U. *J Appl Polym Sci* 2007;105(5):2433-2443.
- [34] Fu SY, Feng XQ, Lauke B, Mai YW. *Composites Part B* 2008;39(6):933-961.
- [35] Tanoue S, Utracki LA, Garcia-Rejon A, Tatibouët J, Kamal MR. *Polym Eng Sci* 2005;45(6):827-837.
- [36] Uribe-Arocha P, Mehler C, Puskas JE, Altstädt V. *Polymer* 2003;44(8):2441-2446.
- [37] Dekkers MEJ, Heikens D. *J Mater Sci* 1983;18(11):3281-3287.
- [38] Boo WJ, Liu J, Sue HJ. *Mater Sci Technol* 2006;22(7):829-834.
- [39] Gam KT, Miyamoto M, Nishimura R, Sue HJ. *Polym Eng Sci* 2003;43(10):1635-1645.
- [40] Weon JI, Sue HJ. *Polymer* 2005;46(17):6325-6334.

Supporting Information

1. Characterization methods

1.1. Static light scattering (SLS)

The particle size distributions (PSD) curves were recorded using a Retsch Horiba LA-950 static light scattering instrument for dispersions (~1% solid content) of O-heck and Bentone in tetrahydrofuran (THF) in a stand cell. The dynamic radius obtained from the measurement can be well correlated with the lateral extension [1].

1.2. Powder X-ray diffraction (PXRD)

The PXRD patterns were obtained in reflection mode on a PANalytical Xpert-Pro equipped with an X'Celerator Scientific RTMS detector using Cu-K α radiation. The "Full Width at Half Maximum" (FWHM) of the 001 reflection was determined and related to the thickness of the platelets applying the Scherer equation [2,3].

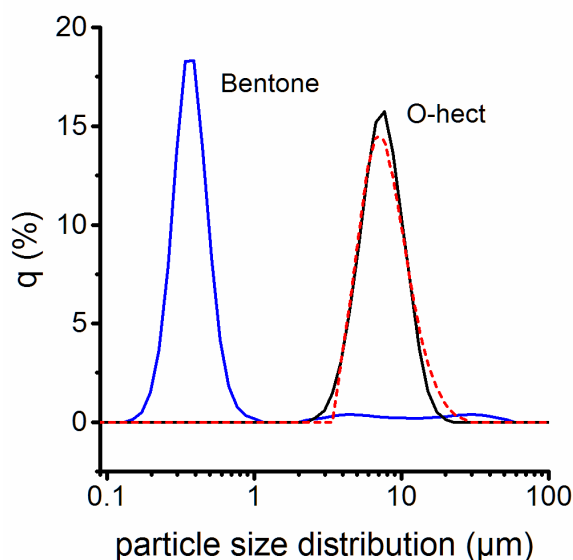


Figure S1. Volume weighted ($q\%$) particle size distributions of (—) Bentone and (—) O-heck before compounding and (---) after compounding. The data were obtained by static light scattering using clay dispersions in THF (1 wt%) using the following refractive indexes RI_{clay} : 1.590, RI_{THF} : 1.407. The D_{50} values are 6.4 μm and 0.30 μm for O-heck and Bentone, respectively

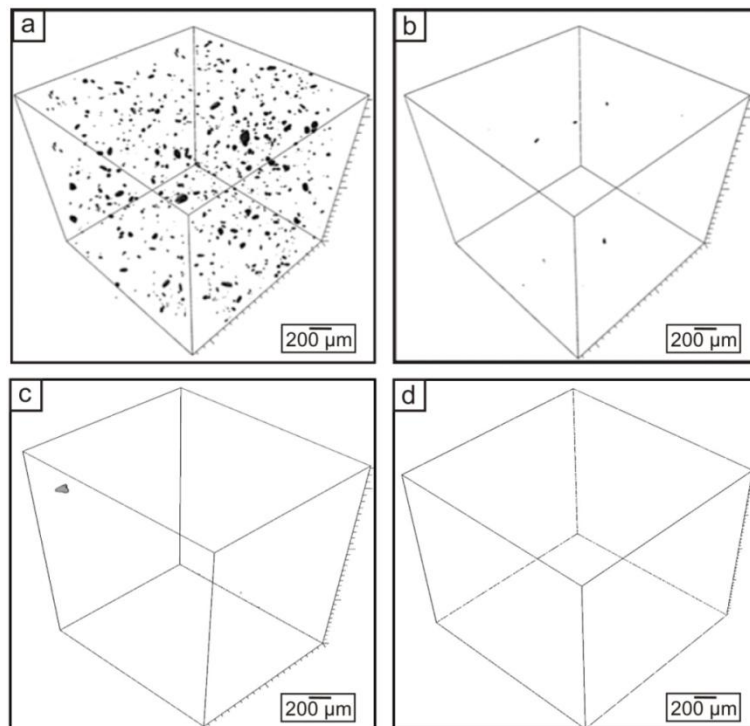


Figure S2. Three-dimensional reconstruction applying μ -CT of different PMMA/clay nanocomposites at 4 wt.-% content; a) Bentone and b) O-hect: prepared by melt compounding, c) Bentone and d) O-hect: prepared by solution blending.

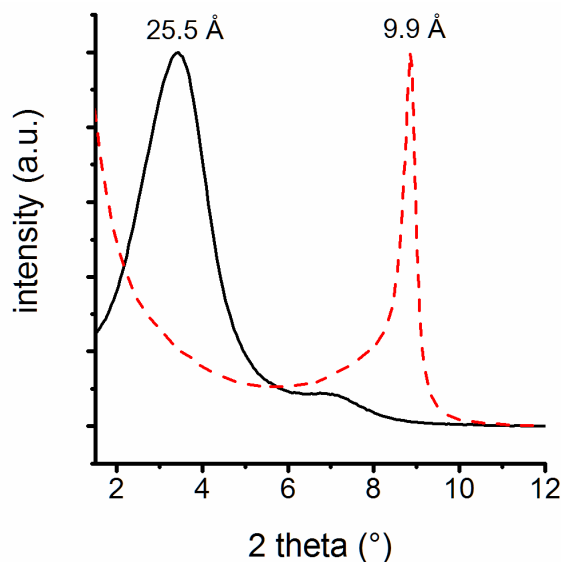


Figure S3. PXRD patterns of Bentone (—) and O-hect (---) showing the (001) reflexes corresponding to a d -spacing of 25.7 and 9.9 Å, respectively.

1. Goossens D. Sedimentology 2008;55(1):65-96.
2. Burton AW, Ong K, Rea T, Chan IY. Microporous and Mesoporous Mater 2009;117(1-2):75-90.
3. Scherrer P. Nachr Ges Wiss Goettingen 1918;2(98-100).

List of publications and conferences

[1]. **Ziadeh, M.**, Fischer, B.; Schmid, J., Altstädt, V.; Breu, J., On the importance of specific interface area in clay nanocomposites of PMMA filled with synthetic nano-mica, *Polymer*, **2014**, (DOI: 10.1016/j.Polymer.2014.05.063).

[2]. **Ziadeh, M.**; Weiss, S.; Fischer, B.; Förster, S.; Altstädt, V.; Müller, A. H. E. Breu, J., Towards completely miscible PMMA nanocomposites reinforced by shear-stiff, nano-mica, *J Colloid Interface Sci.*, **2014**, 425, 143-151.

[3]. Fischer, B.; **Ziadeh, M.**; Pfaff, A.; Breu, J. Altstädt, V., Impact of large aspect ratio, shear-stiff, mica-like clay on mechanical behaviour of PMMA/clay nanocomposites, *Polymer*, **2012**, 53, 3230–3237.

[4]. **Ziadeh, M.**; Chwalka, B.; Kalo, H.; Schütz, M. R. Breu, A simple approach for producing high aspect ratio fluorohectorite nanoplatelets utilizing a stirred media mill (ball mill), *J. Clay Miner.*, **2012**, 47, 341–353.

[5]. Kothmann, M., **Ziadeh, M.**, Bakis, G., Breu, J., Altstädt, V., New generation of high aspect ratio shear-stiff mica-like based epoxy nanocomposites. **2014**, (to be submitted to Composite Part B: Engineering).

[6]. Diar Bakerly, B.; Hausner, J.; Kalo, H.; Edenharter, A.; **Ziadeh, M.**; Beyer, G.; Breu, J. Multi-Component Flame Retardants: Combining Anionic and Cationic Clays as Trojan Horses for Molecular Flame Retardants, **2014**, (to be submitted).

[7]. Weiss, S.; Hirsemann, D.; Biersack, B.; **Ziadeh, M.**; Müller, A. H. E. Breu, J., Hybrid Janus particles based on polymer-modified kaolinite, *Polymer*, **2013**, 54, 1388–1396.

[8]. Fischer, B.; **Ziadeh, M.**; Breu, J. Altstädt, V., PMMA nanocomposites based on 2nd generation layered silicate, Proceedings of the Polymer Processing Society 28th Annual Meeting PPS-28, **2012**.

[9]. Kalo, H.; Möller, M. W.; **Ziadeh, M.**; Dolejs, D. Breu, Large scale melt synthesis in an open crucible of Na-fluorohectorite with superb charge homogeneity and particle size, *J. Appl Clay Sci.*, **2010**, 48, 39–45.

[10]. **Ziadeh, M.**; Breu, J., Dabbit, O., Organic Synthesis of Various Quaternary Ammonium and Phosphonium Cationic Molecules for the Modification of Clay Minerals, *R J of Aleppo Univ.: Basic Science Series*, **2009**, 65, 18–35.

II. Conferences

[1]. **Euroclay 2011**, Antalya, Turkey (26.06 – 01.07.2011)

Poster# 622: A Facile Approach for Producing High Aspect Ratio Fluorohectorite Nanoplatelets by Utilizing a Stirred Media Mill.

Poster# 623: Surface Initiated ATRP of PMMA Brushes from High Aspect Ratio Shear-Stiff, K-fluorohectorite Surface.

Acknowledgment

I would like to dedicate this last page to thank all those who helped me finish this academic work through their encouragement and help.

Probably these few lines won't be enough to express my sincere appreciation for my supervisor and academic mentor Prof. Dr. Josef Breu. I would like to thank him for his trust and the great chances he gave me since I met him in Aleppo few years ago. During my work period he gave me the freedom to develop my own approaches and to learn from my mistakes. I have learned a lot from him for which I am grateful. I am also thankful for his patience and great efforts which he invested in the publications.

I had the chance to be part within an excellent team in ACI department and I would like to thank all my previous and current colleagues and friends who made the last three years very interesting and productive while I was away from home. Thank you for the exceptionally good and cooperative atmosphere. In particular I would like to thank my lab colleagues: Manuela Stirner, Carina Bojer and my friends Martin Schieder and Patrick Feicht (big brother). I would like also to thank Josef Hausner and Jasmin Schmid for their help and collaboration while working on the SFB - Project B3.

I am glad that I had the chance to meet during this few years so many friendly and helpful people in particular from the ACIII department and I would like to thank all of my friends there for their support.

Working in a mutual collaboration with the Polymer Engineering Department gave me the chance to expand and gain new expertise in the mechanical properties of nanocomposites. I appreciate very much the contribution and discussions provided by Prof. Dr.-Ing. Volker Altstädt to the publications. I would like to thank my cooperation partner Bianca Fischer for the great contribution and collaboration during the last two years. In addition, I would like to thank Martin Kothmann for his effort and contribution to the joint publication.

I am very thankful for all the back stage helpers in the background, without their help I would not have been able to finish this research work in a smooth process especially: Dr. Wolfgang Milius, the ACI secretaries, the technical assistance staff: Beate Bojer, Bernd Putz for the large scale synthesis of the layered silicate and Lena Geiling for here help and patience during all the compounding and extruding trails and for the electron microscope micrographs.

Last but not least, I am a very lucky person to have such great parents like you mom and dad. Since the unpleasant situation back home being away from you and not able to help was very hard on me. Your thoughts and trust made me always look forward. Thank you for everything and hope we meet again soon. My brother and my best friend Samer, you inspire me dude, love you and I will always be on your side. Thank you for being the best brother a person can have, wish you all the success in your life.

Finally, I am very thankful for the financial and personal support from the KAAD during my research at Bayreuth University.

Erklärung des Verfassers

Hiermit erkläre ich, dass ich die Arbeit selbständig verfasst und keine anderen als die von mir angegebene Quellen und Hilfsmittel benutzt habe.

Ferner erkläre ich, dass ich anderweitig mit oder ohne Erfolg nicht versucht habe, diese Dissertation einzureichen. Ich habe keine gleichartige Doktorprüfung an einer anderen Hochschule endgültig nicht bestanden.

Bayreuth, den 23.06.2014

Mazen Ziadeh